

Algerian Democratic and Popular Republic  
Ministry of High Education and Scientific Research



University SAAD DAHLAB of Blida  
Faculty of Engineering Sciences  
Department of Electronics

*A Thesis Proposal Submitted in Partial Fulfillment of the Requirements for the Degree of*

## Doctor of Sciences in Electronics

# OPTIMAL IMAGE RESTORATION USING SWARM INTELLIGENCE ALGORITHMS AND THEIR SYNERGY:

*Comparative Study with Application to Nuclear Imaging*

**Slami SAADI**

Committee members:

N.BENBLIDIA	MCA, USD, Blida	President
A.NAMANE	MCA, USD, Blida	Examiner
A.MAYOUF	MCA, UZA, Djelfa	Examiner
M.HALIMI	MRA, CSC, Algiers	Examiner
A. GUESSOUM	Professor, USD, Blida	Supervisor
M.BETTAYEB	Professor, University of Sharjah, UAE	Co-Supervisor

**UNIVERSITE SAAD DAHLEB DE BLIDA**

**Faculté des Sciences de l'Ingénieur**

Département d'Electronique

**THESE DE DOCTORAT EN SCIENCES**

Spécialité: Electronique

Option: Image & Parole

**OPTIMAL IMAGE RESTORATION USING SWARM INTELLIGENCE**

**ALGORITHMS AND THEIR SYNERGY:**

*Comparative Study with Application to Nuclear Imaging*

**Slami SAADI**

**Jury:**

<b>N.BENBLIDIA</b>	<b>MCA, USD, BLIDA</b>	<b>President</b>
<b>A.NAMANE</b>	<b>MCA, USD, BLIDA</b>	<b>Examiner</b>
<b>A.MAYOUF</b>	<b>MCA, UZA, DJELFA</b>	<b>Examiner</b>
<b>M.HALIMI</b>	<b>MRA, CSC, ALGIERS</b>	<b>Examiner</b>
<b>A. GUESSOUM</b>	<b>Professor, USD, BLIDA</b>	<b>Supervisor</b>
<b>M.BETTAYEB</b>	<b>Professor, University of Sharjah, UAE</b>	<b>Co-Supervisor</b>

**Blida, Juin 2012**

*To my parents*  
*To my wife and my children*  
*To my teachers and students*  
*To all my friends*

## ACKNOWLEDGEMENTS

**My deepest gratitude is to my creator the Almighty who guided me always in my life and made me know that science is the torch that leads to true knowledge of His Majesty**

I would like to express my sincere gratitude to my supervisors, Professor **A. Guessoum** from Blida University and Professor **M. Bettayeb** from Sharjah University for their friendly welcome, their open and warm attitude, for their attention, time and flexibility and for their support in hard times. Also, I am indebted to all my mentors, in Electronics Department.

Honest thanks to **Dr. N.Benblidia** (Maître de Conference,USD,Blida) for accepting the presidency of the jury, sincere gratitude also to **Dr.A.Namane** (Maître de Conference,USD,Blida), **Dr.A.Mayouf** (Maître de Conference,UZA,Djelfa) and **Dr.M.Halimi** (Maître de Recherche, CSC, Algiers) who honoured me by examining this work.

Particular gratitude to my good friends for their constant encouragement, during all our research works realized partly in the Nuclear Research Center of Birine (CRNB). Thanks to all researchers in CRNB and teachers in Ziane Achour University of Djelfa, for their kindness and helpful nature, for their encouragement and technical advices.

As it is impossible to mention in this brief acknowledgment every single person, I would like to thank all those who have contributed in a way or another to this achievement and have made my time enjoyable by providing a pleasant environment.

I owe my deepest gratitude to my parents (**Ali and Aicha**) for their sacrifices, their support and their love; they gave me everything in life. I can not find the words to thank my wife (**Djamila**) for her devotion, endurance, patience, understanding and love. She stood besides me and inspired me during my life. Special thanks go to my children (**Abderrahmane, Hadjer, Sajida and Mohamed Younes**) for creating the lovely working environment for me. This achievement is also theirs.

## ABREVIATIONS & NOMENCLATURE

### 1. Abbreviations

*PSF: point spread function*

*FFT: Fast Fourier Transform*

*SVD: Singular Value Decomposition*

*TSVD: Truncated Singular Value Decomposition*

*TV: Total Variation*

*PDE : Partial Differential Equation*

*PSO: Particle Swarm Optimization*

*BFO: Bacterial Foraging Optimization*

*DCT: Discret Cosine Transform*

*GCV: Generalized cross validation*

*CG: Conjugate Gradient*

*ROF: Rudin, Osher, Fatemi*

*BID: Blind Image Deconvolution*

*ARMA: Autoregressive moving average*

*NN: Neural Network*

*RMSE: Root mean squares error*

*PSNR: peak signal to noise ratio*

*NCC: Normalized Cross-Correlation*

*AD: Average Difference*

*SC: Structural Content*

*MD: Maximum Difference*

*NAE: Normalized Absolute Error*

## 2. Nomenclature

$g$  : degraded image

$H$  : blurring operator

$f$  : original image

$\eta$  : additive noise

$U, V^T$  : two column-orthogonal matrices

$\Sigma$  : diagonal matrix with entries  $\sigma_1 \geq \sigma_2 \geq \dots \geq \sigma_N \geq 0$

$\alpha$  : Tikhonov regularization parameter

$\lambda$  : Total Variation regularization parameter

$\omega$  : inertia weight

$C_1, C_2$  : acceleration constants

$P$  : dimension of search space

$S$  : population of the *E. coli* bacteria

$\phi(j)$  : random direction of the bacteria

$J(i, j, k, l)$  : cost at the location of *i*th bacterium

$\theta^i(j, k, l)$  : location of the *i*th bacterium at *j*th chemotactic step, *k*th reproduction step and *l*th elimination–dispersal step

$N_c$  : maximum number of chemotactic steps

$N_s$  : maximum number of swims

$N_{re}$  : maximum number of reproduction steps

$N_{ed}$  : number of elimination–dispersal events

$P_{ed}$  : the probability that each bacteria will be eliminated/dispersed

$S_r = S/2$  : the number of bacteria reproductions (splits) per generation

$C(i)$  : step length of the bacterium

## Abstract

In this thesis, we introduced a new optimal approach to the nonlinear degraded images restoration problem which is useful for the enhancement of neutron radiography gray-level images. We attempt to reconstruct or recover images that have been degraded, using some a priori knowledge of the degradation phenomenon. Our approach is based on using Swarm intelligence optimization methods, Particle Swarm (PSO) and Bacterial Foraging (BFO) algorithms, in addition to their synergy, to solve such ill-posed inverse problem. Many works have been done using a room of techniques, ranging from linear and nonlinear filters, matrix algebra and discrete mathematics methods and regularized deconvolution, to optimization methods such as neural networks, fuzzy logic and genetic evolutionary algorithms. We selected the Total variation (TV) regularization as an approach which requires linearization of a highly nonlinear penalty term and take advantage of swarm intelligence in order to facilitate computation. To get smoothed images in presence of noise, a Laplacian constraint is introduced in the optimization process for regularization task. Another approach is presented in this thesis based on modelling the nonlinear degradation process as an ARMA (autoregressive moving average) process, this model is identified using an optimized neural network which is fast trained using a hybrid swarm implementation based on the synergy of PSO and BFO algorithms. Both original image and blur function are identified through this model. A computational comparison based on some recent image quality metrics is performed between these approaches.

## Résumé

Dans cette thèse, nous avons introduit une nouvelle approche optimale au problème de la restauration des images dégradées non linéaire qui est utile pour l'amélioration des images obtenues par radiographie neutronique. Ces images sont en niveaux de Gris. Nous essayons de reconstruire ou restaurer une image qui a été dégradé pendant l'acquisition, en utilisant des connaissances à priori du phénomène de dégradation. Notre approche est basée sur les méthodes d'optimisation en utilisant l'intelligence en essaims, comme les essaims des particules (PSO) et les bactéries en recherche de nourriture (BFO), en plus de leur synergie, pour résoudre un tel problème inverse mal posé. De nombreux travaux ont été fait en utilisant plusieurs techniques, allant des filtres linéaires et non linéaires, l'algèbre des matrices et mathématique discrète et la dé-convolution régularisée, à des méthodes d'optimisation tels que les réseaux de neurones, la logique floue et les algorithmes évolutionnaires génétiques. Nous avons choisi la méthode de régularisation des variations totales (TV) qui exige la linéarisation d'un terme de pénalité hautement non linéaire, et on a profité des avantages de l'intelligence en essaims, afin de faciliter les calculs. Pour obtenir des images lissées en présence de bruit, une contrainte Laplacienne est introduite dans le processus d'optimisation pour la régularisation. Une autre approche est présentée dans cette thèse basée sur la modélisation du processus nonlinéaire de dégradation par un modèle ARMA (autoregressive moving average). Ce modèle est identifié en utilisant un réseau de neurones optimisé. L'apprentissage de ce réseau est réalisé à l'aide d'une implémentation hybride de deux algorithmes : PSO et BFO. L'image originale et la fonction de dégradation sont déterminés en même temps à travers ce modèle. Une étude comparative basée sur des mesures de qualité d'image est effectuée entre ces approches.



## ملخص

في هذه الأطروحة، اقترحنا إتباع نهج جديد كحل أمثل لمشكلة استعادة الصور المتدهورة غير خطيا التي هي مفيدة لتعزيز و تحسين الصور الرمادية الملتقطة عن طريق الأشعة النيوترونية. حاولنا إعادة بناء أو استعادة الصور التي قد تدهورت ،وذلك باستخدام بعض المعرفة المسبقة لظاهرة التدهور. ويقوم منهجنا على استخدام الأساليب المثلى للذكاء الجماعي للسرب: خوارزمية أسراب الجسيمات (PSO) وخوارزمية أسراب البكتيرية (BFO) في بحثها عن الأكل لحل هذه المشكلة المعكوسة و المعروفة بسوء الطرح.

لقد سبق و أن طرحت عدة حلول باستخدام العديد من التقنيات في أعمال سابقة مثل المرشحات الخطية وغير الخطية، جبر المصفوفات، الرياضيات الرقمية، و الالتفاف المعدل. إلى أساليب التحسين مثل الشبكات العصبية، والمنطق الغامض وخوارزميات التطور الجيني. اخترنا تعديل مجموع التغيرات كنهج يتطلب إعادة إلى الصيغة الخطية لجزء كبير يتميز بالصفة الغير خطية العالية والاستفادة من ذكاء السرب من أجل تسهيل الحساب. للحصول على صور مصقولة جيدا في وجود ضوضاء عالية، أطفنا قيد لابلاس في عملية التحسين من أجل مهمة التعديل.

نقدم مقارنة أخرى في هذه الرسالة تركز على أساس النمذجة لعملية تدهور الصور (باعتبارها غير خطية) . يتم تحديد هذا النموذج باستخدام الشبكة العصبية الأمثل التي يشرف على تدريب عناصرها تطبيق سرب الهجين المستندة على خوارزميات PSO و BFO . في هذه المقارنة يتم تحديد كل من الصورة الأصلية ودالة التدهور في نفس الوقت من خلال هذا النموذج . قمنا بإجراء مقارنة حسابية تقوم على مقاييس جودة الصورة بين هذه المناهج المقترحة والمناهج السابقة.

## CONTENTS

Dedication	II
Acknowledgment	III
Notations	IV
Abstract	V
Contents	VIII
List of figures and tables	X
<b>1. GENERAL INTRODUCTION</b>	<b>15</b>
<b>2. IMAGE RESTORATION: AN OVERVIEW</b>	<b>20</b>
2.1 Introduction	20
2.2 Image degradation	21
2.2.1 Blurring	21
2.2.2 Noise	22
2.3 Restoration Using a General Linear Model	23
2.3.1 Wiener filter Restoration	24
2.3.2 Restoration using regularized filter	25
2.4 Nonlinear image restoration	26
2.4.1 Order Statistic Filters	27
2.4.2 Adaptive Median Filter	27
2.4.3 Restoration using Lucy-Richardson Algorithm	28
2.4.4 Blind Restoration	29
2.4.5 Restoration using Topological derivatives	29
2.5 Direct methods	30
2.5.1 Singular Value Decomposition	30
2.5.2 Tikhonov Regularization	31
2.6 Total Variation Regularization	31
2.6.1 TV Implementation using Chambolle algorithm	32
2.6.2 TV implementation using First-Order Algorithms	33
2.7 Wavelet Shrinkage	33
2.8 Homomorphic Filtering	33
<b>3. SWARM INTELLIGENCE</b>	<b>35</b>
3.1 Introduction to Optimization	35
3.2 Particle Swarm Optimization (PSO)	36
3.3 Bacterial Foraging Optimization Algorithm (BFO)	40

3.4 Synergy of PSO and BFO Algorithms	44
3.5 Testing Swarm Optimization Algorithms	45
<b>4. SIMULATION RESULTS</b>	<b>50</b>
4.1 Introduction	50
4.2 Restoration using naïve and regularized filter	51
4.3 Restoration using some classical methods	53
4.4 Adaptive spatial filtering for image restoration	53
4.4.1 Adaptive Median Filter	53
4.4.2 Decision-Based Algorithm for Removal of High-Density Impulse Noises	54
4.4.3 Some other new filters for Multiplicative noise reduction	54
4.5 Image Restoration Using Direct methods	54
4.6 Regularized Total Variation	55
4.7 Image restoration using Swarm Intelligence	56
4.7.1 Simulation experiment Using PSO algorithm	57
4.7.2 Simulation experiment Using BFO algorithm	60
4.7.3 Simulation experiment Using hybrid implementation (BFO-PSO)	67
4.7.4 Blind Restoration Using Hybrid Swarm Optimized ARMA-NN Model	69
4.7.4.1. Image Degradation Representation by ARMA Model	69
4.7.4.2. ARMA Neural Network modelling	71
4.7.4.3. Application to Radiological Images	74
4.7.5 Comparison with other methods	80
4.7.6 Application to Neutron Radiography Images Restoration	82
4.7.7 Some examples of image denoising and deblurring using PSO and BFO	86
4.8 Conclusion	87
<b>CONCLUSIONS AND FUTURE WORK</b>	<b>88</b>
<b>REFERENCES</b>	<b>90</b>
<b>APPENDIX: SCIENTIFIC PARTICIPATIONS RELATED TO THESIS</b>	

## 1. LIST OF FIGURES

Figure 2.1: Simplified model for image degradation/restoration process. The image signal  $f(x, y)$  is subjected to a linear degrading function  $H(x, y)$  and an arbitrary noise  $\eta(x, y)$  is added to produce the degraded signal  $g(x, y)$

Figure 2.2: Some Blurring Functions: Disk, Motion, Gaussian and Unsharp

Figure 3.1: Swarm of particles searching for maximum fitness and converging to the global solution

Figure 3.2: Swim and tumble of a bacterium

Figure 3.3: Progress towards the optima for One-variable benchmark function using three optimization methods

Figure 3.4: Improving Classical BFO with a synergy between PSO and BFO to reach the best global optimum

Figure.3.5:: Progress towards the optima for Two-variables benchmark function using three optimization methods

Figure.3.6: Improving Classical BFO with a synergy between PSO and BFO to reach the best global optimum

Figure.3.7: Progress towards the optima for Four-variables benchmark function using three optimization methods

Figure.3.8: Improving Classical BFO with a synergy between PSO and BFO to reach the best global optimum

Figure 4.1: a) original b) motion blurred c) motion blurred with gaussian noise

Figure 4.2: Restoring blurred/noisy images: a) direct inverse filtering b) Zero padding FFT filter and c) regularized filter

Figure 4.3: Restoring blurred/Noisy image: a) Lucy-Ridchardson algorithm b) Blind restoration and c) wiener filtering

Figure 4.4: Restoration of Hardly noised image using randam Impluse Noise : a) Original, b) Degraded, and c) Restored with Adaptive median Filter

- Figure 4.5: Restoration Using Decision Based Algorithm for high density impulse noise
- Figure 4.6: a) Noisy image, b) Filtered image using: Kuan, c) Lee, d) Frost and e) SRAD filters
- Figure 4.7: Restored with a) Tikhonov regularization and b) Truncated Singular Value Decomposition (TSVD), the condition number  $\text{cond}(A)=\sigma_1/\sigma_N$  is found to be  $7.337638 \times 10^4$ , c) Iterative Weighted GCV Method
- Figure 4.8: a) Restoration with ROF method, b) TV Energy evolution with iterations
- Figure 4.9: a) Image Restored using Chambolle Algorithm, b) Regularization parameter estimation and TV energy evolution
- Figure 4.10: Restoration of Blurred and Noisy Images without Regularization Constraint: a) Original, b) Noisy and c),d),e),f) Restored with swarm size and iterations: (10,20), (20,50), (50,100), and (120,200)
- Figure 4.11: Restoration of Blurred and Noisy Images with Regularization Constraint: a) Original, b) Noisy, c),d),e),f) Restored with swarm size and iterations: (10,20), (20,50), (50,100), and (120,200)
- Figure 4.12: Evolution of cost function: a) Without regularization, b) With regularization
- Figure.4.13. a: RMSE Evolution with Swarm Size & Number of Iterations
- Figure.4.13. b: PSNR Evolution with Swarm Size & Number of Iterations
- Figure 4.14: a) Health of each Bacterium in Ascending Order, b) Minimum Cost function for each Bacterium
- Figure 4.15: Restoration of Blurred with Noise Images without Regularization Constraint: a) Original, b) Blurred, c) Restored with  $p=8 \times 8$  d) Restored with  $p=16 \times 16$
- Figure 4.16: Restoration of Blurred with Noise Images with Regularization Constraint: a) Original, b) Blurred, c) Restored with  $p=8 \times 8$  d) Restored with  $p=16 \times 16$
- Figure 4.17: Restoration of Blurred/Noisy images: a) Original, b) Blurred, c) With PSO, d) With BFO, e) With hybrid BFO-PSO
- Figure 4.18: PSNR progress with increasing number of bacteria, chemotactic and reproduction steps
- Figure 4.19: ARMA Model of the degraded image
- Figure.4.20: Schematic diagram of a multi-layer feed-forward NN

Figure.4.21: Information processing in a NN unit

Figure.4.22: Comparison between Different Learning Algorithms using MSE Evolution

Figure.4.23: The resultant Simulated Neural Network on Matlab/Simulink

Figure.4.24: a)Original image, b)Blurred image, c)Restored image with iterative blind deconvolution algorithm, d)Restored with the ARMA-NN model

Figure.4.25: a)Original image, b)blurred image, c)restored image with iterative blind deconvolution algorithm, d)restored with the ARMA-NN model

Figure.4.26: Mean Square Error Comparison Between classical BID and ARMA-NN Model

Figure.4.27: Peak Signal to Noise Ratio Comparison Between classical BID and ARMA-NN Model

Figure.4.28: Normalized Cross-Correlation Comparison Between classical BID and ARMA-NN Model

Figure.4.29: Average Difference Comparison Between classical BID and ARMA-NN Model

Figure.4.30: Structural Content Comparison Between classical BID and ARMA-NN Model

Figure.4.31: Maximum Difference Comparison Between classical BID and ARMA-NN Model

Figure.4.32: Normalized Absolute Error Comparison Between classical BID and ARMA-NN Model

Figure.4.33: Quality comparison between the best four methods (TSVD, Tikhonov regularization, Tikhonov in Sobolev space and TV regularization solved with iterative method) and the Hybrid Algorithms BFO-PSO

Fig.4.34: a) original, b) stained with impulse noise, c) restored with median Filter, d) with soft heuristic SURE thresholding in wavelet decomposition, e) with split Bregman denoise, f) with hybrid BFO-PSO, g) with regularized hybrid BFO-PSO

Figure.4.35: Neutron Imaging System

Figure.4.36: Neutron Radiography Image restoration using PSO: a)Original, b)blurred, c)Blurred/Noisy, d)Restored Image with PSO

Figure.4.37: Neutron Radiography Image Restoration: a)Original, b)Blurred/Noisy, c)Restored image with BFO

Fig.4.38: a) original image, b) with added noise, c) using median filter, d) using hybrid BFO-PSO

Figure.4.39: a)Original image of an electrical relay, b) Hardly motion blurred image, c)TSVD, d)Tikhonov regularization, e)Tikhonov (sobolev), f)TV regularization, g) Restored with PSO, h)Restored with BFO, i) restores with BFO-PSO Synergy

Figure.4.40: a) Original image of computer hard disk, b) Hardly motion blurred image, c) Restored with TSVD, d) Restored with Tikhonov regularization, e) Restored with Tikhonov (sobolev), f) Restored with TV regularization, g)Restored with PSO, h)Restored with BFO, i) restores with BFO-PSO Synergy

Figure.4.41: Gaussian Noise removal using (TV) Swarm Optimization

Figure.4.42: Image deblurring using (TV) Swarm Optimization

## 2. LIST OF TABLES

Table 4.1: Evolution of the (RMSE) and the peak signal to noise ratio (PSNR) with swarm size and number of iterations

Table 4.2: Values of the RMSE and the PSNR for five selected different methods

Table 4.3: Sensitivity analysis for Bacterial Foraging Algorithm with varying parameters: Restoring Blurred Image with Regularization

Table 4.4: Sensitivity analysis for Bacterial Foraging Algorithm with varying parameters: Restoring Blurred/Noisy Image with Regularization

Table 4.5: The ANOVA TABLE for Restoring Blurred Image with Regularization

Table 4.6: The ANOVA TABLE for Restoring Blurred/Noisy Image with Regularization

Table 4.7: Best BFO parameters for restoring blurred images with regularization (Best Regularization parameter is 0.01)

Table 4.8: Best BFO parameters for restoring blurred/Noisy images with regularization (Best Regularization parameter is 0.01)

Table 4.9: RMSE and PSNR values of the three Algorithms reached with the identical computation time and population size

Table 4.10: PSNR progress with increasing number of bacteria, chemotactic and reproduction steps

Table 4.11: Image metrics for the checkerboard image

Table 4.12: Image metrics for the first x-ray image

Table 4.13: Image metrics for the second x-ray image

Table 4.14: Image metrics for the magnetic resonance image

Table 4.15: Image metrics for the brain image

Table 4.16: Image metrics for the blood vessel image

Table 4.17: Quality comparison based on RMSE and PSNR values between the best four methods and the proposed Swarm Intelligence Algorithms

Table 4.18: Regularized Neutron Radiography Image Restoration with Hybrid BFO-PSO of mixing light water (H<sub>2</sub>O) and heavy water (D<sub>2</sub>O)



## CHAPTER 1

### GENERAL INTRODUCTION

By image restoration, we seek to recover the original sharp image by using a mathematical model of the blurring process. The key issue is that some information on the lost details is indeed present in the blurred image, but this information is “hidden” and can only be recovered if we know the details of the blurring process. Due to various unavoidable errors in the recorded image, we can recover the original image exactly. The most important errors are fluctuations in the recording process and approximation errors when representing the image with a limited number of digits [1].

The image restoration techniques are widely used in various applications such as medical imaging (Rathee et al., 1992, satellite imaging (Jalobeanu et al., 2000; Bretschneider, 2002; Bratsolis and Sigelle, 2003); Lee et al., 2004), astronomical imaging (Molina, 1994; Molina et al., 2001), forensic science (Wen and Lee, 2002) and many other poor-quality imaging. In this work, we especially focus on the problem of image restoration in neutron radiography.

We can broadly classify restoration techniques into two classes: the filtering reconstruction techniques and the algebraic techniques. The filtering techniques are rather classical and they make use of the fact that noise signals usually have higher frequencies than image signals. This means that image signals die out faster than noise signals in high frequencies. By selecting the proper filter, one can get a good estimate of the original image signal, by reducing the effect of noise. Examples of the restoration filters are the deconvolution filter, in which the transfer function of the degraded system is inverted to produce a restored image, and the Wiener filter that the mean-squared error (MSE) criterion to minimize the error signal between the original and degraded image signals. The Wiener filter acts as a band-pass filter. At low spatial frequencies, it acts as an inverse filter, whereas at higher frequencies, it acts as a smooth rolloff low-pass filter. This filter is not very suitable for use in cases in which images are investigated by the human eye. The MSE technique treats all errors equally, regardless of their spatial location in the

image. The human eye, on the other hand, has high degree of tolerance to errors in darker areas on the image than elsewhere. Another limitation in this filter is that it cannot handle dynamically changing image and noise signals. (A. Khireddine et al.,2007) used this filter in 2D case for digital image restoration [2]. The Lucy-Richardson algorithm can be used effectively when the point-spread function PSF (blurring operator) is known, but little or no information is available for the noise. The blurred and noisy image is restored by the iterative, accelerated, damped Lucy-Richardson algorithm. The Blind deconvolution algorithm maximizes the likelihood that the resulting image, when convolved with the resulting PSF, is an instance of the blurred image, assuming Poisson noise statistics. This Algorithm can be used effectively when no information about the distortion (blurring and noise) is known. The algorithm restores the image and the point-spread function (PSF) simultaneously. The accelerated, damped Richardson-Lucy algorithm is used in each iteration. The linear Algebraic techniques utilize matrix algebra and discrete mathematics for solving the problem of image restoration. Some of the algebraic restoration techniques are: the unconstrained reconstruction technique and the constrained reconstruction technique. Regularized deconvolution can be used effectively when constraints are applied on the recovered image (e.g., smoothness) and limited information is known about the additive noise. The blurred and noisy image is restored by a constrained least square restoration algorithm that uses a regularized filter.

Optimization methods can be used to solve a large-scale constrained linear least-squares optimization problem to recover blurred images, and many works have been done using, for example, simulated annealing. In [3] (Lamotte et al., 1994) did a comparative study of four "essian" tion algorithms based on simulated annealing: the Gibbs Sampler, the Metropolis algorithm, the Iterated Conditional Modes, and an original method of random descent. In (Z. Réiti,1995) in [4] made use of some formulas from the theory of basic hypergeometric series to to deblur images blurred by a modified Gaussian blur. Another solution for this type of image blur has been proposed by (Hummel et al.,1987) in [5]. They gave constructive formulas for the deblurring kernels in terms of Hermite polynomials, and observe that their use yields optimal approximate deblurring solutions among the space of bounded degree polynomials. A simple and fast deblurring algorithm for Gaussian has recently presented by (Firsov et al., 2006) [6] in which they

solved the ill-posed problem of backward heat equation by truncation of a Neumann's expansion of the backward heat operator followed by a forward heat operator to stabilize the procedure. (J.Kamm et al.,1998) in [7] proposed an approximate Singular value decomposition (SVD) as a direct method, the computed restorations are comparable to iterative methods but are computationally less expensive and may be used with the generalized Cross Validation method to choose regularization parameters. (Chen et al.,1999) in [8] modeled the restoration problem as an optimization problem and used the genetic algorithm for gray images restoration. (Barcelos et al.,2000) in [9] new anisotropic diffusion model is proposed for image restoration and segmentation, which is closely related to the minimization problems for the unconstrained total variation. Because filters include adjustable parameters such as the regularization parameter or threshold, (Sugiyama et al.,2002) in [10] optimized the filter type and parameters based on subspace information criterion (SIC), which is an unbiased estimator of the expected squared error between the restored and original images. The same approach has been used by (Lin et al., 2004) in [11] by proposing a novel adaptive median-based filter, called the partition fuzzy median (PFM) filter to preserve image details while effectively suppressing impulsive noises, through a summation of the weighted output of the median filter and the related weighted input signal and The weights are set in accordance with the fuzzy rules. Stack filters that are non-linear spatial operators used for noise suppression have been formulated by (Undrill et al.,1997) as an optimization problem solved by genetic algorithm for restoring magnetic resonance images corrupted with uncorrelated additive noise [12]. (Chan et al.,2005) in [13] proposed a regularized constrained iterative algorithm for restoring color-quantized images that makes good use of the available color palette to derive useful a priori information for restoration. In [14] they introduced a new algorithm based on simulated annealing to solve the problem of image color quantization with halftoning. In [15] (Chao et al.,2006) proposed a modified anisotropic diffusion scheme to tackle the problem of image restoration in astronomy, that incorporates both gradient and gray-level variance information. (Belaid et al.,2008) in [16] used the topological gradient method for modeling and solving image restoration problems considered in the frame of variational diffusive approaches for the minimization of potential energy with respect to conductivity. Statistical models introduced by (Rajesh et al., 2007) for

satellite images restoration in [17]. They proposed a non-causal eight neighbourhood image restoration model based on autocorrelation and triple correlation function of the noise corrupted satellite image. General variational model for image restoration based on the minimization of a convex functional of gradient under minimal growth conditions has been discussed in the paper of (Barbu et al., 2007). The nonlinear diffusion techniques and PDE-based variational models are used for image restoration [18].

A new method for the restoration of images degraded by noise and spatially invariant blur has been proposed by (G. Landi, 2007), in which image restoration problem is replaced by an equality constrained minimization problem. A quasi-Newton method is applied to the first-order optimality conditions. In each quasi-Newton iteration, the hessian of the Lagrangian is approximated by a circulant matrix and the Fast Fourier Transform is used to compute the quasi-Newton step. The quasi-Newton iteration is terminated according to the discrepancy principle [19]. A novel method called edge-preserving regularization is presented in the paper of (Xiaojuan Gu et al., 2008). This method is used to solve an optimization problem whose objective function has a data fidelity term and a regularization term, the two terms are balanced by a parameter  $\lambda$  [20]. Most of the optimal techniques that have been proposed in literature over the past few decades to solve such problem by iterative optimization procedures are computationally demanding and time consuming.

Total variation (TV) is a regularization approach that performs edge preserving image restoration, but at a high computational cost. TV regularization requires linearization of a highly nonlinear penalty term, which increases the restoration time considerably for large scale images. In TV method, we will consider an iterative regularization approach in the spatial domain, which was first addressed in optimization as the Barzilai-Borwein minimization (BB) method [21]. Iterative techniques have a common problem: the error starts increasing after it reaches a minimum. The first few iterations restore the low frequency components of the signal and, as the number of iterations increases, the algorithm attempts to restore the high frequency components, which are dominated by noise. Solution to such problem can be attained by adding a median filter to maintain a low error by preserving the edge information while reducing the high frequency error [22].

The novel approach introduced in this thesis is to take advantage of swarm intelligence in order to facilitate optimization process in total variation regularized methods. An ARMA (autoregressive moving average) model used for the non linearly degraded image deconvolution, is identified using a neural network which is fast trained by a hybrid implementation of the two swarm algorithms: PSO and BFO. Both estimated image and blur function are identified through this representation. Some applications on radiological images are presented in simulation results. This optimized model will be implemented on reconfigurable hardware.

Chapter two introduces the theoretical aspects of image restoration problem with the classical methods used previously, and highlights other new strong methods that proved their potential in image deblurring, such as non linear filters, direct iterative methods: Tikonove regularization and Truncated SVD, and Rudin-Osher-Fatemi Total variation approaches.

In chapter three, we surf through new swarm intelligence methods as proposed by their inventors with applications to some benchmark functions, in addition to synergy of two powerful algorithms to boost up optimization towards better solutions.

Chapter four is devoted for computer simulation of on hand methods, and then we present the state of art results for solving such ill-posed inverse problem through total variation minimization approach and introduce swarm intelligence approach using Particle Swarm Optimization (PSO), Bacterial Foraging Optimization (BFO) and synergy of both algorithms. A computational comparison based on image quality reached is made between these approaches and other recent approaches.

We conclude this work by highlighting results obtained using these techniques especially for their real time implementation on adaptively reconfigurable systems, with suggestions of future works.

Going through references, we can notice the new enormous works made to solve such ill-posed problem by means of various methods.

## CHAPTER 2

### IMAGE RESTORATION: AN OVERVIEW

#### 2.1 Introduction

When we use a camera, we want the recorded image to be a faithful representation of the scene that we see, but every image is more or less blurry. Thus, image deblurring is fundamental in making pictures sharp and useful. A digital image is composed of picture elements called pixels. Each pixel is assigned an intensity, meant to characterize the color of a small rectangular segment of the scene. A small image typically has around  $256 \times 256 = 65536$  pixels while a high-resolution image often has 5 to 10 million pixels. Some blurring always arises in the recording of a digital image, because it is unavoidable that scene information "spills over" to neighboring pixels. For example, the optical system in a camera lens may be out of focus, so that the incoming light is smeared out. The same problem arises, for example, in astronomical imaging where the incoming light in the telescope has been slightly bent by turbulence in the atmosphere. In neutron radiography, neutron flux behavior used for imaging encounters random radiations especially gamma perturbation. In these and similar situations, the inevitable result is that we record a blurred image.

In image deblurring, we seek to recover the original, sharp image by using a mathematical model of the blurring process. The key issue is that some information on the lost details is indeed present in the blurred image, but this information is "hidden" and can only be recovered if we know the details of the blurring process. Unfortunately there is no hope that we can recover the original image exactly! This is due to various unavoidable errors in the recorded image. The most important errors are fluctuations in the recording process and approximation errors when representing the image with a limited number of digits.

## 2.2 Image Degradation

The degradation process is modeled as a degradation function  $H(x,y)$  that, together with an additive noise term  $\eta(x,y)$ , operates on an input image  $f(x,y)$  to produce a degraded image  $g(x,y)$ , Fig.1:

$$g(x, y) = H(x, y) f(x, y) + \eta(x, y) \quad 1.1$$

Where,  $H$  represents a convolution matrix that models the blurring that many imaging systems introduce. For example, camera defocus, motion blur, imperfections of the lenses, all can be modeled by  $H$ . The vectors  $g$ ,  $f$ , and  $\eta$  represent the observed, the original and the noise images. More specifically,  $\eta$  is a random vector that models the random errors in the observed data. These errors can be due to the electronics used (thermal and shot noise) the recording medium (film grain) or the imaging process (photon noise).

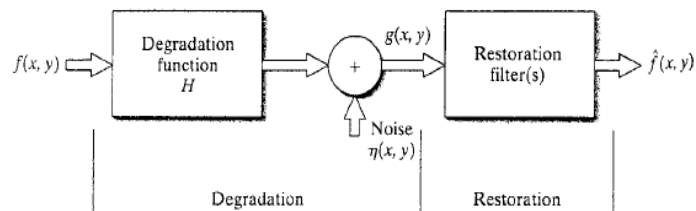


Figure.2.1: Simplified model for image degradation/restoration process. The image signal  $f(x, y)$  is subjected to a linear degrading function  $H(x, y)$  and an arbitrary noise  $\eta(x, y)$  is added to produce the degraded signal  $g(x, y)$

Given  $g(x,y)$ , some knowledge about the degradation function  $H(x,y)$ , and some knowledge about the additive noise  $\eta(x,y)$ , the objective of restoration is to obtain an estimate of the original image  $f(x, y)$ . We want the estimate to be close as possible to the original input image. In general, the more we know about noise, the closer the estimate will be to  $f(x, y)$ .

### 2.2.1 Blurring

Blurring in images can arise from many sources. The blurring matrix  $H$  is determined from two ingredients: the point spread function PSF, which defines how each pixel is blurred, and the boundary conditions, which specify our assumptions on the scene just outside our image [1]. In some cases the PSF can be described analytically, and thus it can be constructed from a function, Fig.1.2, rather than through experimentation.

1. *Motion blurs* : which occurs when there is a relative motion between the object and the camera during exposure and can be modeled using the following 1D degradation function:

$$h(x) = \begin{cases} \frac{1}{L}, & \text{if } -\frac{L}{2} \leq x \leq \frac{L}{2} \\ 0, & \text{otherwise} \end{cases} \quad 2.2$$

L is the length of degradation vector

2. *Atmospheric turbulence blur*: is due to long term exposure through the atmosphere and can be modeled by the below Gaussian function:

$$h(x, y) = Ke^{-\left[\frac{x^2 + y^2}{2\sigma^2}\right]} \quad 2.3$$

Where  $K$  is a normalizing constant and  $\sigma^2$  is the variance that determines the severity of the blur.

3. *Uniform out-of-focus blur*. is described by 2D degradation function below:

$$h(x, y) = \begin{cases} \frac{1}{\pi R^2}, & \text{if } \sqrt{x^2 + y^2} \leq R \\ 0, & \text{otherwise} \end{cases} \quad 2.4$$

Boundary conditions specify our assumptions on the behavior of the image outside its boundaries.

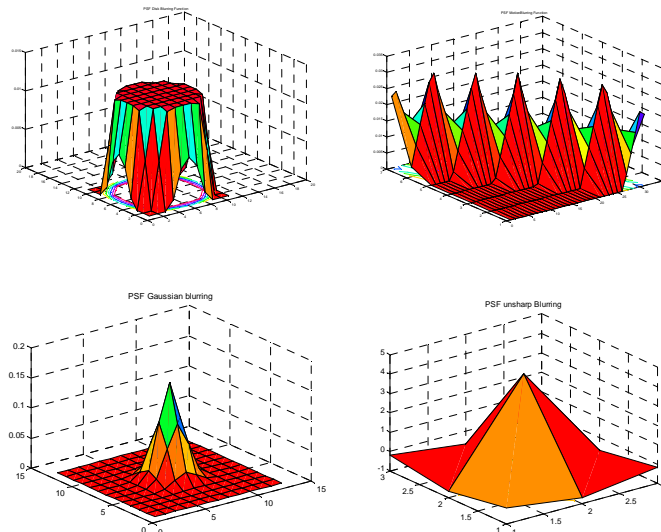


Figure.2.2 : Some Blurring Functions: Disk, Motion, Gaussian and Unsharp

### 2.2.2 Noise

In addition to blurring, observed images are usually contaminated with noise. Noise can arise from several sources and can be linear, nonlinear, multiplicative,



and additive. In our application we consider a common additive noise model that comes essentially from the following three sources:

- \* Photoelectric noise of background photons, from both natural and artificial sources. This kind of noise is typically modeled by a Poisson process.
- \* Noise from electronics used to capture images, modeled usually by a white Gaussian noise, with zero mean and a fixed standard deviation proportional to the amplitude of the noise with probability density function :
- \* Film grain noise, from the randomness of silver halid grains in the film used for recording, modeled by impluse random noise.
- \* Quantization noise which occurs during image digitization.

### 2.3 Restoration Using a General Linear Model

We model the blurring of images as a linear process characterized by a blurring matrix  $H$  of dimensions  $N \times N$ , with  $N = m \times n$  and an observed image  $g$  which, in vector form, are related by the equation:

$$Hf = g \quad 2.5$$

The reason  $H^{-1}g$  can not be used to deblur images is the amplification of high-frequency components of the noise in the data, caused by the inversion of very small singular values of  $H$ . Practical methods for image deblurring need to avoid this pitfall [1]. Obtaining  $f$  from Equation (5) is not a straight forward task since, in most cases of interest, the matrix  $H$  is ill-posed. Mathematically this means that certain eigenvalues of this matrix are close to zero, which makes the inversion process very unstable. For practical purposes, this implies that the inverse or the pseudo-inverse solutions:

$$f_1 = H^{-1}g \text{ and } f_2 = (H^T H)^{-1} H^T g \quad 2.6$$

Amplify the noise and provide incorrect results. This means that image signals die out faster than noise signals in high frequencies.

In frequency domain, we use the two dimensions FFT to form an estimate of the form:

$$\hat{F}(u, v) = \frac{G(u, v)}{H(u, v)} \quad 2.7$$

And then obtain the corresponding estimate of the image by taking the inverse Fourier transform of  $\hat{F}(u, v)$  ( $\hat{G}(u, v)$  is the Fourier transform of the

degraded image). This approach is appropriately called *inverse filtering*. From the model (1), we can express our estimate as:

$$\hat{F}(u, v) = F(u, v) + \frac{N(u, v)}{H(u, v)} \quad 2.8$$

This deceptively simple expression tells us that, if we knew  $\hat{H}(u, v)$  exactly, we could not recover  $F(u, v)$  and hence the original image  $f(x, y)$  because the noise component is a random function whose Fourier transform,  $N(u, v)$ , is not known. The typical approach when attempting inverse filtering is to form the ratio  $\hat{F}(u, v) = \frac{G(u, v)}{H(u, v)}$  and then limit the frequency range for obtaining the inverse, to frequencies “near” the origin. The idea is that zeros in  $H(u, v)$  are less likely to occur near the origin because the magnitude of the transform typically is at its highest value in that region. This type of approach some times is called pseudo inverse filtering and is seldom practical.

### 2.3.1 Wiener filter Restoration

Wiener filtering (after N.Wiener, who first proposed the method in 1942 [23]) is one of the earliest and best known approaches to linear image restoration. A Wiener filter seeks an estimate  $\hat{f}$  that minimizes the statistical error function:

$$e^2 = E \left\{ \left( f - \hat{f} \right)^2 \right\} \quad 2.9$$

Where  $E$  is the expected value operator and  $f$  is the undegraded image. The solution to this expression in the frequency domain is:

$$\hat{F}(u, v) = \left[ \frac{1}{H(u, v)} \frac{|H(u, v)|^2}{|H(u, v)|^2 + S_\eta(u, v) / S_f(u, v)} \right] G(u, v) \quad 2.10$$

Where:

$H(u, v)$  = the degradation function

$$|H(u, v)|^2 = H^*(u, v) H(u, v)$$

$H^*(u, v)$  = the complex conjugate of  $H(u, v)$

$S_\eta(u, v) = |N(u, v)|^2$  = the power spectrum of the noise

$S_f(u, v) = |F(u, v)|^2$  = the power spectrum of the undegraded image

The ratio  $S_\eta(u, v) / S_f(u, v)$  is called the noise-to-signal power ratio. We see that if the noise power spectrum is zero and the Wiener filter reduces to the inverse filter discussed in the previous section. Replacing this ratio by a constant array in the preceding filter equation results in the so-called parametric Wiener filter which yields significant improvements over direct inverse filtering.

### 2.3.2 Restoration using regularized filter

Another well-established approach to linear restoration is *constrained least squares filtering*, called regularized filtering in image processing documentation [27]. The definition of 2-D discrete convolution is:

$$h(x, y) * f(x, y) = \frac{1}{MN} \sum_{m=0}^{M-1} \sum_{n=0}^{N-1} f(m, n) h(x - m, y - n) \quad 2.11$$

Using this equation, we can express the linear degradation model (1),  $g(x, y) = H(x, y) f(x, y) + \eta(x, y)$ , in vector-matrix form, as:  $g = H f + \eta$ , suppose that  $g(x, y)$  is of size  $M \times N$ , then we can form the first  $N$  elements of the vector  $g$  by using the image elements in the first row of  $g(x, y)$ , the next  $N$  elements from the second row, and so on. The resulting vector will have dimensions  $MN \times 1$ . These also are the dimensions of  $f$  and  $\eta$ , as these vectors are formed in the same manner. The matrix  $H$  then has dimensions  $MN \times MN$ . Its elements are given by the elements of the preceding convolution equation.

It would be reasonable to arrive at the conclusion that the restoration problem can now be reduced to simple matrix manipulations. Unfortunately, this is not the case. For instance, suppose that we are working with images of medium size; say  $M=N=512$ . Then the vectors in the preceding matrix equation would be of dimension  $262144 \times 1$ , and matrix  $H$  would be of dimensions  $262144 \times 262144 \times 1$ . Manipulating vectors and matrices of these sizes is not a trivial task. The problem is complicated further by the fact that the inverse of  $H$  does not always exist due to zeros in the transfer function. However, formulating the restoration problem in matrix form does facilitate derivation of restoration techniques. We base optimality of restoration on a measure of smoothness, such as the second derivative of an image (e.g. the Laplacian). To be meaningful, the restoration must be constrained by the parameters of the problem at hand. Thus, what is desired is to find the minimum of a criterion function,  $C$ , defined as:

$$C = \sum_{x=0}^{M-1} \sum_{y=0}^{N-1} [\nabla^2 f(x, y)]^2 \quad 2.12$$

Subject to the constraint:

$$\|g - H \hat{f}\|^2 = \|\eta\|^2 \quad 2.13$$

Where  $\|w\|^2 \triangleq w^T w$  is the Euclidean vector norm,  $\hat{f}$  is the estimate of the undegraded image, and  $\nabla^2$  is the Laplacian. The frequency domain solution to this optimization problem is given by the expression:

$$\hat{F}(u, v) = \left[ \frac{H^*(u, v)}{|H(u, v)|^2 + \gamma |P(u, v)|^2} \right] G(u, v) \quad 2.14$$

Where  $\gamma$  is a parameter that must be adjusted so that the constraint is satisfied (if  $\gamma$  is zero we have an inverse filter solution), and  $P(u, v)$  is the Fourier transform of the function:

$$P(x, y) = \begin{bmatrix} 0 & 1 & 0 \\ 1 & -4 & 1 \\ 0 & 1 & 0 \end{bmatrix}$$

We recognize this function as the Laplacian operator. The only unknowns in the preceding formulation are  $\gamma$  and  $\|\eta\|^2$ . However, it can be shown that  $\gamma$  can be found iteratively if  $\|\eta\|^2$ , which is proportional to the noise power (a scalar), is known.

#### 2.4. Nonlinear image restoration

Nonlinear filters are often designed to remedy deficiencies of linear filtering approaches. Nonlinear filters cannot be implemented by convolution and do not provide a predictable modification of image frequencies. However, for this very reason, powerful nonlinear filters can provide performance attributes not attainable by linear filters, since frequency separation (between image and noise) is often not possible. Nonlinear filters are usually defined by local operations on windows of pixels. So, the nonlinear filtering operation may be expressed as a function of the image a defined moving window. The size of the window determines the scale of the filtering operation [23]. Larger windows will tend to produce more coarse scale representations, eliminating fine detail.

### 2.4.1 Order Statistic Filters

Within the class of nonlinear filters, order statistic (OS) filters encompass a large group of effective image enhancers. The OS filters are based on an arithmetic ordering (from smallest to largest) of the pixels in each window (local neighborhood). The most popular nonlinear filter is the median filter. It is an OS filter. The median filter smoothes additive white noise while maintaining edge information - a property that differentiates it from all linear filters. Particularly effective at eliminating impulse noise, it has strong optimality properties when the noise is Laplacian-distributed.

### 2.4.2 Adaptive Median Filter

When the only degradation present is noise, the method of choice for reduction of noise in this case is spatial filtering. These filters can adapt their behavior depending on the characteristics of the image in the area being filtered. Therefore, the adaptive median filtering has been applied widely as an advanced method compared with standard median filtering. It performs spatial processing to determine which pixels in an image have been affected by impulse noise, and classifies pixels as noise by comparing each pixel in the image to its surrounding neighbor pixels. The size of the neighborhood is adjustable, as well as the threshold for the comparison. A pixel that is different from a majority of its neighbors, as well as being not structurally aligned with those pixels to which it is similar, is labeled as impulse noise. These noise pixels are then replaced by the median pixel value of the pixels in the neighborhood that have passed the noise labeling test. Some advantages of this filter are:

- a. The standard median filter does not perform well when impulse noise is greater than 0.2, while the adaptive median filter can better handle these noises.
- b. The adaptive median filter preserves detail and smooth non-impulsive noise.

#### Adaptive Median Filter Algorithm:

$S_{xy}$  denotes a subimage (window) centered at location  $(x,y)$  in the image being processed. The algorithm is as follows:

Let:

$Z_{min}$  = minimum gray level value in  $S_{xy}$

$Z_{max}$  = maximum gray level value in  $S_{xy}$

$Z_{med}$  = median gray level values in  $S_{xy}$

$Z_{xy}$  = gray level value at coordinates  $S_{xy}$

The adaptive median filtering algorithm works in two levels, denoted level A and level B:

Level A: if  $Z_{min} < Z_{med} < Z_{max}$ , go to level B  
 Else increase the window size  
 If window size  $\leq S_{max}$ , repeat level A  
 Else output  $Z_{med}$   
 Level B: if  $Z_{min} < Z_{xy} < Z_{max}$ , output  $Z_{xy}$   
 Else output  $Z_{med}$

Where  $S_{max}$  denotes the maximum allowed size of the adaptive filter window. Another option in the last step in Level A is to output  $Z_{xy}$  instead of the median. This produces a slightly less blurred result but can fail to detect salt & pepper noise.

### 2.4.3 Restoration using Lucy-Ridchardson Algorithm

The simplicity of implementation, coupled with modest computational requirements and a well-established theoretical base, have made linear techniques a fundamental tool in image restoration for many years. During the last decades, nonlinear iterative techniques have been gaining acceptance tools that often yield results superior to those obtained with linear methods. The principal objections to nonlinear methods are that their behavior is not always predictable and that they generally require significant computational resources. This nonlinear technique developed by Richardson (1972) and by Lucy (1974), working independently and called L-R algorithm. The L-R algorithm arises from a maximum-likelihood formulation in which the image is modeled with Poisson statistics Maximizing the likelihood function of the model yields an equation that is satisfied when the following iteration converges:

$$\hat{f}_{k+1}(x, y) = \hat{f}_k(x, y) \left[ h(-x, -y) * \frac{g(x, y)}{h(x, y) * \hat{f}_k(x, y)} \right] \quad 2.15$$

As before, “\*” indicates convolution,  $\hat{f}$  is the estimate of the undegraded image, and both  $g$  and  $h$  are as defined before. The iterative nature of the algorithm is evident. Its nonlinear nature arises from the division by  $\hat{f}$  on the right side of this equation. As with most nonlinear methods, the question of when to stop the L-R algorithm is difficult to answer in general. The approach often

followed is to observe the output and stop the algorithm when a result acceptable is a given application has been obtained.

#### 2.4.4 Blind Restoration

One of the most difficult problems in image restoration is obtaining a suitable estimate of the PSF to use in restoration algorithms such as those discussed previously [28]. Image restoration methods that are not based on specific knowledge of the PSF are called *blind deconvolution algorithms*.

Blind Deconvolution Algorithms can be used effectively when no information about the distortion (blurring and noise) is known. These algorithms restore the image and the point-spread function (PSF) simultaneously. The accelerated, damped Richardson-Lucy algorithm is used in each iteration. Additional optical system (e.g. camera) characteristics can be used as input parameters that could help to improve the quality of the image restoration. PSF constraints can be passed in through a user-specified function.

#### 2.4.5 Restoration using Topological derivatives

The main idea behind this algorithm is to compute the topological derivative for an appropriate functional (the energy norm and the gradient norm in the case of continuum) and a perturbation given by the introduction of cracks between pixels (straight crack in the domain in the case of discret). This derivative is used as an indicator function to find the best pixels (places) to introduce the cracks that, in the presence of diffusion, will most remove noise preserving relevant image characteristics [25].

##### Topological derivative Algorithm:

Require: a 2-D image  $f$  and the parameter  $\alpha$

Ensure: the enhanced image  $\hat{f}$  has same dimensions as  $f$

Set  $k_j^s = 1, j = 1..4, s = 1..N * M$

For every pixel  $\omega^s$  do

For every neighborhood case  $k^\sigma \in C$  do

Compute  $D_T^\sigma(\omega^s)$

End for

If  $\min\{D_T^\sigma(\omega^s), \sigma = 1, \dots, N_c\} < \alpha$  then

$K^T = k^\sigma$

End if

End for

While  $\Psi^\sigma > \epsilon$  do

Apply diffusion equation over the image  $f$  and calculate  $k$ .

End while

## 2.5 Direct methods

### 2.5.1 Singular Value Decomposition

Singular value decomposition (SVD) is one of the most successful tools in the theory of inverse problems. It can be used to understand the ill-posed inverse problem and for describing the effect of the regularization method. It has been widely applied in image processing. In numerical analysis, the SVD provides a measure of the effective rank of a given matrix. In statistics and time series analysis, the SVD is particularly a useful tool for finding least-squares solutions and approximations.

Singular value decomposition has been successfully applied to many image restoration problems. Usual applications include linear space invariant and linear space variant pseudoinverse filtering, image enhancement, separation of 2-D filtering operations into 1-D filtering operations, generation of small convolution kernels, etc... Among all unitary transformations, SVD is optimal for a given image in the sense that the energy packed in a given number of transformation coefficients is maximized. Although applicable in many image restoration applications, SVD is severely limited because of a large number of computations required for calculating singular values and singular vectors of large image matrices [26].

The SVD of an  $m \times n$  matrix  $A$  is given by:

$$A = U \Sigma V^T \quad 2.16$$

Where  $U = (u_1, u_2, \dots, u_n) \in R^{m \times m}$  and  $V = (v_1, v_2, \dots, v_n) \in R^{n \times n}$  are two column-orthogonal matrices.  $\Sigma$  is a diagonal matrix with entries  $\sigma_1 \geq \sigma_2 \geq \dots \geq \sigma_N \geq 0$ . For a blurring matrix, all the singular values decay gradually to zero and the condition number  $\text{cond}(A) = \sigma_1/\sigma_N$  is very large. One approach to damp the effects caused by division of small singular values is to simply discard all SVD components that are dominated by noise, typically the ones above a certain truncation parameter  $k$ . The resulting method is, for obvious reasons, referred to as the truncated SVD, or TSVD method [26].

In the TSVD method, we define the filter factors to be one for large singular values, and zero for the rest. The number of large singular values is  $k$  that determines the number of SVD components maintained in the regularized solution.



### 2.5.2 Tikhonov Regularization

The main objective of regularization is to incorporate more information about the desired solution in order to stabilize the problem and find a useful and stable solution. The most common and well-known form of regularization is that of Tikhonov [27]. In the Tikhonov method, we define the filter factors to be:

$$\phi_i = \frac{\sigma_i^2}{\sigma_i^2 + \alpha^2} \quad i=1, \dots, N, \quad 2.17$$

Where  $\alpha > 0$  is called the regularization parameter. This choice of filter factors yields the solution vector  $x_\alpha$  for the minimization problem :

$$\min_x \left\{ \|g - Hf\|_2^2 + \alpha^2 \|f\|_2^2 \right\} \quad 2.18$$

We want  $\|g - Hf\|_2$  to be small, but if we make it zero by choosing  $f = H^{-1}g$ , then the Laplacian of the solution will be very large when the magnitude of noise exceeds the magnitude of singular values  $\sigma_i$ .

Thus, we also want to keep  $\|f\|_2$  reasonably small, our minimization ensures that both  $\|g - Hf\|_2$  and  $\|f\|_2$  are small by choosing the appropriate TSVD truncation parameter  $k$  or the appropriate Tikhonov regularization parameter  $\alpha$ . Regularization by means of spectral filtering requires finding a suitable balance between the regularization error and the perturbation error by choosing the filter factors appropriately.

For a low pass filter, the filter parameters for low frequency components are close to one, while filter parameters for high frequency components are close to zero. The TSVD and Tikhonov methods are analogous to this. As a consequence, the noise affects the high frequency components which are associated with the smaller singular values. Results are illustrated in chapter three.

### 2.6 Total Variation Regularization

Total variation (TV) is often used for image filtering and restoration. Total variation based filtering was introduced by Rudin, Osher, and Fatemi [28]. TV denoising is an effective filtering method for recovering piecewise-constant signals. Many algorithms have been proposed to implement total variation filtering. The most famous one is by Chambolle [29]. The derivation in this algorithm is based on the min-max property and the majorization-minimization procedure. Rudin, Osher and Fatemi introduced in 1992 the following idea:

Instead of minimizing: 
$$\|Hf - g\|_2^2 + \lambda \|Lf\|_2^2 \quad 2.19$$

Let us minimize: 
$$\|Hf - g\|_2^2 + \lambda \|Lf\|_1 \quad 2.20$$

Recall that: 
$$\|Z\|_2^2 = |Z_1|^2 + \dots + |Z_N|^2 \quad 2.21$$

And: 
$$\|Z\|_1 = |Z_1| + \dots + |Z_N| \quad 2.22$$

The idea is that (1.20) should allow occasional larger jumps in the reconstruction leading to piecewise smoothness instead of overall smoothness. It turns out that minimizing (8) is really a powerful method, but numerical minimization is more difficult.

Since their introduction in a classic paper by Rudin, Osher and Fatemi [28], total variation minimizing models have become one of the most popular and successful methodology for image restoration. Variational models have been extremely successful in a wide variety of restoration problems, and remain one of the most active areas of research in mathematical image processing and computer vision. The minimization technique of choice for such models routinely involves the solution of nonlinear partial differential equations (PDEs) derived as necessary optimality conditions. Perhaps the most basic (fundamental) image restoration problem is denoising. It forms a significant preliminary step in many machine vision tasks, such as object detection and recognition. It is also one of the mathematically most interesting problems in vision. A major concern in designing image denoising models is to preserve important image features, such as those most easily detected by the human visual system, while removing noise. All successful denoising models take advantage of the fact that there is an inherent regularity found in natural images; this is how they attempt to tell apart noise and actual image information. Variational and PDE based models make it particularly easy to impose geometric regularity on the solutions obtained as denoised images, such as smoothness of boundaries. This is one of the main reasons behind their success.

### 2.6.1 TV Implementation using Chambolle algorithm

Antonin Chambolle describes in [29] an iterative algorithm for the resolution of the TV regularized restoration problem (the so called "Rudin-Osher-Fatemi" method). This algorithm exploits a dual formulation of the minimization problem, and uses a fixed point iteration to find a solution of the dual formulation. Chambolle proves that these iterations are contractant, and thus converge to a

solution with linear speed. Chambolle also exposes some important extensions of this algorithm such as the regularization parameter  $\lambda$  that can be updated during the iterations in order to solve the  $L_1$  constrained problem (instead of Lagrangian regularization). This is very useful if one knows the level of noise that perturbs the measurements.

### 2.6.2 TV implementation using First-Order Algorithms

The first-order numerical schemes for image restoration rely on a duality-based algorithm proposed in 1979 by Bermúdez and Moreno [30]. This is an old and forgotten algorithm that is revealed wider than recent schemes (such as the Chambolle projection algorithm) and able to improve contemporary schemes.

### 2.7 Wavelet Shrinkage

Recently, *wavelet shrinkage* has been recognized as a powerful tool for signal estimation and noise reduction or simply *de-noising* [31]. The wavelet transform utilizes scaled and translated versions of a fixed function, which is called a “wavelet,” and is localized in both the spatial and frequency domains. Such a joint spatial-frequency representation can be naturally adapted to both the global and local features in images. The wavelet shrinkage estimate is computed via thresholding wavelet transform coefficients.

The key idea of wavelet shrinkage derives from the approximation property of wavelet bases. The wavelet transform compresses the image into a small number of coefficients of large magnitude, and it packs most of the image energy into these coefficients. On the other hand, the coefficients of the noise have small magnitudes; that is, the noise energy is spread over a large number of coefficients. Therefore, among the coefficients of the degraded image  $g$ , those having large magnitudes correspond to the original image  $f$  and those having small magnitudes correspond to the noise  $\eta$ . Apparently, thresholding coefficients with an appropriate threshold removes a large amount of noise and maintains most image energy.

### 2.8 Homomorphic Filtering

To this point, we have described methods that only deal with additive noise. In several imaging scenarios, such as radar and laser-based imaging, signal-dependent noise is encountered. The signal-dependent noise can be modeled as a multiplicative process.

Applying the traditional low-pass filters or nonlinear filters is fruitless, since the noise is signal dependent. But we can decouple the noise from the signal using a homomorphic approach [32]. The first step of the homomorphic approach is the application of a logarithmic point operation on the degraded image to transform it to an addition, image with noise. Then we can apply one of the filters discussed above and then transform the image back to its original range with an exponential point operation.

## CHAPTER 3

### SWARM INTELLIGENCE

#### 3.1 Introduction to Optimization:

The task of optimization is seeking to achieve the best result possible for a given system. However, dependent upon the context or environment, the optimal result could be represented by either a maximum or a minimum result. In most contexts, optimization to find a maximum output is often referred to as maximizing a system's fitness, whereas optimization to find a minimum output is often referred to as minimizing a system's cost. Thus, fitness is the negative of cost (Haupt et al.,2004) in [33].

A common challenge is finding the global minima/maxima with any number of local minima/maxima. This is more easily visualized using the concept of a cost surface for which there may exist any number of smaller peaks and troughs.

Multiple variable systems are more complex than single variable systems and are more difficult to model and solve mathematically. The number of variables can be used to express the number of dimensions within the system. Dynamic systems are systems for which the output is a function of time and static systems are time invariant (Haupt et al.,2004) in [33].

System variables can be classified as either discrete or continuous. Continuous variables can take an infinite number of values; whereas discrete variables can only be assigned a finite number of possible values. A common approach to optimizing continuous systems is to first discretise the system and then attempt to optimize using digital processes. Constrained systems are systems for which variables can only take values within set limits. Variables in unconstrained systems have no such limits applied. Mathematical optimization works best on unconstrained systems.

Minimum seeking optimization methods use a single set of inputs in order to, normally, numerically find the optimal outputs. Such methods are challenged by the problem of local minima/maxima. Unlike minimum seeking optimization methods, random methods use probabilistic calculations to find the variable sets

on which to perform optimization, thus finding local minima/maxima is not as problematic. This is why minimum seeking methods are computationally faster than random methods. Most classical optimization methods can be described as minimum-seeking algorithms searching the cost surface for minimum cost and hence suffer from the challenge of local minima. Such classical methods are often calculus based and solved numerically [34].

More recently, natural optimization methods have been developed in order to address the inherent limitations of calculus-based optimization. Some natural optimization methods we will use are:

- a) Particle Swarm Optimization (PSO),
- b) Bacterial Foraging Optimization (BFO),

These methods provide an intelligent search of the solution space using statistical methods and hence do not require finding the cost function's derivatives; thus natural methods can handle systems with multiple, non-continuous and discrete variables.

### 3.2 Particle Swarm Optimization (PSO)

The PSO algorithm was first described in 1995 by James Kennedy and Russell C. Eberhart [35]. The techniques have evolved greatly since then, and the original version of the algorithm is barely recognizable in the current ones. It is a stochastic, population-based evolutionary computer algorithm for problem solving. It is a kind of swarm intelligence that is based on social-psychological principles and provides insights into social behavior, as well as contributing to engineering applications.

In a PSO system, a swarm of individuals (called particles) fly through the search space. Each particle represents a candidate solution to the optimization problem. The position of a particle is influenced by the best position visited by itself (i.e. its own experience) and the position of the best particle in its neighborhood (i.e. the experience of neighboring particles). When the neighborhood of a particle is the entire swarm, the best position in the neighborhood is referred to as the global best particle, and the resulting algorithm is referred to as a gbest PSO. When smaller neighborhoods are used, the algorithm is generally referred to a lbest PSO. The performance of each particle (i.e. how close the particle is from the global optimum) is measured using a fitness function that varies depending on the optimization problem.

Each particle in the swarm is represented by the following characteristics:

$x_i$ : The current position of the particle;

$v_i$ : The current velocity of the particle;

$y_i$ : The personal best position of the particle.

$\hat{y}$ : The neighborhood best position of the particle.

The personal best position of particle  $i$  is the best position (i.e. the one resulting in the best fitness value) visited by particle  $i$  so far. Let  $F$  denote the objective function. Then the personal best of a particle at time step  $t$  is updated as:

$$y_i(t+1) = \begin{cases} y_i(t) & \text{if } F(x_i(t+1)) \geq F(y_i(t)) \\ x_i(t+1) & \text{if } F(x_i(t+1)) < F(y_i(t)) \end{cases} \quad 3.1$$

For the *gbest* model, the best particle is determined from the entire swarm by selecting the best personal best position. If the position of the global best particle is denoted by the vector  $\hat{y}$ , then:

$$\hat{y} = \in \{y_0, y_1, y_2, \dots, y_{s-1}, y_s\} \quad 3.2$$

Where:

$$\hat{y} = \min\{F(y_0(t)), \dots, F(y_s(t))\} \quad 3.3$$

Where:  $s$  denotes the size of the swarm.

The velocity update step is specified for each dimension  $j$ :  $j \in \{1, \dots, N_d\}$

Hence,  $v_{i,j}$  represents the  $j^{\text{th}}$  element of the velocity vector of the  $i^{\text{th}}$  particle. Thus the velocity of particle  $i$  is updated using the following equation:

$$v_{i,j} = \omega \cdot v_{i,j}(t) + C_1 \cdot \Delta_1 + C_2 \cdot \Delta_2 \quad 3.4$$

Where:

$$\Delta_1 = r_{1,j} \cdot (y_{i,j}(t) - x_{i,j}(t)) \quad 3.5$$

$$\Delta_2 = r_{2,j} \cdot (y_j^n(t) - x_{i,j}(t)) \quad 3.6$$

$\omega$  is the inertia weight,  $C_1$  and  $C_2$  are the acceleration constants, and  $r_{1,j}$ ,  $r_{2,j}$  are random coefficients distributed as:

$$r_{1,j} \text{ and } r_{2,j} \in [0,1] \quad 3.7$$

The position of particle  $i$ ,  $x_i$  is then updated using the following equation:

$$x_i(t+1) = x_i(t) + v_i(t+1) \quad 3.8$$

This process is repeated until a specified number of iterations is exceeded, or velocity updates are close to zero. The quality of particles is measured using a fitness function which reflects the optimality of a particular solution. The following steps summarize the basic PSO algorithm [36]:

PSO Algorithm:

```

For each particle  $i = 1, \dots, s$  do
    Randomly initialize  $x_i$ 
    Randomly initialize  $v_i$  (or just set  $v_i$  to zero)
    Set  $y_i = x_i$ 
endfor
Repeat
For each particle  $i = 1, \dots, s$  do
    Evaluate the fitness of particle  $i$ ,  $f(x_i)$ 
    Update  $y_i$  using equation (3.1)
    Update  $\hat{y}$  using equation (3.3)
    For each dimension  $j = 1, \dots, Nd$  do
        Apply velocity update using equation (3.4)
    end loop
    Apply position update using equation (3.8)
end loop
Until some convergence criteria is satisfied

```



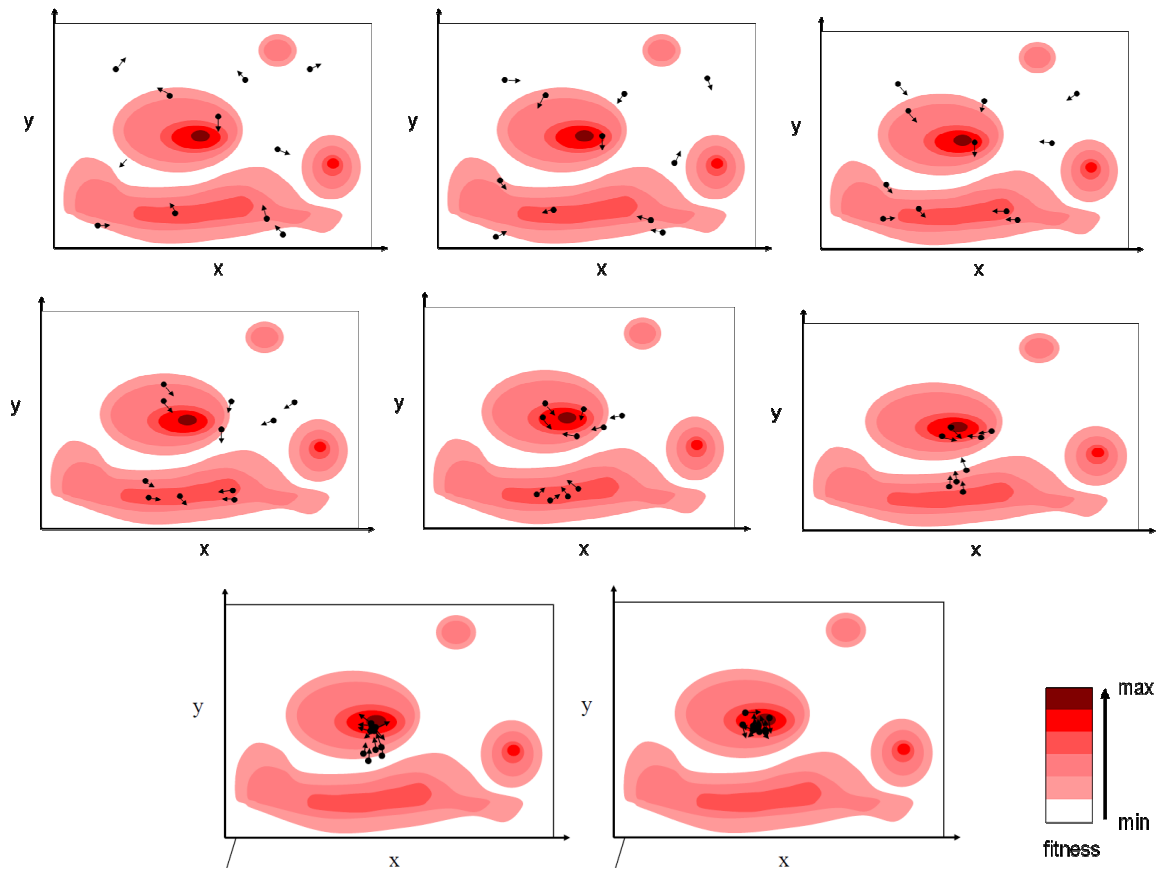


Figure.3.1: Swarm of particles searching for maximum fitness and converging to the global solution

It is important to clarify that good choice of the initial population can make the PSO faster to the global minimum, for this reason some works used the normal cloud method to find the best initial populations [37-38]. In this paper for the presented case, the choice of the initial population is made by a simple instruction:

$$x_{i,j}(0) = \frac{\pi}{2k} \cdot (j-1 + rand) \quad 3.9$$

Where  $k$  is the dimension of the objective function.

### 3.3 Bacterial Foraging Optimization Algorithm (BFO)

Foraging means locating, handling, and ingesting food. Animals that have successful foraging strategies are favored since they obtain enough food to enable them to reproduce, so they are more likely to enjoy reproductive success [39]. This has led scientists to model the activity of foraging as an optimization process. (Kevin et al.2002) in [40] explain the biology and physics underlying the chemotactic (foraging) behavior of E.coli bacteria (the ones that are living in your intestines), and gives a computer program that emulates the distributed optimization process represented by the activity of social bacterial foraging and apply that in adaptive controllers.

The foraging strategy of E. coli bacteria present in human intestine can be explained by four processes namely: Chemotaxis, Swarming, Reproduction, Elimination and Dispersal [40].

a) *Chemotaxis*: The characteristics of movement of bacteria in search of food can be defined in two ways, i.e. swimming and tumbling together known as chemotaxis. A bacterium is said to be 'swimming' if it moves in a predefined direction; and 'tumbling' if it moves randomly in different directions. Mathematically, tumble of any bacterium can be represented by a unit length of random direction  $\phi(j)$  multiplied by step length of that bacterium  $C(i)$ . In case of Swimming this random length is predefined.

b) *Swarming*: For the bacteria to reach at the richest food location (i.e. for the algorithm to converge at the solution point), it is desired that the optimum bacterium till a point of time in the search period should try to attract other bacteria so that together they converge at the desired location (solution point) more rapidly. To achieve this, a penalty function based upon the relative distances of each bacterium from the fittest bacterium till that search duration, is added to the original cost function. Finally, when all the bacteria have merged into the solution point this penalty function becomes zero. The effect of Swarming is to make the bacteria congregate into groups and move as concentric patterns with high bacterial density.

c) *Reproduction*: The original set of bacteria, after getting evolved through several chemotactic stages reach the reproduction stage. Here best set of bacteria (chosen out of all the chemotactic stages), get divided into two groups. The

healthier half replaces with the other half of bacteria, which gets eliminated, owing to their poorer foraging abilities. This makes the population of bacteria constant in the evolution process.

*d) Elimination and Dispersal:* In the evolution process a sudden unforeseen event can occur, which may drastically alter the smooth process of evolution and cause the elimination of the set of bacteria and/or disperse them to a new environment. Most ironically, instead of disturbing the usual chemotactic growth of the set of bacteria, this unknown event may place a newer set of bacteria nearer to the food location. In its application to optimization it helps in reducing the behavior of stagnation, (i.e. being trapped in a premature solution point or local optima) [40].

We want to find the minimum of  $f(x)$ ,  $x \in \mathfrak{R}^p$ , where we do not have measurements or an analytical description of the gradient  $\nabla f(x)$ . Here we use ideas from bacterial foraging to solve this non gradient optimization problem. First, suppose that  $x$  is the position of a bacterium and  $f(x)$  represents the combined effects of attractants and repellents from the environment, with, for example,  $f(x) < 0$ ,  $f(x) = 0$ , and  $f(x) > 0$  representing that the bacterium at location  $x$  is in nutrient-rich, neutral, and noxious environments, respectively. Bacteria try to climb up the nutrient concentration (find lower and lower values of  $f(x)$ , avoid noxious substances, and search for ways out of neutral media). Chemotactic is a tumble followed by a tumble or a tumble followed by a run. Let  $j$  be the index for the chemotactic step. Let  $k$  be the index for reproduction step. Let  $l$  be the index of the elimination-dispersal event.

$$\text{Let: } p(j, k, l) = \{ \theta^i(j, k, l) | i = 1, 2, \dots, S \} \quad 3.9$$

represents the position of each member in the population of the  $S$  bacteria at the  $j$ th chemotactic step.  $k$ th reproduction step, and  $l$ th elimination-dispersal event.

Here  $f(i, j, k, l)$  denotes the cost at the location of the  $i$ th bacterium  $\theta^i(j, k, l) \in \mathfrak{R}^p$ . For actual bacterial populations,  $S$  can be very large ( $S=10^9$ ), but  $p$  is the dimension of the cost function. Let  $N_c$  be the length of the lifetime of the bacteria as measured by the number of chemotactic steps they take during their life. Let  $C(i) > 0$ ,  $i=1, 2, \dots, S$ , denote a basic chemotactic step size that we will use to define the lengths of steps during runs. To represent a tumble, a unit length random

direction, say  $\phi(j)$ , is generated; this will be used to define the direction of movement after a tumble. In particular, we let:

$$\theta^i(j+1, k, l) = \theta^i(j, k, l) + C(i)\phi(j) \quad 3.10$$

So that  $C(i)$  is the size of the step taken in the random direction specified by the tumble. If at  $\theta^i(j+1, k, l)$  the cost  $f(i, j+1, k, l)$  is better (lower) than at  $\theta^i(j, k, l)$ , then another step of size  $C(i)$  in the same direction will be taken, and again, if that step resulted in a position with a better cost value than at the previous step another step is taken. This swim is continued as long as it continues to reduce the cost function, but only up to a maximum number of steps  $N_s$  [39]. We can represent swarming as follows:

$$f_{cc}(\theta, P(j, k, l)) = \sum_{i=1}^S f_{cc}^i(\theta, \theta^i(j, k, l))$$

$$= \sum_{i=1}^S \left[ -d_{attract} \exp\left(-\omega_{attract} \sum_{m=1}^P (\theta_m - \theta_m^i)^2\right) \right] + \sum_{i=1}^S \left[ h_{repellent} \exp\left(-\omega_{repellent} \sum_{m=1}^P (\theta_m - \theta_m^i)^2\right) \right] \quad 3.11$$

The function  $f_{cc}$  represents the combined cell-to-cell attraction and repelling effects, where  $\theta = [\theta_1, \dots, \theta_p]^T$  is a point on the optimization domain and  $\theta_m^i$  is the  $m$ th component of the  $i$ th bacterium position  $\theta^i$ . This function is time varying in that if many cells come close together there will be a high amount of attractant and hence an increasing likelihood that other cells will move toward the group. This produces the swarming effect.

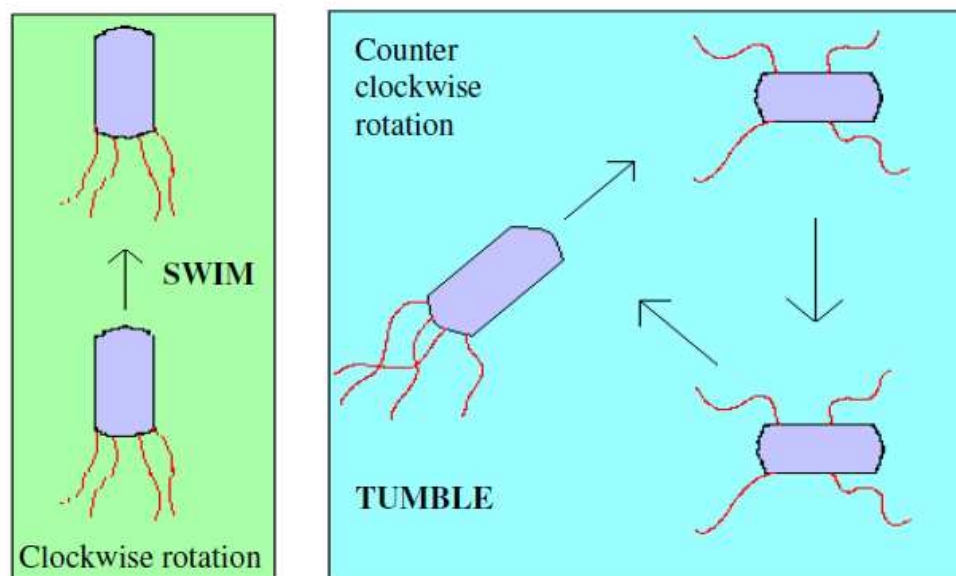


Figure.3.2: Swim and tumble of a bacterium

BFO Algorithm:

1. Initialization: We choose  $p, S, N_c, N_{re}, N_{ed}, P_{ed}$  and the  $C(i), i=1,2,\dots,S$ . for swarming, we choose also parameters of the cell-to-cell attractant functions. Initial values for  $\theta^i, i=1,2,\dots,S$  are also chosen.

2. Elimination-dispersal loop:  $l=l+1$

3. Reproduction loop:  $k=k+1$

4. Chemotaxis loop:  $j=j+1$

a) For  $i=1$  to  $S$  take a chemotaxis step for bacterium  $l$  as follows.

b) Compute  $f(i,j,k,l)$  and let:

$$f(i,j,k,l) = f(i,j,k,l) + f_{cc}(\theta^i(j,k,l), P(j,k,l)),$$

we add on the cell-to-cell attractant effect to the nutrient concentration.

c) Let  $flast = f(i,j,k,l)$  to save this value since we may find a better cost via a run.

d) Tumble: generate a random vector  $\Delta(i) \in \mathfrak{R}^p$  with each element  $\Delta_m(i), m=1,2,\dots,P$ , a random number on  $[-1,1]$ .

$$\theta^i(j+1,k,l) = \theta^i(j,k,l) + C(i) \frac{\Delta(i)}{\sqrt{\Delta^T(i)\Delta(i)}}$$

e) Move let:

this results in a step of size  $C(i)$  in the direction of the tumble for bacterium  $i$ .

f) Compute  $f(i,j+1,k,l)$ , and then let:

$$f(i,j+1,k,l) = f(i,j+1,k,l) + f_{cc}(\theta^i(j+1,k,l), P(j+1,k,l))$$

g) Swim: let  $m=0$  and While  $m < N_s$  put  $m=m+1$ , if  $f(i,j+1,k,l) < flast$  let  $flast = f(i,j+1,k,l)$

$$\theta^i(j+1,k,l) = \theta^i(j+1,k,l) + C(i) \frac{\Delta(i)}{\sqrt{\Delta^T(i)\Delta(i)}}$$

and let:

and use this position to calculate the new cost value.

Else, let  $m=N_s$

end while.

h) Go to the next bacterium.

5. if  $j < N_c$  then go to step 4.

6. Reproduction: For  $i=1,2,\dots,S$ .  $f_{health}^i = \sum_{j=1}^{N_c+1} f(i,j,k,l)$  (health of bacterium

$i$ ). Sort bacteria and chemotactic parameters  $C(i)$  in order of ascending cost  $f_{health}$  (higher cost means lower health). The  $S/2$  bacteria of the highest cost will die and the healthiest are placed at the same location as their parent.

7. if  $k < N_{re}$  go to step 4.

8. Elimination-dispersal: for  $i=1,2,\dots,S$ , with probability  $P_{ed}$ , eliminate and disperse each bacterium.

9. if  $l < N_{ed}$  then go to step 1, otherwise end algorithm.

### 3.4 Synergy of PSO and BFO Algorithms:

In the proposed hybrid approach, after undergoing a chemo-tactic step, each bacterium also gets mutated by a PSO operator. In this phase, the bacterium is stochastically attracted towards the globally best position found so far in the entire population at current time and also towards its previous heading direction. The PSO operator uses only the 'social' component and eliminates the 'cognitive' component as the local search in different regions of the search space. BFO has been changed by directing positions of bacteria and updating their velocities from the first chemotactic step using the power of PSO reaching the global solution in addition to its rapid convergence compared to BFO.

This hybridization improved the convergence speed and accuracy of solutions got by classical BFO, however, what is requested in image restoration is attaining a best approach to the original image by finding the best solution, which is accomplished by a hybrid implementation of BFO-PSO.

In the previous BFO Algorithm, inside the *Chemotaxis loop* (step 4, point g), we introduce the PSO operator to update the global position of each bacterium, then calculating the cost function and subsequently we update both global position and velocity of each bacterium before letting bacteria swimming with the new speed on the way of the new updated direction:

g) We introduce PSO operator (for each chemotactic step S):

- Update the  $\theta_{g\_best}$  and  $f_{best}(i, j, k, l)$
- Update position and velocity of the  $d$ -th coordinate of the  $i$ -th bacterium to the following rule :

$$V_{id}^{new} = \omega \cdot V_{id}^{old} + C_1 \cdot \varphi_1 \cdot (\theta_{g\_best_d} - \theta_d^{old}(i, j+1, k))$$

$$\theta_d^{new}(i, j+1, k) = \theta_d^{old}(i, j+1, k) + V_{id}^{new}$$

### 3.5 Testing Swarm Optimization Algorithms

By comparison with the unconstrained nonlinear optimization method that uses the Nelder-Mead simplex algorithm which is a direct search method that does not use numerical or analytic gradients (implemented in MATLAB with the function *fminsearch*) [41], performance metrics proved the robustness and solution quality of the employed methods (PSO and BFO). Their performance has been evaluated on a bed of eight known benchmark functions with different dimensions as shown below:

Problem 1:  $f = x^4 - 14x^3 + 60x^2 - 70x$  with  $-10 < x < 10$

*fminsearch*:  $f_{\min}(0.7809) = -24.3696$

PSO:  $f_{\min}(0.7809) = -24.3696$

BFO :  $f_{\min}(0.7961) = -24.3696$

Hybrid PSO-BFO :  $f_{\min}(0.7809) = -24.3696$

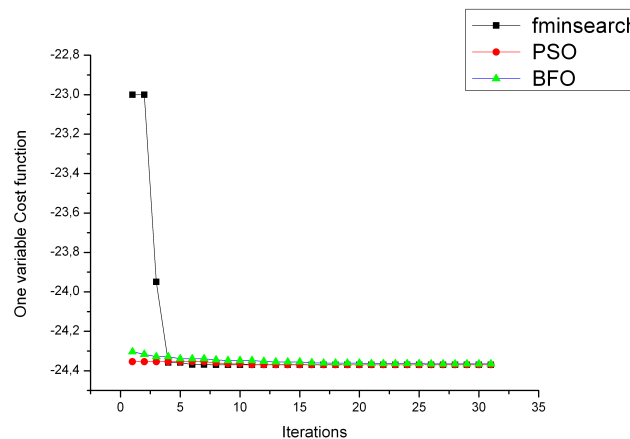


Figure.3.3: Progress towards the optima for One-variable benchmark function using three optimization methods

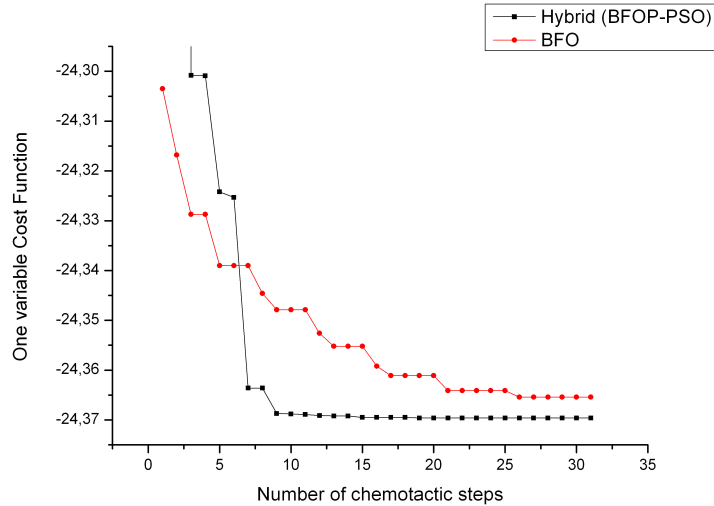


Figure.3.4: Improving Classical BFO with a synergy between PSO and BFO to reach the best global optimum

Problem 2:  $f = x.\sin(4x) + 1.1y.\sin(2y)$  with  $0 < x, y < 10$

*fminsearch*:  $f_{\min}(9.0390, 8.6682) = -18.5547$

PSO:  $f_{\min}(9.0390, -8.6682) = -18.5547$

BFO :  $f_{\min}(9.0380, -8.6834) = -18.5547$

Hybrid PSO-BFO :  $f_{\min}(9.0390, 8.6682) = -18.55474$

Problem 3:  $f = (x^2 + y^2)^{0.25} \times \sin\left\{30\left[(x + 0.5)^2 + y^2\right]^{0.1}\right\} + |x| + |y|$

*fminsearch*:  $f_{\min}(-0.2022, -0.0000) = -0.2474$

PSO:  $f_{\min}(-0.2021, 0.0000) = -0.2474$

BFO :  $f_{\min}(-0.2065, -0.0030) = -0.2474$

Hybrid PSO-BFO :  $f_{\min}(-0.2022, 0.0000) = -0.2475$

Problem 4:  $f = 100(y - x^2)^2 + (1 - x)^2$  with  $-10 < x, y < 10$

*fminsearch*:  $f_{\min}(1.0000, 1.0000) = 8.1777e - 10$

PSO:  $f_{\min}(1.0000, 1.0000) = 0.0000$

BFO :  $f_{\min}(1.0002, 1.0014) = 1.6625e - 007$

Hybrid PSO-BFO :  $f_{\min}(1.0000, 10000) = 0.0000$



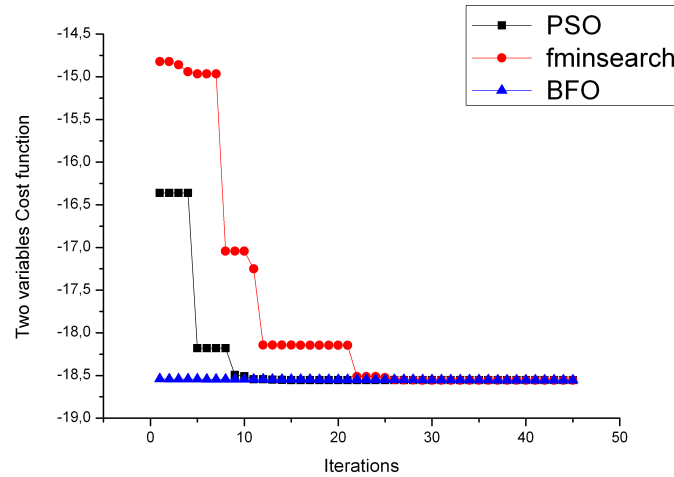


Figure.3.5: Progress towards the optima for Two-variables benchmark function using three optimization methods

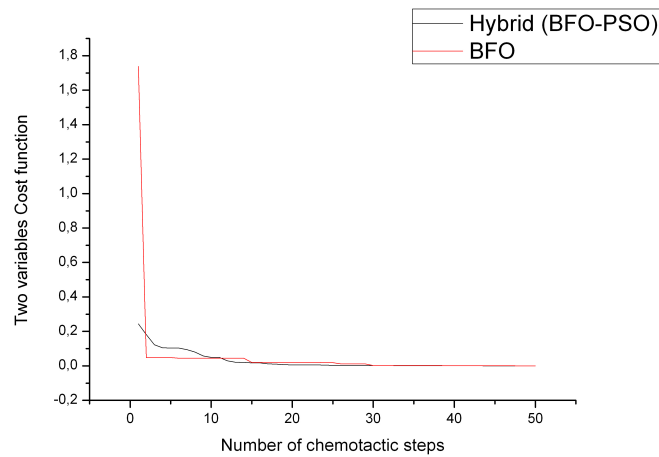


Figure.3.6: Improving Classical BFO with a synergy between PSO and BFO to reach the best global optimum

**Problem 5:**  $f = 1.5x^2 + 2y^2 + 1.5z^2 + xz + 2yz - 3x - z$  with  $-10 < x, y, z < 10$

*fminsearch:*  $f_{\min}(1.0000, 0.0000, 0.0000) = -1.5000$

PSO:  $f_{\min}(1.0000, -0.0000, -0.0000) = -1.5000$

BFO :  $f_{\min}(0.9983, -0.0004, -0.0031) = -1.4998$

Hybrid PSO-BFO :  $f_{\min}(1.0000, 0.0000, 0.0000) = -1.5000$

**Problem 6:**  $f = (x + 10y)^2 + 5(z - t)^2 + (y - 2z)^4 + 10(x - t)^4$  with  $-10 < x, y, z, t < 10$

*fminsearch:*  $f_{\min}(0.0316e-3, -0.0316e-3, 0.2160e-3, 0.2160e-3) = 8.2563e-14$

PSO:  $f_{\min}(-0.0007, 0.0001, -0.0004, -0.0004) = 0.0000$

BFO :  $f_{\min}(-0.0273, -0.0009, -0.0052, -0.0063) = 9.7615e - 006$

Hybrid PSO-BFO :  $f_{\min}(0.0005, -0.0001, 0.0005, -0.0003) = 0.0000$

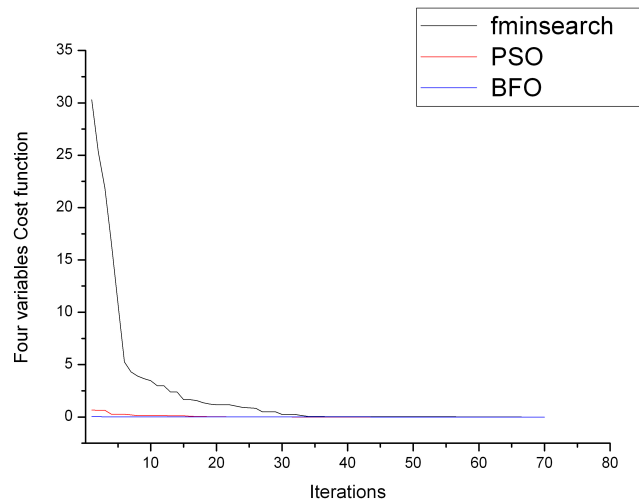


Figure.3.7: Progress towards the optima for Four-variables benchmark function using three optimization methods

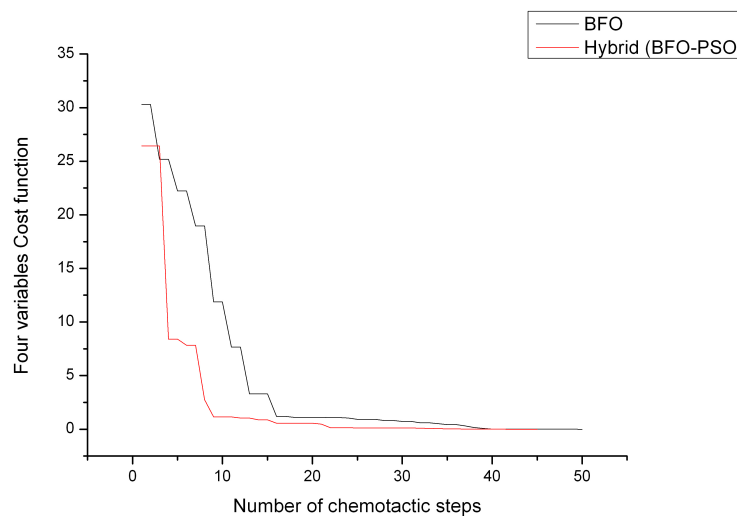


Figure.3.8: Improving Classical BFO with a synergy between PSO and BFO to reach the best global optimum

**Problem 7:** Function with thirty variables (Rosenbrock function):

$$f = \sum_{i=1}^{29} \left( 100(x_{i+1} - x_i^2)^2 + (x_i - 1)^2 \right) \text{ with } x \in [-30, 30]^{30}$$

*fminsearch:*

$f_{\min}(0.0510, 0.2059, -0.1223, 0.1282, -0.0131, 0.0326, -0.0939, 0.1484, -0.1841, 0.1148, 0.0689, -0.0309, 0.0876, -0.0581, 0.1476, -0.0962, 0.0191, 0.0263, -0.1047, 0.2639, 0.1275, 0.0257, 0.1943, 0.2798, 0.2334, 0.0511, 0.0245, 0.0626, 0.1364, -0.8415) = 2.7323e+003$



## CHAPTER 4

### SIMULATION RESULTS

#### 4.1 Introduction

In this chapter, we present some numerical examples with the schemes introduced in this thesis. Notice that all the experiments presented in this thesis were run with Matlab, on a desktop with a processor at 1.80 GHz and 2Gb of RAM. In all the presented algorithms, the cost of one iteration of the algorithm is proportional to the size of the image. This cost is some seconds for a 256×256 image with either the fixed point algorithms or the gradient algorithms or algebraic direct methods. Swarm algorithms have a computation cost which is twice higher. This cost is between 8 and 10 times higher with the different variants of images.

A digital image is a two or three dimensional array of numbers representing intensities on a grayscale or color scale. Denote a two-dimensional digital image of gray-level intensities by  $I$ . The image  $I$  is ordinarily represented in software accessible form as an  $M \times N$  matrix containing indexed elements  $I(i, j)$ , where  $0 \leq i \leq M-1$ ,  $0 \leq j \leq N-1$ . The elements  $I(i, j)$  represent samples of the image intensities, usually called *pixels* (*picture elements*). For simplicity, we assume that these come from a finite integer-valued range. This is not unreasonable, since a finite wordlength must be used to represent the intensities. Typically, the pixels represent optical intensity, but they may also represent other attributes of sensed radiation, such as radar, electron micrographs, x-rays, or thermal imagery.

This thesis is concerned with grayscale images. However, at the end of our simulations, we extend our implementation to some color images.

When comparing, in a given situation, the suitability of the various approaches discussed in this thesis, it is useful to use the same image or test pattern so that comparisons are meaningful. The test pattern generated by function checkerboard is particularly useful for this purpose because its size can be scaled without affecting its principal features. The images generated by this function are of class double with values in the range [0,1]. Because some restoration algorithms are slow for large images, a good approach is to experiment

with small images to reduce computation time and thus improve interactivity, then we can extend our experiment to real gray level images taken by neutron radiography imaging system.

Image restoration may be defined as the process of undoing imaging degradations based on a mathematical model of these degradations. The aim of image restoration is to remove blur and the noise incurred in recording the image.

Before we can deblur an image, we must have a mathematical model that relates the given blurred image to the unknown true image. Consider the example shown in Figure 4.1. The left is an original test image, and right ones are a blurred and blurred/noisy versions of the same image. The last images are what would be recorded during acquisition in bad conditions.

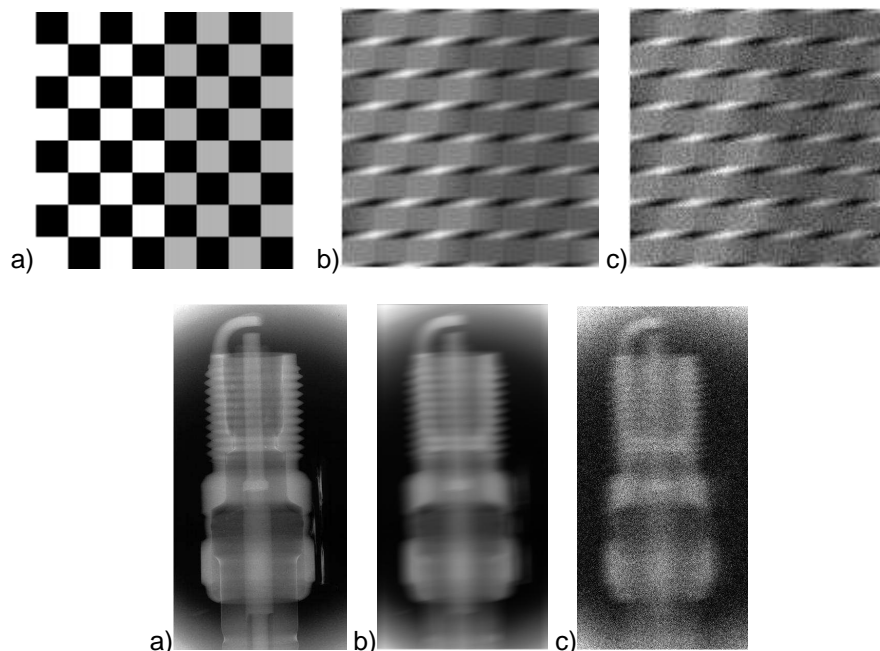


Figure.4.1: a) original b) motion blurred c) motion blurred with gaussian noise

#### 4.2 Restoration using naïve and regularized filter

If we neglect the presence of noise in the degradation model (1), we can derive a simple restoration technique, in which the frequency response of the deconvolution filter, is found to be the inverse of the frequency response of the PSF, the degradation function.

Inverse filtering can efficiently be implemented in the frequency domain with the FFT. However, image restoration by direct inversion is often ill-posed owing to the presence of observation noise. This follows because the direct inverse of the blur transfer function usually has a very large magnitude at high frequencies and is

in finite at those frequencies where the blur transfer function has zeros. This result in excessive amplification at these frequencies of any sensor noise.

Regularization techniques using information about the image generation process attempt to roll-off the transfer function of the inverse filter at these frequencies in an attempt to limit the noise amplification during the signal restoration process. Inevitably, the regularized filter deviates from the exact inverse at these frequencies. It is this deviation of the regularized filter from the exact inverse that causes the ringing artifacts. We define such ringing artifacts as periodic overshoots and under-shoots about an edge that decay in spatial coordinates as we move further from the edge. Ringing artifacts are encountered in the regions of an image at those frequencies where the regularized inverse transfer function differs from the exact inverse because sharp edges contain almost all frequencies.

Regularization of the inversion can either be achieved via deterministic iterative procedures or via stochastic filtering techniques. The first usually do not utilize an image model and are implemented by iterative procedures to alleviate the computational problems. Stochastic techniques, on the other hand incorporate an image model and the noise statistics for optimal filtering. Almost universally, the minimum mean squared error (MSE) criterion has been chosen because of the simplicity it provides.

In the following, we gathered some results using these methods for both blurred and blurred with additive noise image restoration:

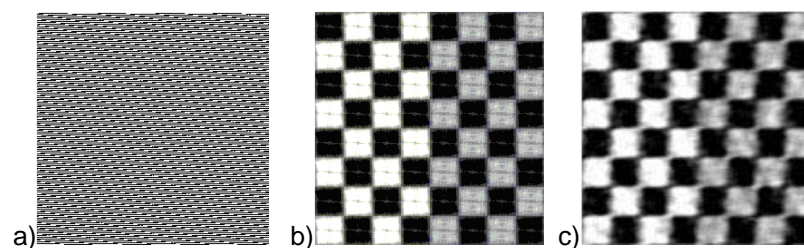


Figure.4.2: Restoring blurred/noisy image: a) Direct inverse filtering b) Zero padding FFT filter and c) Regularized filter

### 4.3 Restoration using some classical methods

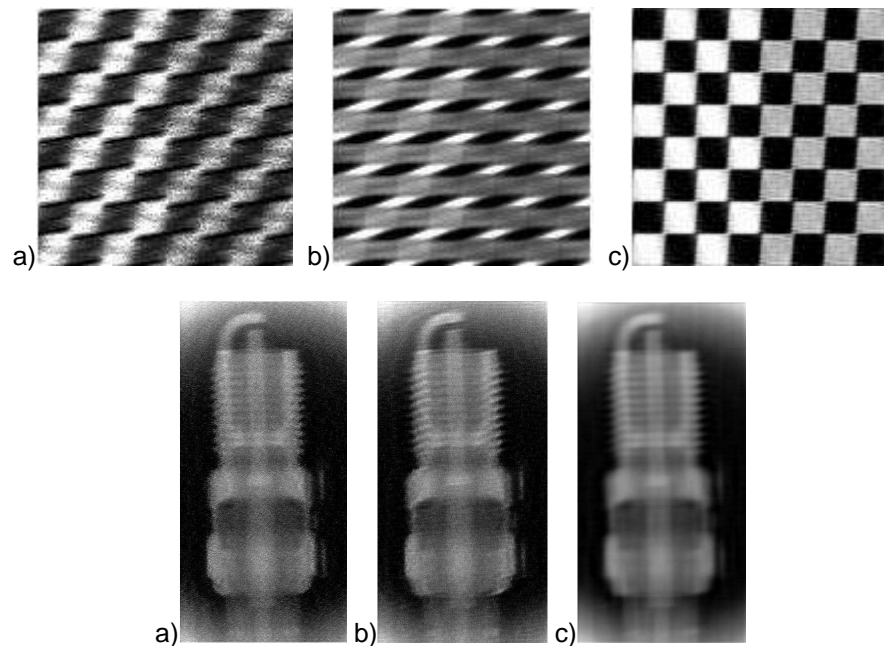


Figure.4.3: Restoring blurred/Noisy image: a) Lucy-Ridchardson algorithm  
b) Blind restoration and c) Wiener filtering

### 4.4 Adaptive Spatial filtering for image restoration

When the only degradation present is noise, the method of choice for reduction of noise in this case is spatial filtering. These filters can adapt their behavior depending on the characteristics of the image in the area being filtered.

#### 4.4.1 Adaptive Median Filter

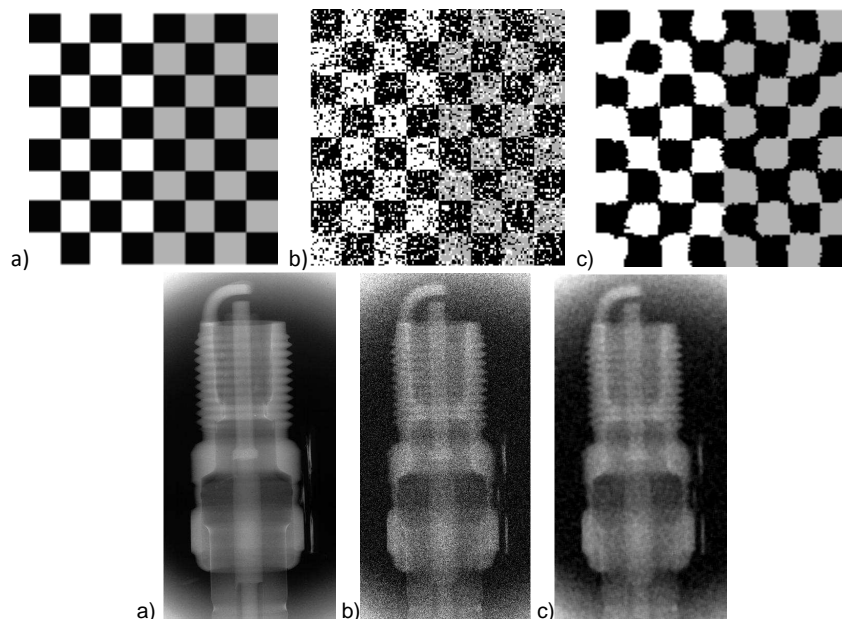


Figure.4.4: Restoration of Hardly noisy image using random Impulse Noise : a)Original, b)Degraded, and c)Restored with Adaptive median Filter

#### 4.4.2 Decision-Based Algorithm for Removal of High-Density Impulse Noises

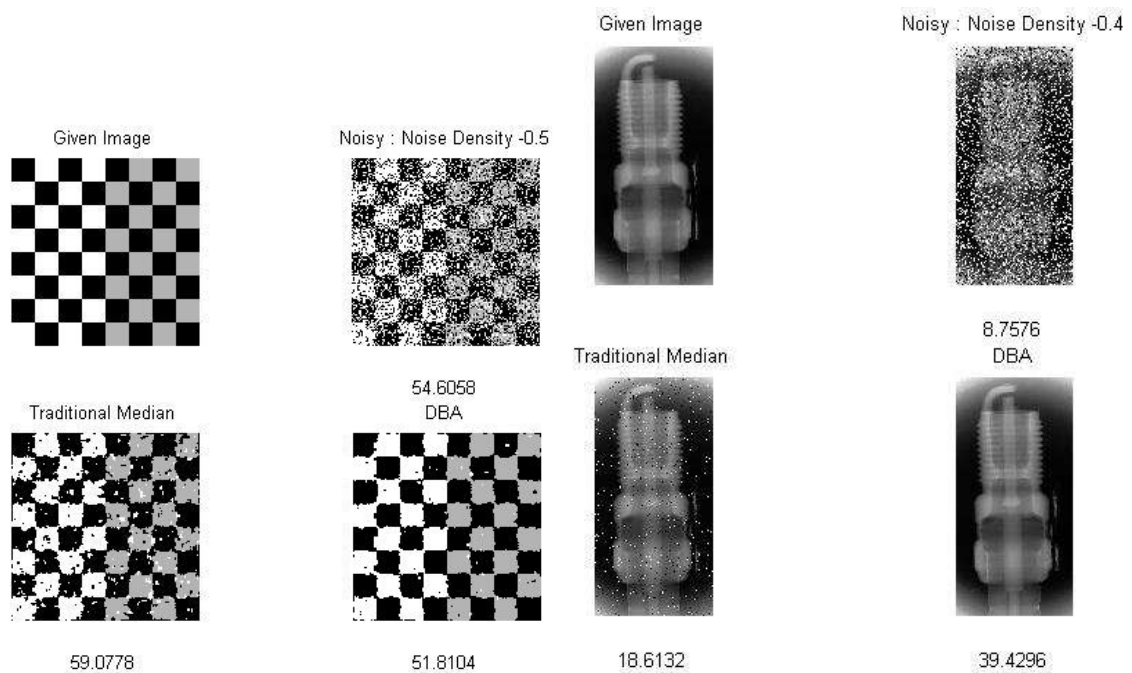


Figure.4.5: Restoration Using Decision Based Algorithm for high density impulse noise

#### 4.4.3 Some other new filters for Multiplicative noise reduction

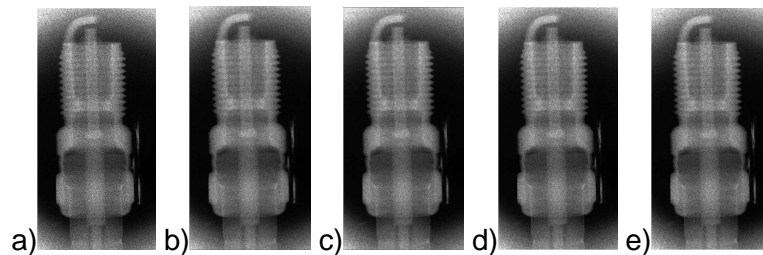


Figure.4.6: a) Noisy image, b) Filtered image using: Kuan, c) Lee, d) Frost and e) SRAD filters

#### 4.5 Image Restoration Using Direct methods

There are two important direct methods: TSVD and Tikhonov. To implement them, we use the following six spectral filtering methods:

1. Tikhonov image deblurring using the DCT algorithm.
2. Tikhonov image deblurring using the FFT algorithm.
3. Tikhonov image deblurring using the Kronecker decomposition.
4. Truncated SVD image deblurring using the DCT algorithm.
5. Truncated SVD image deblurring using the FFT algorithm.
6. Truncated SVD image deblurring using Kronecker decomposition.



These methods give us control, via the filter parameters, over the spectral contents of the deblurring images. Spectral filtering methods work by choosing the filter parameters in the computed solution in order to obtain a solution with desirable properties. We use the generalized cross validation (GCV) method for choosing parameters for both direct methods.

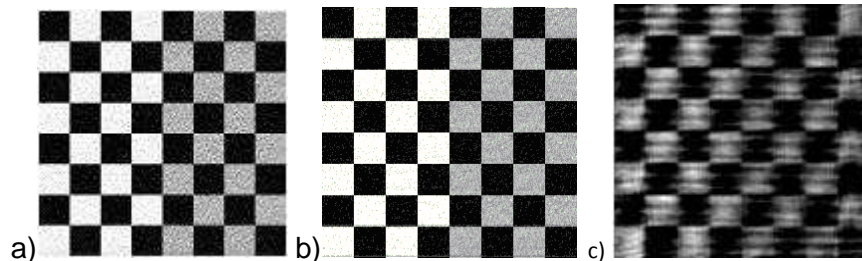


Figure.4.7: Restored with a) Tikhonov regularization and b) Truncated Singular Value Decomposition (TSVD), the condition number  $\text{cond}(A)=\sigma_1/\sigma_N$  is found to be  $7.337638 \times 10^4$ , c) Iterative Weighted GCV Method

#### 4.6 Regularized Total Variation

An implementation of the Total Variation based filtering was made using the conjugate gradient (CG) method and the Newton Algorithm for minimizing Total Variations with Laplacian regularization. Figure.4.8 shows restorations with ROF (Rudin, Osher, Fatemi), Figure.4.8.a, and shows TV energy evolution with iterations, Figure.4.8.b:

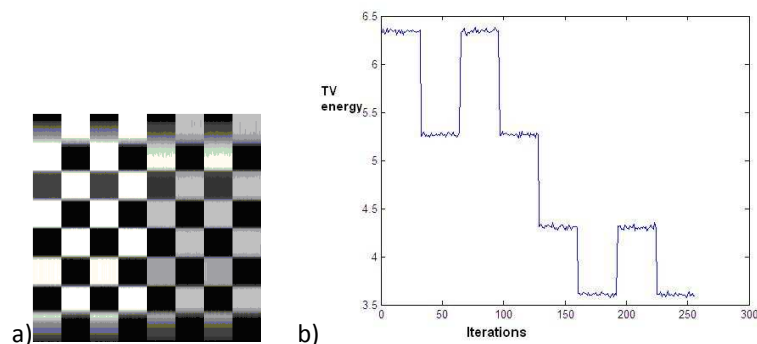


Figure.4.8: a) Restoration with ROF method, b) TV Energy evolution with iterations

Figure.4.9 illustrates a restoration result of the previous blurred/noisy image, using Chambolle Algorithm, with automatic estimation of regularization parameter and TV energy evolution with iterations.

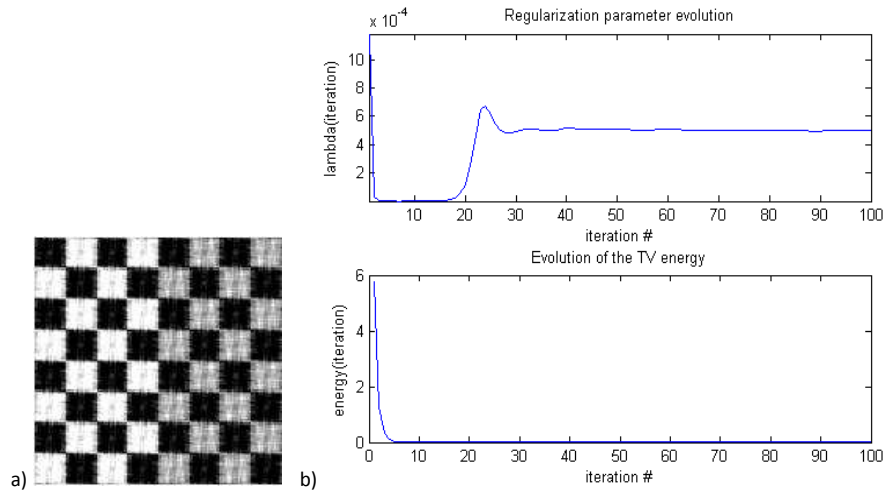


Figure.4.9: a) Image Restored using Chambolle Algorithm, b) Regularization parameter estimation and TV energy evolution

#### 4.7 Image restoration using Swarm Intelligence

We will establish a new approach that can be used to solve a constrained optimization ill-posed problem in order to improve a blurred and noisy image. We will corrupt images of different sizes using many types of degradation functions and noises, and then try to restore the original. Our starting image is a gray-level image contained in the  $m \times n$  matrix. Each element in the matrix represents a pixel's gray intensity between black and white (0 and 255). The simplest approach is to solve the least squares problem:

$$\min(\|H * X - G\|^2) \quad (12)$$

In practice the results obtained with this simple approach tend to be noisy, because this term expresses only the fidelity to the available data  $g$ . To compensate for this, the below regularization term is added to improve smoothness of the estimate:

$$0.004 * \|L * X\|^2 \quad (13)$$

$L$  is the discrete Laplacian, which relates each pixel to those surrounding it.  $L = \text{del}2(X)$  is a discrete approximation of:

$$l = \frac{\nabla^2 X}{2N} = \frac{1}{2N} \left( \frac{d^2 X}{dx^2} + \frac{d^2 X}{dy^2} \right) \quad (14)$$

Where  $X$  is the estimated matrix. The matrix  $L$  has the same size as  $X$  with each element equal to the difference between an element of  $X$  and the average of its four neighbors. Since we know we are looking for a gray intensity, we also impose the constraint that the elements of  $X$  must fall between 0 and 255. To obtain the deblurred image, we want to solve for  $X$ :

$$\min(\|H * X - G\|^2) + 0.004 * \|L * X\|^2 \quad (15)$$

We can implement our objective function using this expression; the number of variables in this function to be minimized will be  $m \times n$  which is the size of the matrix representing the original image.

#### 4.7.1 Simulation experiment Using PSO algorithm [42,44,47]

We carried out computer simulations to validate the applicability of this algorithm in image restoration. We run the algorithm using Intel Pentium4 Desktop computer with 1.80GHZ CPU and memory size of 2Go. The average processing time is dependent upon computation machine, image size and choice of PSO algorithm parameters (varies from few seconds to few minutes). Some simple images of sizes: 8x8, 16x16, 32x32, 64x64, 256x256 and 512x512 are used. Different PSO parameters are chosen:  $C1=1.5$ ;  $C2=4-C1$ ;  $\text{minInertia}=0.3$ ;  $\text{maxInertia}=0.95$ ;  $\text{Swarm Size}=10,20,50,120$ ;  $\text{Maximum Iterations}=20,50,100,200$ . We took the value 0.004 as a regularization parameter. In Fig.5(a, b, c and d), we increase gradually the swarm size and iterations to reach improved restoration results. The cost function evolution is traced in Figure 4.10 without regularization and in Figure 4.11 with regularization.

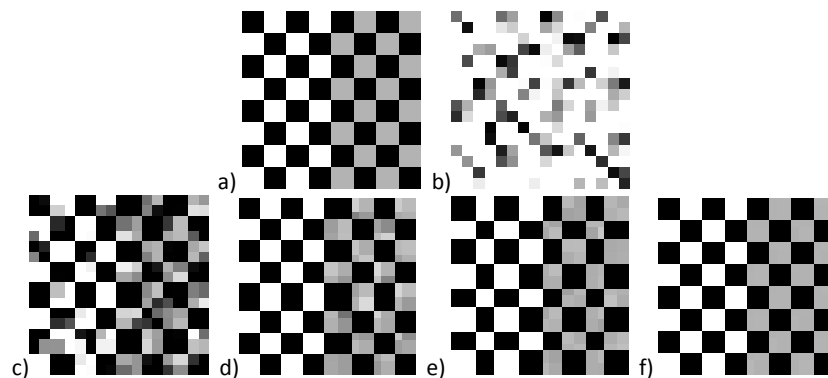


Figure.4.10: Restoration of Blurred and Noisy Images without Regularization Constraint: a)Original, b)Noisy and c),d),e),f) Restored with swarm size and iterations: (10,20), (20,50), (50,100), and (120,200)

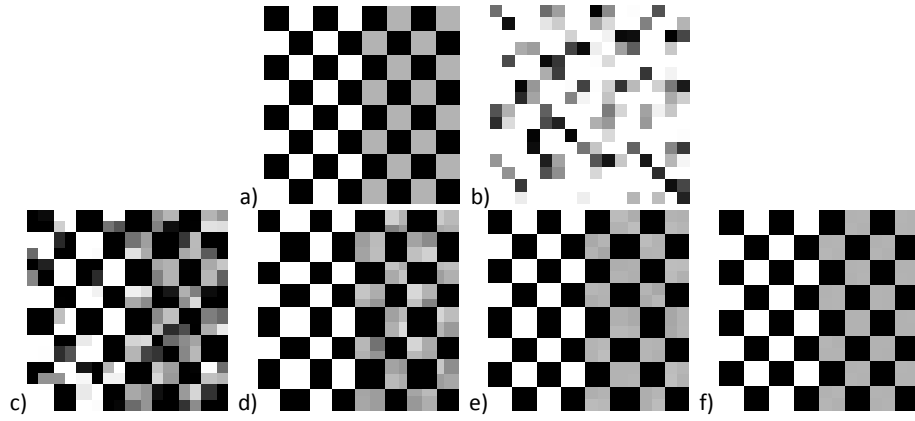


Figure.4.11: Restoration of Blurred and Noisy Images with Regularization Constraint: a) Original, b) Noisy, c),d),e),f)Restored with swarm size and iterations: (10,20), (20,50), (50,100), and (120,200)

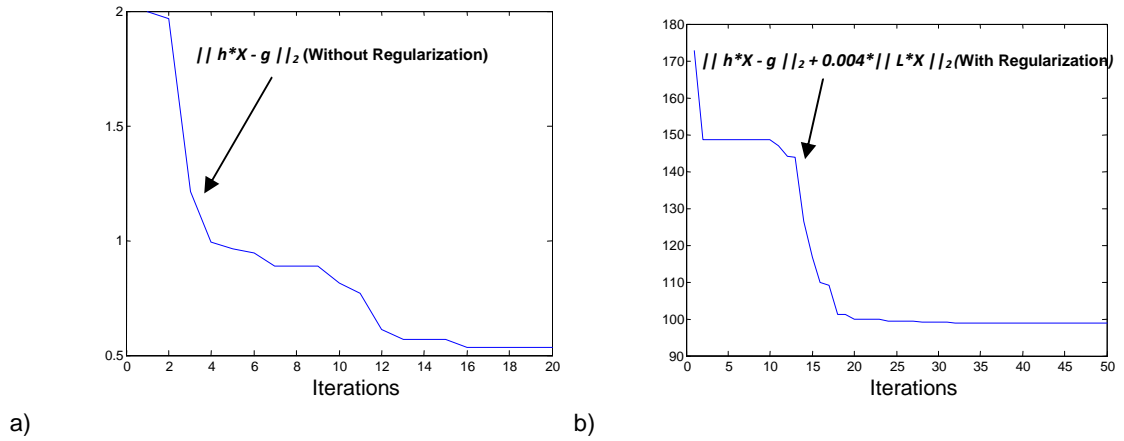


Figure.4.12: Evolution of Cost function: a) Without regularization, b) With regularization

To evaluate the restoration performance of our approach quantitatively, we record the evolution of the root mean squared error (RMSE) and the peak signal to noise ratio (PSNR) in Table 4.1 and Fig.7.a, b:

$$MSE = \frac{1}{m \times n} \sum_{i=1}^{i=m} \sum_{j=1}^{j=n} [original(i, j) - restored(i, j)]^2 \quad (16)$$

$$\text{and } RMSE = \sqrt{MSE}$$

$$PSNR = 20 \cdot \log_{10} \left( \frac{255}{RMSE} \right) \quad (17)$$

Table 4.1: Evolution of the (RMSE) and the peak signal to noise ratio (PSNR) with swarm size and number of iterations

	<i>With Regularization</i>		<i>Without Regularization</i>	
	<i>RMSE</i>	<i>PSNR</i>	<i>RMSE</i>	<i>PSNR</i>
<i>Blured/Noisy</i>	0.92	48.81	0.92	48.81dB
<i>(10,20)</i>	0.16	64.21	0.16	64.18dB
<i>(20,50)</i>	0.04	75.49	0.04	75.50dB
<i>(50,100)</i>	0.014	87.06dB	0.02	83.82dB
<i>(120,200)</i>	0.001	102.17dB	0.001	101.17

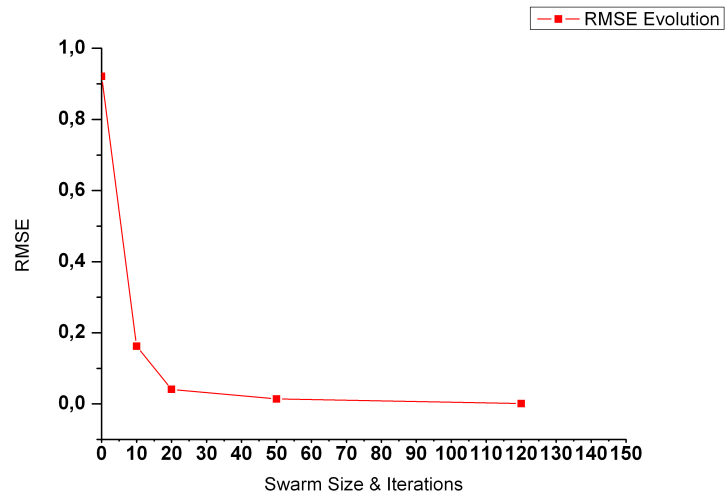


Figure.4.13. a: RMSE Evolution with Swarm Size & Number of Iterations

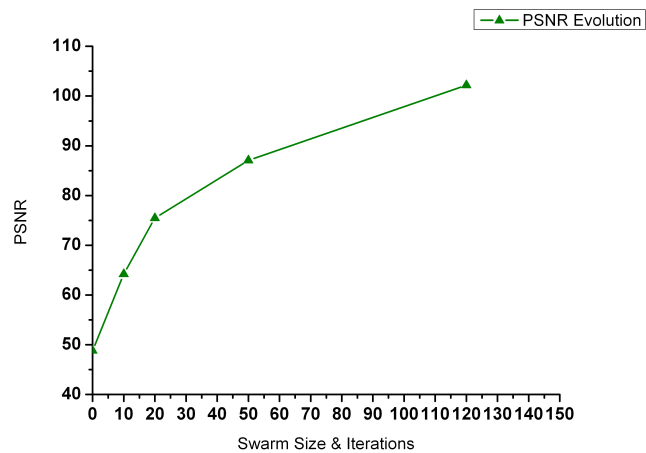


Figure.4.13.b: PSNR Evolution with Swarm Size & Number of Iterations

Table 4.2: Values of the RMSE and the PSNR for five selected different methods[44]

	<i>RMSE</i>	<i>PSNR</i>
<i>Blured/Noisy</i>	0.921	48.81
<i>FFT</i>	0.1680	64.01
<i>TSVD</i>	0.0795	70.47
<i>Tikhonov</i>	0.0682	71.47
<i>TV (CG)</i>	0.2124	61.53
<i>TV (Chambolle)</i>	0.1401	65.26

Using the checkerboard test image (a) blurred and noisy (b) and restored using different swarm sizes and process iterations (c, d, e, f), with and without Laplacian regularization constraint in figures 10 and 11. We can observe evolution of the mean squared error (RMSE) and the peak signal to noise ratio (PSNR) in table 4.1 and remark the effect of regularization both on image quality and cost function evolution, figures 12.a and b. In table 4.2, we computed values of the RMSE and the PSNR for five selected different methods.

#### 4.7.2 Simulation experiment Using BFO algorithm [43,45,46,49]

We have carried out computer simulation to validate the applicability of our implementation for image restoration. We run the algorithm using the same PC as before. The average processing time is dependent on image size and choice of BFO algorithm parameters (varies from few seconds to few minutes). Same test and real images are used for assessment with different BFO parameters as follows:

*The number of bacteria:  $s=6, 10, 20, 30, 50, 80$ ;*

*Number of chemotactic steps:  $N_c=10, 20, 30, 50, 70, 80, 100$ ;*

*Limits the length of a swim:  $N_s=10, 20, 30, 40, 50, 70, 80, 100$ ;*

*The number of reproduction steps:  $N_{re}=10, 20, 30, 40, 50, 70, 80, 100$ ;*

*The number of elimination-dispersal events:  $N_{ed}=1, 2$ ;*

*The number of bacteria reproductions (splits) per generation:  $S_r=s/2$ ;*

*The probability that each bacteria will be eliminated/dispersed:  $P_{ed}=0.25$ ;*

*The run length:  $c(i)=0.05$ ;*

There are many varying parameters on which the quality of restorations depends. Although it is very difficult and almost impossible to determine the best set of these parameters, it is very important that a reasonably effective set of these parameters is chosen, so that the deblurred image quality is accepted enough for use. In tables 4.3 and 4.4 we recorded the sensitivity of the BFO algorithm with variation parameters in terms of MSE, PSNR and objective function minimum. In Figure.15, we show the health (a) of each bacterium in ascending order and the cost function minimum (b) of each bacterium among the 20 bacteria at the 50th chemotactic step and 80th reproduction step. Restoration of a checkerboard test gray level image blurred and noised together with and without regularization constraint is presented in Figure 4.15 and Figure 4.16

Table 4.3: Sensitivity analysis for Bacterial Foraging Algorithm with varying parameters: Restoring Blurred Image with Regularization

	MSE	PSNR	Cost Function
Degraded Image	0.15	64.61	
<b>S=6</b>	<b>0.13</b>	<b>66.02</b>	<b>1.5610</b>
S=10	0.14	65.14	1.6088
S=20	0.15	64.86	1.6214
S=30	0.15	64.01	1.6641
Nc=10	0.24	60.36	6.4967
Nc=20	0.17	63.41	3.2768
Nc=30	0.15	64.65	1.9659
Nc=50	0.13	65.60	1.5910
<b>Nc=70</b>	<b>0.13</b>	<b>66.02</b>	<b>1.5175</b>
Ns=10	0.14	65.04	1.7133
Ns=20	0.14	65.40	1.6566
<b>Ns=30</b>	<b>0.13</b>	<b>66.02</b>	<b>1.5910</b>
Ns=50	0.13	66.02	1.5910
Ns=80	0.13	66.02	1.5910
Nre=10	0.31	58.31	9.3992
Nre=20	0.19	62.46	3.9219
Nre=30	0.17	63.68	2.6595
Nre=40	0.16	64.08	2.1448
Nre=50	0.14	65.52	1.7570
<b>Nre=70</b>	<b>0.13</b>	<b>66.02</b>	<b>1.5910</b>

Table 4.4: Sensitivity analysis for Bacterial Foraging Algorithm with varying parameters: Restoring Blurred/Noisy Image with Regularization

	MSE	PSNR	Cost Function
Degraded Image	0.57	52.99	
S=6	0.12	68.37	2.2035
S=10	0.12	68.44	2.2909
<b>S=20</b>	<b>0.10</b>	<b>68.75</b>	<b>2.2270</b>
S=30	0.11	68.43	2.2090
Nc=10	0.18	66.84	8.0116
Nc=20	0.12	67.67	3.2706
Nc=30	0.11	68.52	2.2263
<b>Nc=50</b>	<b>0.10</b>	<b>68.02</b>	<b>2.1670</b>
Nc=70	0.10	68.02	2.1670
Ns=10	0.11	67.53	2.6089
Ns=20	0.10	68.22	2.3635
Ns=30	0.10	67.94	2.4871
<b>Ns=50</b>	<b>0.10</b>	<b>68.52</b>	<b>2.2263</b>
Ns=80	0.10	68.52	2.2263
Nre=10	0.30	58.53	20.8247
Nre=20	0.19	62.41	9.0574
Nre=30	0.14	65.06	4.5166
Nre=50	0.10	68.28	3.0948
<b>Nre=80</b>	<b>0.09</b>	<b>68.75</b>	<b>2.2270</b>
Nre=100	0.11	67.94	2.3504

To quantitatively judge the quality of several BFO parameters combinations, we recorded in Table 4.3 and Table 4.4 both for blurred and blurred/noisy image the sensitivity of the BFO algorithm with variation parameters in terms of MSE, PSNR and objective function minimum. A full statistical analysis of these results for tuning parameters is accomplished by applying ANOVA test (analysis of variance) [32]. We use a 4-Way ANOVA with a Large Data Set (8x8, 16x16, and 64x64) and with random effects as a statistical test of whether or not the means of several groups are all equal to illustrate the statistical significance of the tuned parameters. The expected value of each mean square depends not only on the variance of the error term, but also on the variances supplied by the random effects.

ANOVA allow us to test the difference between two or more means. ANOVA does this by examining the ratio of variability between two conditions and variability within each condition. Thus, when the variability that we predict between the two groups of parameters is much greater than the variability we don't predict within each group, then we will conclude that our treatments produce different results. We consider the four groups of the four parameters. With the null



hypothesis:  $\mu_1 = \mu_2 = \mu_3 = \mu_4$ , and the alternative: at least two of the means are not equal. At the significance level equal to 0.05(5%), the critical value from the F-table is:  $F_{0.05,3,12} = 3.49$ ; and demonstrate that:  $SST = SSB + SSW$ .

SST: sum of squares total

SSB: sum of squares between the groups

SSW: sum of squares within the groups

1. With the grand mean = 0.13 (0.10 for blurred and Noisy image), first, start with taking the difference between each observation and the grand mean, and then square it for each data point, using the following formula:

$$\sum_{i=1}^4 \sum_{j=1}^{n_i} (X_{ij} - \bar{X})^2 \quad (18)$$

$X_{ij}$  : is the  $j^{\text{th}}$  data in the  $i^{\text{th}}$  experimental group

$\bar{X}$  : is the arithmetic mean all members of the four groups

$n_i$ : is number of members of the  $i^{\text{th}}$  group

2. Second, let all the data in each group have the same value as the mean in that group. This removes any variation WITHIN. Compute SS differences from the grand mean, using the following formula:

$$\sum_{i=1}^k n_i (\bar{X}_i - \bar{X})^2 \quad (19)$$

$\bar{X}_i$  : is the arithmetic mean of the  $i^{\text{th}}$  group elements

$\bar{X}$  : is the arithmetic mean all members of the four groups

$n_i$  : is number of members of the  $i^{\text{th}}$  group

3. Third, compute the SS difference within each group using their own group means. This provides SS deviation WITHIN all groups, using the following formula:

$$\sum_{i=1}^4 \sum_{j=1}^{n_i} (X_{ij} - \bar{X}_i)^2 \quad (20)$$

$X_{ij}$  : is the  $j^{\text{th}}$  data in the  $i^{\text{th}}$  experimental group

$\bar{X}_i$  : is the arithmetic mean of the  $i^{\text{th}}$  group elements

$n_i$  : is number of members of the  $i^{\text{th}}$  group

4. Now, we construct the ANOVA Tables, 4.5 and 4.6 by plugging the results of computation. Note that, the Mean Squares are the Sum of squares divided by their Degrees of Freedom. F-statistics is the ratio of the two Mean Squares.

5. Conclusion: the T-statistics is less than the critical value, so there is not enough evidence to reject the null hypothesis.

Table 4.5: The ANOVA TABLE for Restoring Blurred Image with Regularization

The ANOVA Table				
Sources of Variation	Sum of Squares	Degrees of Freedom	Mean Squares	F-Statistic
Between Groups	0.123	3	0.041	2.226
Within Groups	0.221	12	0.0184	
Total	0.344	15		

Table 4.6: The ANOVA TABLE for Restoring Blurred/Noisy Image with Regularization

The ANOVA Table				
Sources of Variation	Sum of Squares	Degrees of Freedom	Mean Squares	F-Statistic
Between Groups	0.141	3	0.0470	3.065
Within Groups	0.184	12	0.0153	
Total	0.325	15		

We can select the best bacterial foraging parameters both for blurred images in Table 4.7, and blurred/noisy images in Table 4.8. This selection is based on a compromise between restored image quality and expense in terms of both time and computational resources. For example, in blurred/noisy images, if we choose the bacteria size  $S=30$ , we get better cost function and minimum MSE, but this had to be achieved at the expense of more computational complexity. After fixing  $S=20$ , we change  $N_c$  to reach the cost function minimum found before, i.e. with the

same computational resources. After fixing  $S=20$  and  $N_c=50$ , we increase  $N_s$  until stable values of MSE, PSNR and cost function minimum;  $N_s$  is found to be 50.

The rest parameters are also selected following similar logic.

Table 4.7: Best BFO parameters for restoring blurred images with regularization (Best Regularization parameter is 0.01)

BFO Parameters	Values
S	6
$N_c$	70
$N_s$	30
$N_{re}$	70
$N_{ed}$	1
$S_r$	$S/2 = 3$

Table 4.8: Best BFO parameters for restoring blurred/Noisy images with regularization (Best Regularization parameter is 0.01)

BFO Parameters	Values
S	20
$N_c$	50
$N_s$	50
$N_{re}$	80
$N_{ed}$	1
$S_r$	$S/2 = 10$

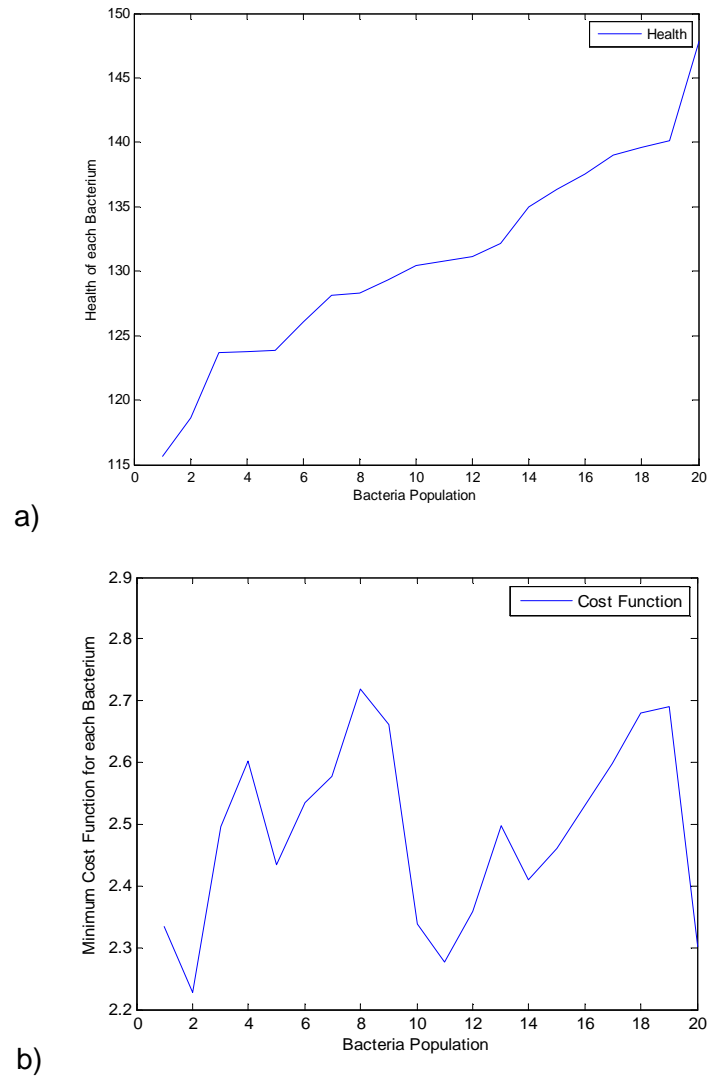


Figure.4.14: a) Health of each Bacterium in Ascending Order, b) Minimum Cost function for each Bacterium

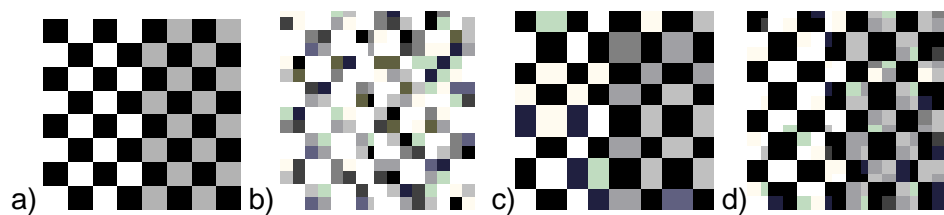


Figure.4.15: Restoration of Blurred with Noise Images without Regularization Constraint: a) Original, b) Blurred, c) Restored with  $p=8 \times 8$  d) Restored with  $p=16 \times 16$

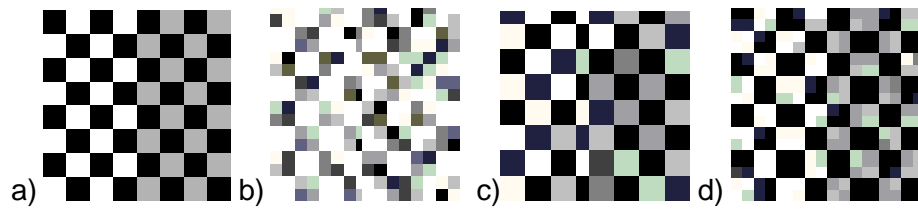


Figure.4.16: Restoration of Blurred with Noise Images with Regularization Constraint: a) Original, b) Blurred, c) Restored with  $p=8 \times 8$  d) Restored with  $p=16 \times 16$

#### 4.7.3 Simulation experiment Using hybrid implementation (BFO-PSO) [48,50]

This hybridization improved the convergence speed and accuracy of solutions got by classical BFO, however, what is requested in image restoration is attaining a best approach to the original image by finding the best solution, which is accomplished by a hybrid implementation of BFO-PSO.

Fig.4.18 and Table 4.9 compare the three algorithms, PSO, BFO, Hybrid BFO-PSO, on quality of the optimum restoration results using the same image and the same degradation function. The PSNR progress, chosen as an image quality metric, throughout chemotactic steps increase reveals the good choice of such scheme, Fig.4.19 and Table 4.10.

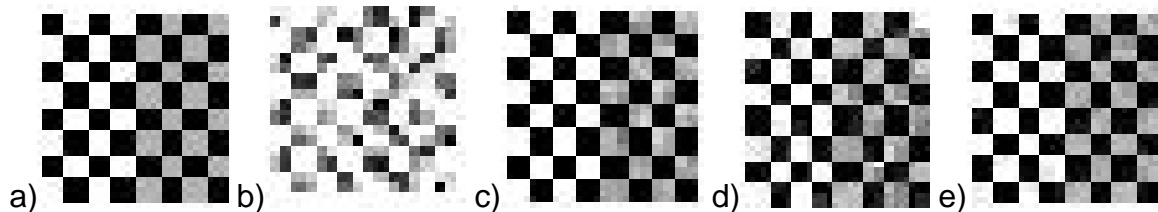


Figure.4.17: Restoration of Blurred/Noisy images: a)Original, b)Blurred, c)With PSO, d)With BFO, e)With hybrid BFO-PSO

Table 4.9: RMSE and PSNR values of the three Algorithms reached with the identical computation time and population size

	<b>Blurred</b>	<b>Restored with PSO</b>	<b>Restored with BFO</b>	<b>Restored with Hybrid</b>
<b>RMSE</b>	0.57	0.05	0.09	0.04
<b>PSNR</b>	52.99dB	75.01dB	68.68dB.	75.50dB

Table 4.10: PSNR progress with increasing number of bacteria, chemotactic and reproduction steps

PSNR	
Classical BFO	Synergy of BFO and PSO
54.21	54.18
54.55	54.78
54.62	54.83
54.75	55.26
55.25	55.75
56.06	56.89
65.53	68.30
68.68	75.50

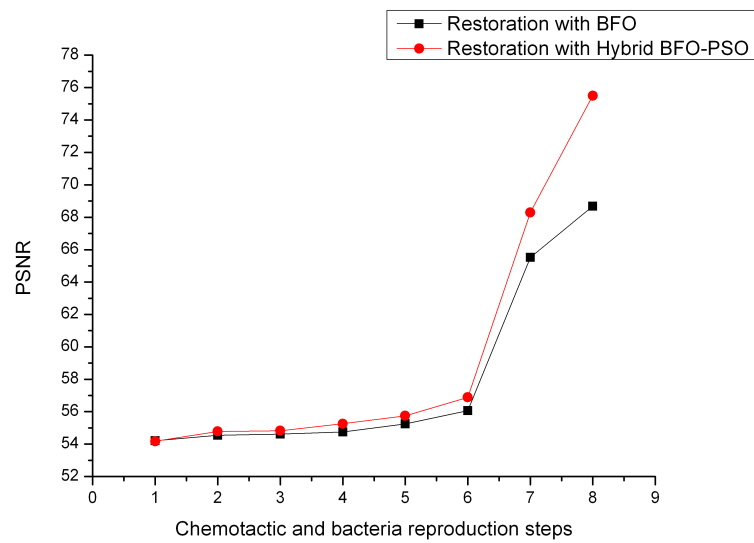


Figure.4.18: PSNR progress with increasing number of bacteria, chemotactic and reproduction steps

#### 4.7.4. Blind Restoration Using Hybrid Swarm Optimized ARMA-Neural Network Model:

##### 4.7.4.1. Image Degradation Representation by ARMA Model

An image can be considered to be a sample function of random variables array. This characterization of an ensemble of images is useful in developing image processing techniques that are valid for an entire class and not just for an individual image. Two dimensional linear stochastic systems led to the modeling of blurred image as an (ARMA) process, where (AR) part determines the image model coefficients and (MA) part determines the blur function of the system [21]. Therefore, blind image deconvolution is transformed into an ARMA parameter estimation problem. Identifying the ARMA parameters allows us to identify the true image and the degradation function. This task can be achieved using neural networks [22] trained with classical optimization Algorithms that have the drawbacks of ill-convergence to local minima and sensitivity to initial conditions.

The true image is modeled as a two-dimensional (AR) process represented by:

$$f(x, y) = \sum_{\substack{(l,m) \in R_a \\ (l,m) \in (0,0)}} a(l, m) f(x-l, y-m) + v(x, y) \quad (21)$$

$f(x,y)$  is the true image, and  $v(x,y)$  is the modelling error which is a zero-mean homogeneous noise process which is statistically independent of  $f(x,y)$ . Using matrix-vector notation, (21) can be written as:

$$f = Af + v \quad (22)$$

For smooth and homogeneous true images (as in photography), only three AR coefficients  $\{a(0, l), a(1,0), a(1,l)\}$  are sufficient to reasonably model the image. In most practical situations, the blurring function is of finite extent and its effect on the true image can be modeled as that of a two-dimensional FIR filter. The linear degradation model can be written:

$$g(x, y) = f(x, y) \otimes h(x, y) + \eta(x, y) \quad (23)$$

Where the degradation function is  $h(x, y)$ , and  $\eta(x, y)$  is the additive noise of the imaging system assumed to be zero-mean Gaussian. The degraded image  $g(x, y)$  can be expressed as:

$$g(x, y) = \sum_{(l,m) \in R_h} h(l, m) f(x-l, y-m) + \eta(x, y) \quad (24)$$

Using matrix-vector notation, equation (4) becomes:

$$g = Hf + \eta \quad (25)$$

Rearranging equation (2), substituting into equation (25) and rearranging yields:

$$g = H(I - A)^{-1}v + \eta \quad (26)$$

Where  $I$  is the identity matrix

A complete model for the blurred image using equation (26) is given in Fig.4.19, where capital letters denote the Z-transforms of their lowercase counterparts. Therefore, the problem of blind deconvolution consists of estimating the AR parameters:  $a(l, m)$  for  $(l, m) \in R_a$ , and the MA parameters:  $h(l, m)$  for  $(l, m) \in R_h$

Once the blurring function  $h(l, m)$  is determined, one of the classical linear image restoration methods can be used to estimate the true image.

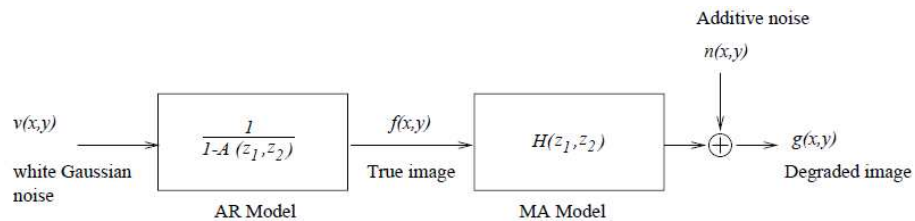


Figure.4.19: ARMA Model of the degraded image

The practical difficulties with estimating  $\{a(l, m), h(l, m)\}$  using equation (26) include high computational complexity with large support, instability of the estimation algorithms, and non-unique solutions. To overcome these problems, the following additional assumptions are commonly made on the blurring function by existing second-order statistics methods.

1. The blurring function is positive, and the mean value of the true image is preserved in the degradation process. That is:  $\sum_{(l, m) \in R_h} h(l, m) = 1$ . The use of these assumptions limits the number of possible ambiguous solutions to the problem.
2. The blurring function is symmetric and zero-phase. These assumptions are made for the stability and the uniqueness of solution of the estimation algorithms.
3. The blurring function has a known parametric form consisting of only a few parameters. Use of such models significantly lowers the computational complexity.



#### 4.7.4.2. ARMA Neural Network modelling

A neural network (NN) is a parallel and distributed network of simple nonlinear processing units interconnected in a layered arrangement. Parallelism, modularity and dynamic adaptation are three computational characteristics typically associated with NN's. The multi-layer perceptron (MLP) consists of various layers: an input and output ones between which lay one or several hidden ones whose outputs are not observable, Fig.4.20:

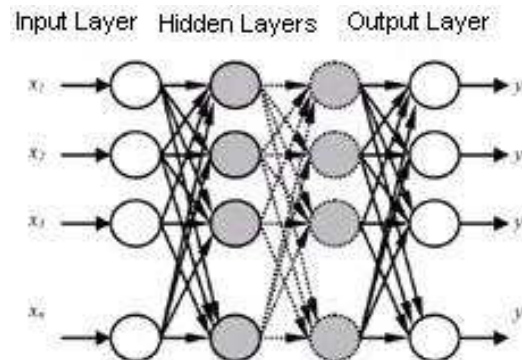


Figure.4.20: Schematic diagram of a multi-layer feed-forward NN

These layers are based upon some processing units (neurons) interconnected by means of feed-forward pondered links. Fig.4.21:

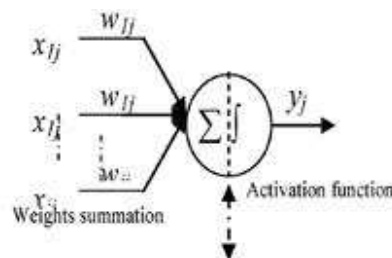


Figure.4.21: Information processing in a NN unit

All these processing units carry out the same operation: the sum of their weighted inputs, equation (27). Then they apply the result to a non-linear function named activation function and generally based upon the sigmoid function, equation (28):

$$y_j = \left[ \left( \sum_i w_{ij} \cdot x_{ij} \right) - b_j \right] \quad (27)$$

$$f(x) = \frac{1}{(1 + e^{-x})} \quad (28)$$

Where  $y_j$  is the output of the processing unit,  $w_{ij}$  are the synaptic weight coefficients and  $b_j$  is the bias

Back-propagation (BP) has been widely adopted as a successful learning rule to find the appropriate values of NN weights. Using the hybrid implementation (PSO-BFO), each bacterium (or particle) position vector is defined by all connecting weights matrix  $w_{ij}$ . The fitness value of each bacterium is the value of the error function evaluated at this position. To achieve the same error goal both with back-propagation (BP) and Hybrid swarm algorithms, we find that the Hybrid PSO-BFO implementation requires less number of computations; which is an observed performance.

For our application, a multi-layer NN structure trained using a hybrid swarm implementation, to minimize the mean squares of errors function in the NN, is used to represent the ARMA model for identifying the blur function and restore the degraded image, simultaneously. The main difficulty in our approach is to learn correctly the perceptron because the learning sets are very large (about 100 examples), Fig.4.22. We developed a (MLP) with 3x3 input/output dimensions and two hidden layers, Fig.4.23. Also the swarm optimization algorithm parameters must be chosen carefully. The input of the NN model is a white Gaussian noise and the output of the last layer is the observed degraded image. The output of the second layer is the estimated original image and the weights between the third and the output layers represent the blurring function.

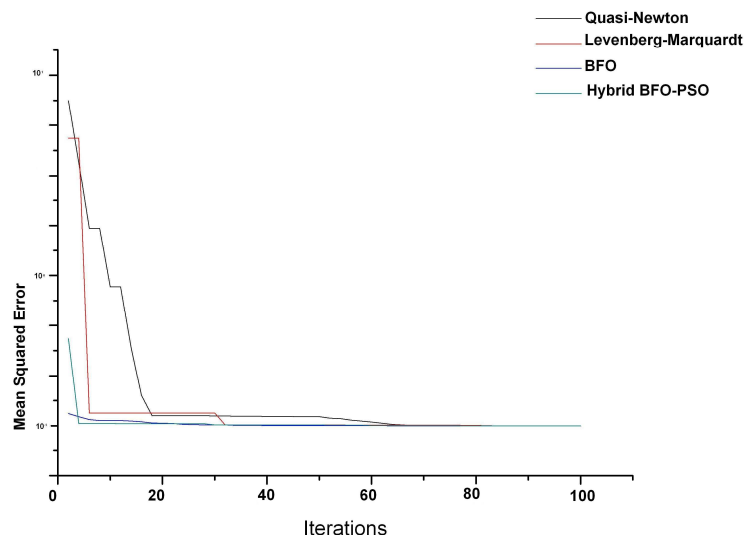


Figure.4.22: Comparison between Different Learning Algorithms using MSE Evolution

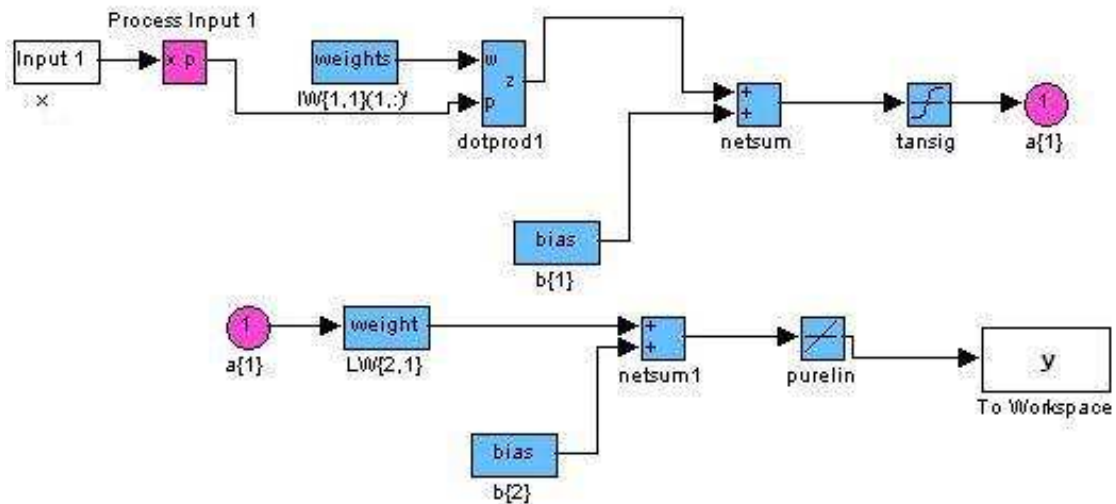


Figure.4.23: The resultant Simulated Neural Network on Matlab/Simulink

In our simulation we use gray scale images with size of 256x256 pixels and 256 gray-levels. Some practical simulation results are given below. Before application to radiological images, we launch a step by step assessment procedure of our model using some test images restoration. Fig.6 shows a comparison between the classical blind iterative deconvolution (BID) that maximizes the likelihood using an iterative process and restoration via the optimized ARMA-NN model. The reference images, used also for comparison, are two text images and one generated by the MATLAB function '*checkerboard*'. The last reference image contains all gray levels (from 0 to 255). The original image in Fig. 4.24(a) is blurred by 5x5 Gaussian blur and Gaussian noise with 10dB was added to the blurred image of Fig.4.24(b). Restoration results presented in Fig.4.24(c) and (d), reveal that the proposed approach gives a better image estimate than the (BID) method.

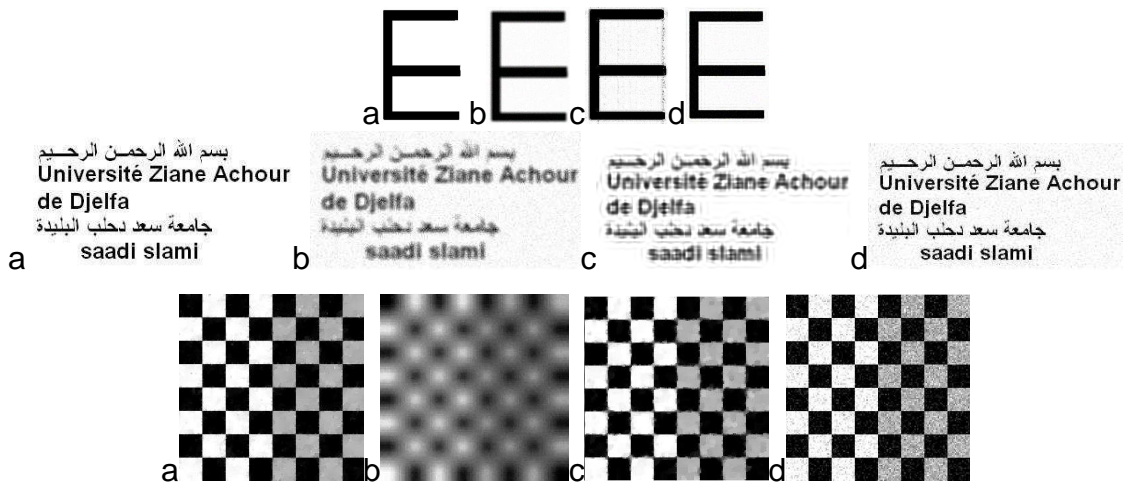


Figure.4.24: a)Original image, b)Blurred image, c)Restored image with iterative blind deconvolution algorithm, d)Restored with the ARMA-NN model

#### 4.7.4.3. Application to Radiological Images:

Medical radiology offers many good techniques helping doctors in their diseases diagnosis work and also it is widely used in medical research. Radiological images used here are gathered from radiological databases. Five images of different types are selected for experimentation to validate the proposed model, Fig.4.25.

Some image quality measures are calculated for all restored images with reference to their original images. To extend tests, a set of six tables and seven graphs are constructed below, Fig.4.26-32. The implemented image quality measures are defined using the following expressions:

$$1. \text{ Mean Square Error (MSE): } MSE = \frac{1}{MN} \sum_{j=1}^M \sum_{k=1}^N (x_{j,k} - x'_{j,k})^2$$

$$2. \text{ Peak Signal to Noise Ratio (PSNR in dB): } PSNR = 10 \log \frac{(2^n - 1)^2}{MSE} = 10 \log \frac{255^2}{MSE}$$

$$3. \text{ Normalized Cross-Correlation (NCC): } NK = \frac{\sum_{j=1}^M \sum_{k=1}^N x_{j,k} \cdot x'_{j,k}}{\sum_{j=1}^M \sum_{k=1}^N x_{j,k}^2}$$

$$4. \text{ Average Difference (AD): } AD = \sum_{j=1}^M \sum_{k=1}^N \frac{(x_{j,k} - x'_{j,k})}{MN}$$

5. Structural Content (SC): 
$$SC = \frac{\sum_{j=1}^M \sum_{k=1}^N x_{j,k}^2}{\sum_{j=1}^M \sum_{k=1}^N x_{j,k}'^2}$$

6. Maximum Difference (MD): 
$$MD = \text{Max}(|x_{j,k} - x_{j,k}'|)$$

7. Normalized Absolute Error (NAE): 
$$NAE = \frac{\sum_{j=1}^M \sum_{k=1}^N |x_{j,k} - x_{j,k}'|}{\sum_{j=1}^M \sum_{k=1}^N |x_{j,k}|}$$

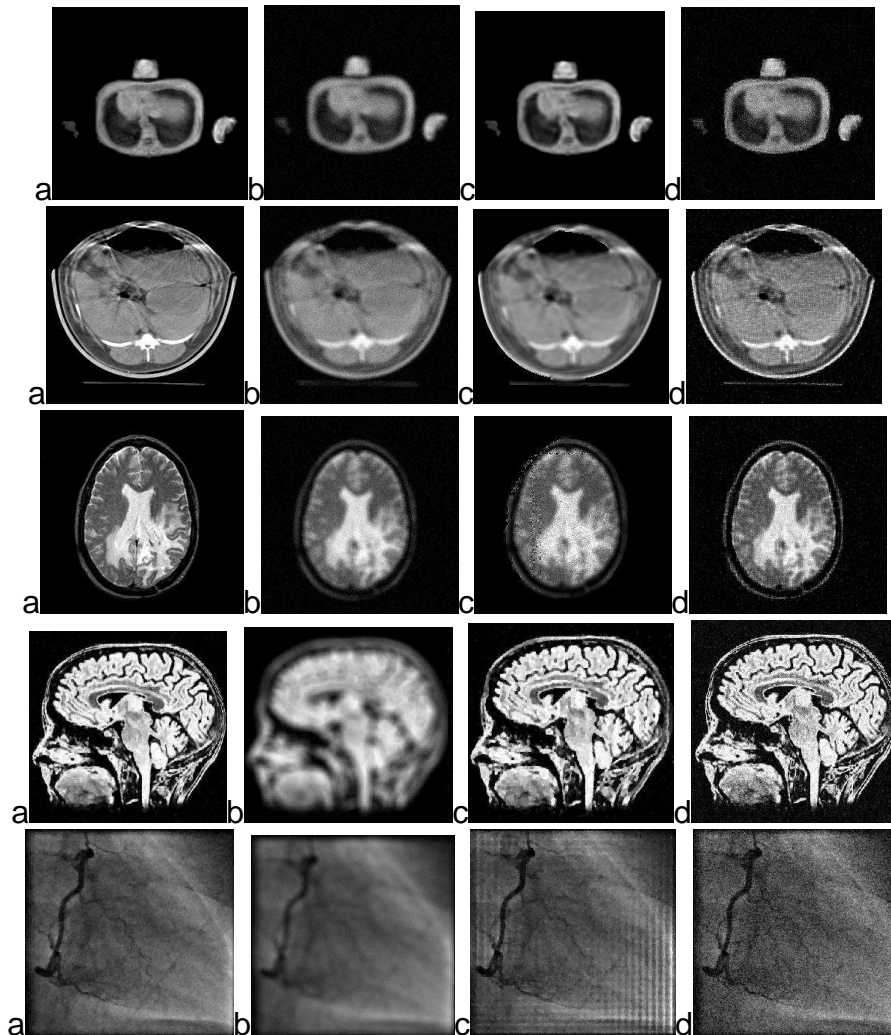


Figure.4.25: a)Original image, b)blurred image, c)restored image with iterative blind deconvolution algorithm, d)restored with the ARMA-NN model

Table 4.11: Image metrics for the checkerboard image

	Degraded Image	Restored with BID	Restored with: ARMA-NN model
Mean Square Error	6.7657e+003	2.2163e+003	1.8347e+003
Peak Signal to Noise Ratio	9.8277	14.6746	15.4951
Normalized Cross-Correlation	0.6518	0.9488	0.9597
Average Difference	-0.5576	-2.4622	-2.8398
Structural Content	1.6781	1.0048	1.0237
Maximum Difference	255	152	149
Normalized Absolute Error	0.7074	0.1805	0.1863

Table 4.12: Image metrics for the first x-ray image

	Degraded Image	Restored with BID	Restored with: ARMA-NN model
Mean Square Error	675.6993	535.6264	360.4974
Peak Signal to Noise Ratio	19.8333	20.8422	22.5618
Normalized Cross-Correlation	0.9316	0.9257	0.9727
Average Difference	0.2043	-1.1556	-1.6216
Structural Content	1.0656	1.0976	1.0146
Maximum Difference	189	188	149
Normalized Absolute Error	0.1843	0.2042	0.1833

Table 4.13: Image metrics for the second x-ray image

	Degraded Image	Restored with BID	Restored with: ARMA-NN model
Mean Square Error	158.2443	75.0939	12.4176
Peak Signal to Noise Ratio	26.1375	29.3748	37.1904
Normalized Cross-Correlation	0.9820	0.9539	0.9954
Average Difference	-2.8710	-2.2942	0.0352
Structural Content	0.9805	1.0704	1.0048
Maximum Difference	149	130	51
Normalized Absolute Error	0.3183	0.2359	0.0556

Table 4.14: Image metrics for the magnetic resonance image

	Degraded Image	Restored with BID	Restored with: ARMA-NN model
Mean Square Error	801.1238	265.2525	263.7717
Peak Signal to Noise Ratio	19.0938	23.8942	23.9185
Normalized Cross-Correlation	0.9156	0.9500	0.9802
Average Difference	0.5833	-1.7516	-2.4985
Structural Content	1.0480	1.0630	0.9992
Maximum Difference	255	148	142
Normalized Absolute Error	0.3130	0.2191	0.2254

Table 4.15: Image metrics for the brain image

	Degraded Image	Restored with BID	Restored with: ARMA-NN model
Mean Square Error	3.9938e+003	3.0085e+003	1.3441e+003
Peak Signal to Noise Ratio	12.1169	13.3473	16.8464
Normalized Cross-Correlation	0.9028	0.8235	0.9594
Average Difference	-2.9687	0.9376	0.2043
Structural Content	0.9846	1.2418	1.0106
Maximum Difference	255	246	210
Normalized Absolute Error	0.4029	0.3876	0.2102

Table 4.16: Image metrics for the blood vessel image

	Degraded Image	Restored with BID	Restored with: ARMA-NN model
Mean Square Error	761.1953	381.9748	61.0878
Peak Signal to Noise Ratio	19.3158	22.3105	30.2713
Normalized Cross-Correlation	0.9978	0.9939	0.9865
Average Difference	-0.5042	-1.2890	0.4166
Structural Content	0.9141	0.9641	1.0194
Maximum Difference	147	122	51
Normalized Absolute Error	0.2660	0.1616	0.0690

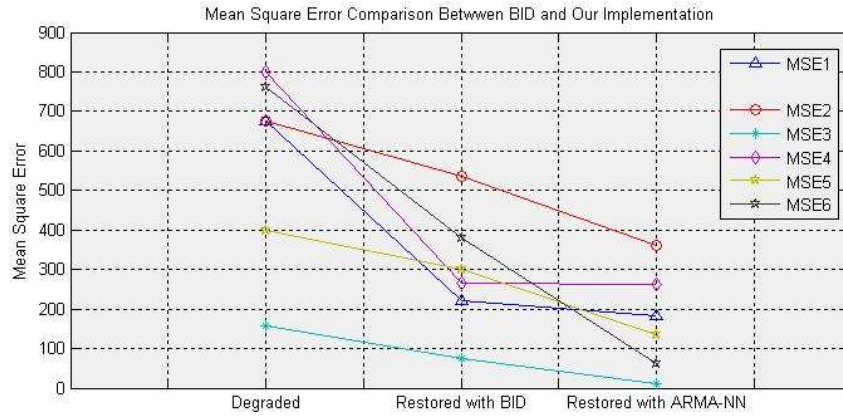


Figure.4.26: Mean Square Error Comparison Between classical BID and ARMA-NN Model

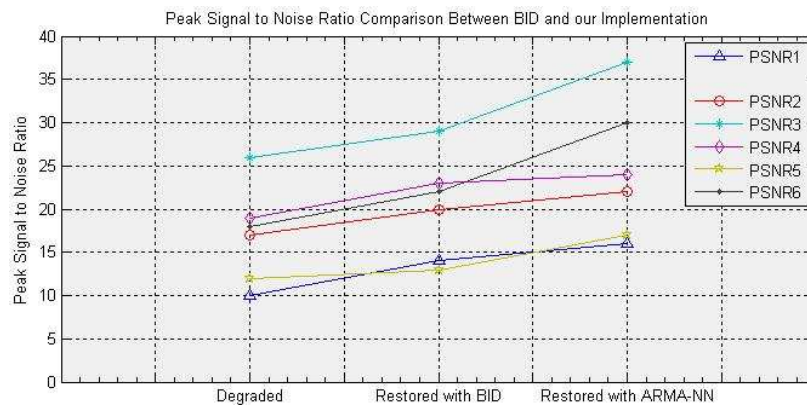


Figure.4.27: Peak Signal to Noise Ratio Comparison Between classical BID and ARMA-NN Model

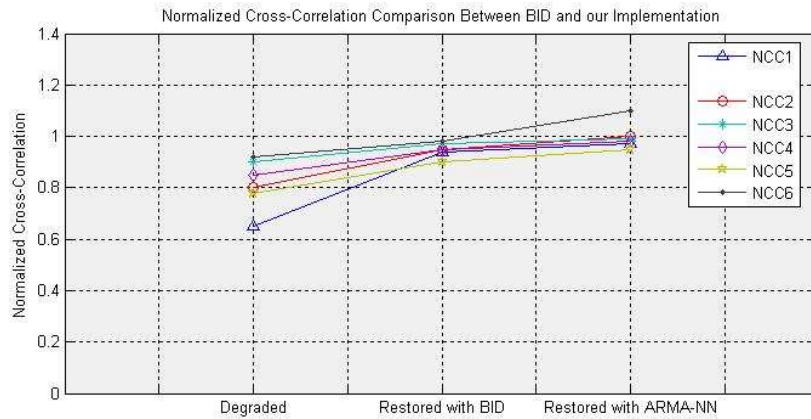


Figure.4.28: Normalized Cross-Correlation Comparison Between classical BID and ARMA-NN Model



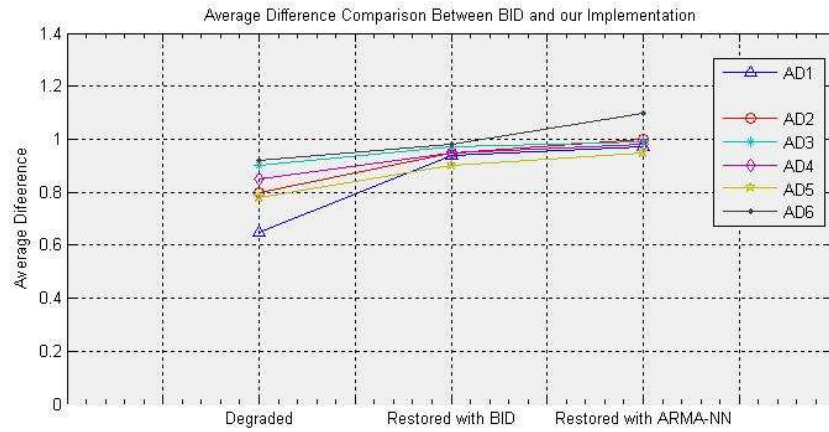


Figure.4.29: Average Difference Comparison Between classical BID and ARMA-NN Model

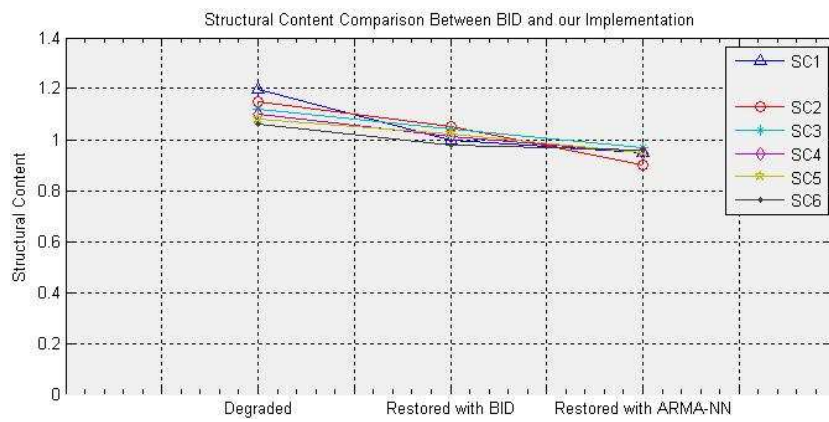


Figure.4.30: Structural Content Comparison Between classical BID and ARMA-NN Model

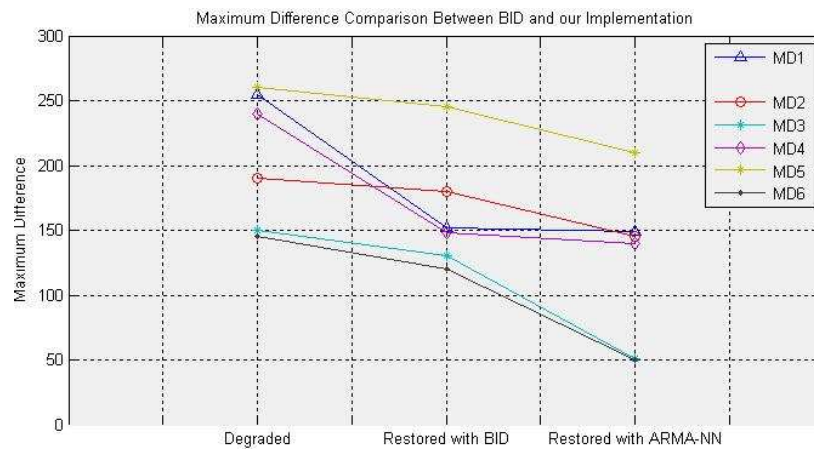


Figure.4.31: Maximum Difference Comparison Between classical BID and ARMA-NN Model

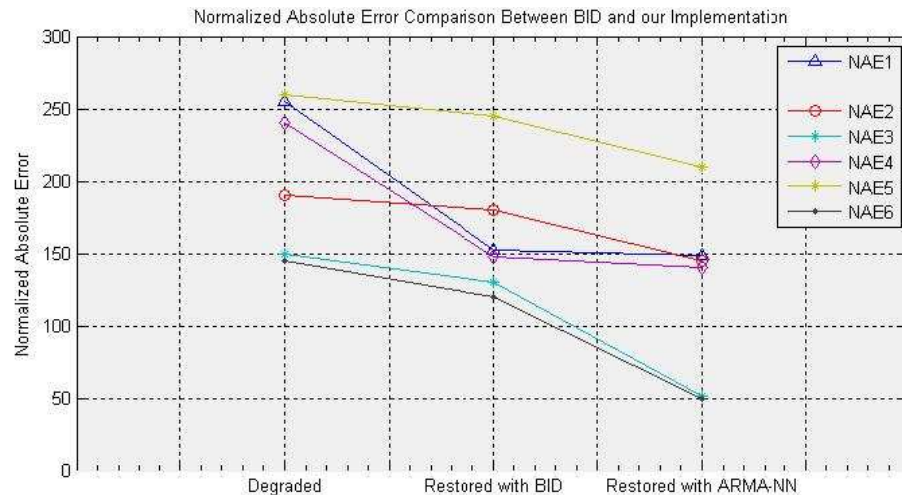


Figure.4.32: Normalized Absolute Error Comparison Between classical BID and ARMA-NN Model

From images visual inspection with numerical evaluation from Figures: 4.26-32, we can judge that the PSNR is a little enhanced using the proposed model compared to standard (BID). The performance of this approach for restoring radiological images degraded by Gaussian and motion blur and an additive noise is revealed from experiments performed on some database images. Although the performance is demonstrated for such images, the proposed approach can be used to restore others images degraded with the same blurring function. In the future, we will try to implement models for other known blurring functions encountered in radiological images to further improve the performance.

#### 4.7.5. Comparison with other methods

In the following, Table 4.11 and Fig.4.33, we have selected four best methods used for image and signal restoration: Truncated Singular Value Decomposition (TSVD), Tikhonov regularization, normalized Tikhonov in Sobolev space and Total Variation (TV) regularization solved with iterative recursive least squares method. For TSVD, the truncation parameter used in simulation is  $4e-3$ .

Tikhonov regularization used here is feasible by direct computation for such inverse problem using the Kronecker product structure, regularization parameter found as the used in simulation is  $4e-5$ . The second Tikhonov regularization is an approximation of the popular Sobolev seminorm penalization, regularization

parameter found as the best used in simulation is  $1e-5$ . In (TV), regularization parameter found as the used in simulation is  $1e-3$ .

Finally, in solving TV regularization problem using swarm intelligence, the regularization parameter found as the used in simulation is  $1e-3$ .

To get rid of impulse noise, it is found that the hybrid implementation of BFO and PSO (with and without regularization) can offer good quality results compared to the enhanced median filter and the soft heuristic SURE thresholding in wavelet decomposition, Fig.4.34. The recent split Bregman approach seems to be a good choice.

Table 4.17: Quality comparison based on RMSE and PSNR values between the best four methods and the proposed Swarm Intelligence Algorithms

	RMSE	PSNR
Blurred	0.57	52.99dB
TSVD Restoration	0.08	69.86
Tikhonov Restoration	0.06	71.92
Tikhonov (sobolev) Restoration	0.12	66.83
TV Regularization Iterative LS Restoration	0.24	60.41
PSO Restoration	0.05	74.01dB
BFO Restoration	0.09	68.68dB
Hybrid BFO-PSO Restoration	0.04	75.50dB

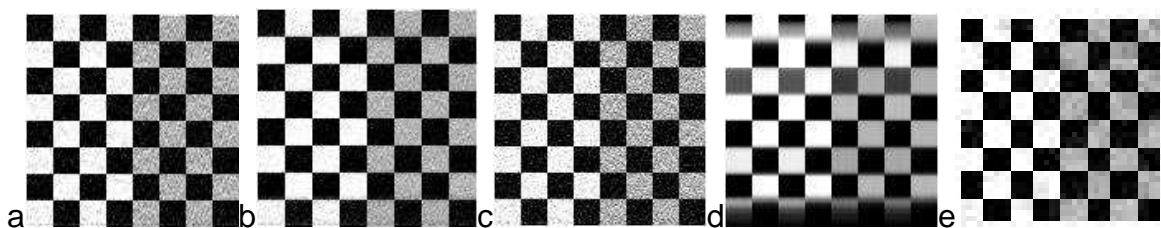


Figure.4.33: Quality comparison between the best four methods (TSVD, Tikhonov regularization, Tikhonov in Sobolev space and TV regularization solved with iterative method) and the Hybrid Algorithms BFO-PSO

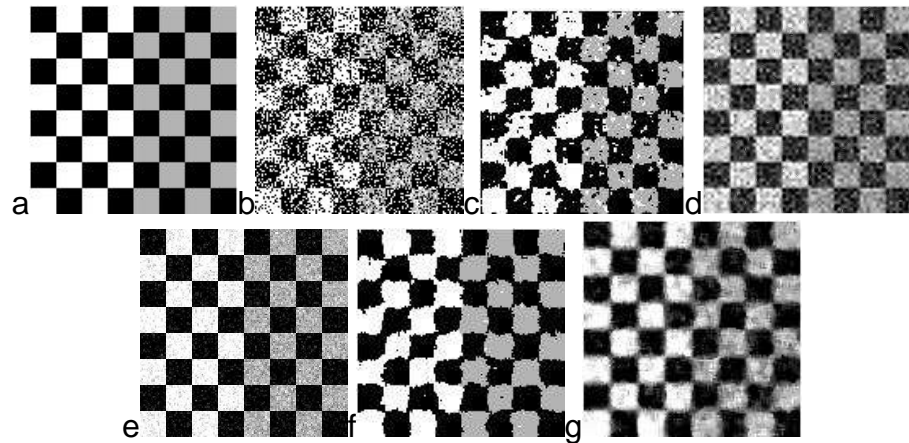


Fig.4.34: a) original, b) stained with impulse noise, c) restored with median Filter, d) with soft heuristic SURE thresholding in wavelet decomposition, e) with split Bregman denoise, f) with hybrid BFO-PSO, g) with regularized hybrid BFO-PSO

#### 4.7.6 Application to Neutron Radiography Images Restoration:

Digital radiological image is a digital image acquired by a certain radiological procedure which can be X-rays, gamma camera, nuclear magnetic resonance or neutron radiography. It is a two-dimensional  $M \times N$  array of non-negative integers (gray levels). For neutron radiography, Fig.4.35, the gray level value represents the relative linear attenuation coefficient of the object. Each of these gray images has 8-bit representations of their intensity levels. Hence, there are 256 gray levels. Degradations in this imaging technique are essentially due to bad situation with respect to randomly distributed neutron flux causing dissimilarity in images taken for the same object, in addition to the presence of gamma radiations causing additive noises.

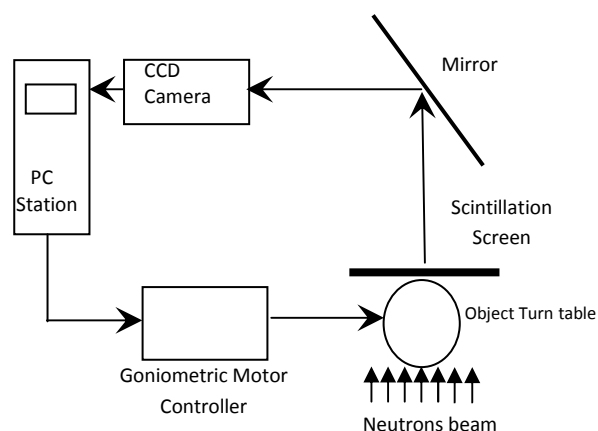


Figure.4.35: Neutron Imaging System

In order to evaluate the performance of the proposed approaches when applied to neutron radiography images, we make use of corrupted images due to degradation (neutron flux perturbation) and additive noise (gamma radiations) taken by neutron radiography in a hostile site. Computer simulations prove that PSO, BFO algorithms, Fig.4.36 and 37; in addition to their Synergy of them, yield excellent results and present good efficiency in neutron images restoration, as illustrated in Figures.4.38, 4.39, 4.40 and Table 4.12.

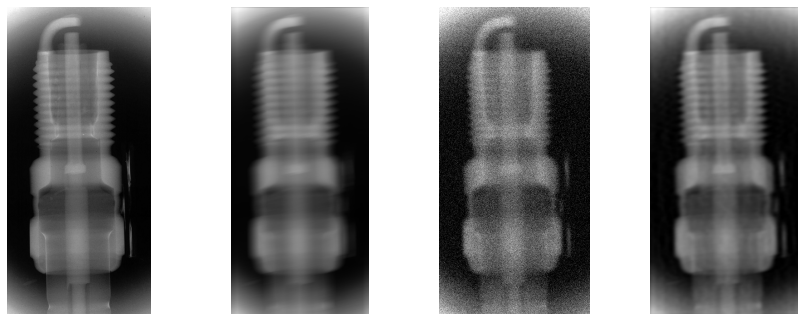


Figure.4.36: Neutron Radiography Image restoration using PSO: a)Original, b)blurred, c)Blurred/Noisy, d)Restored Image with PSO

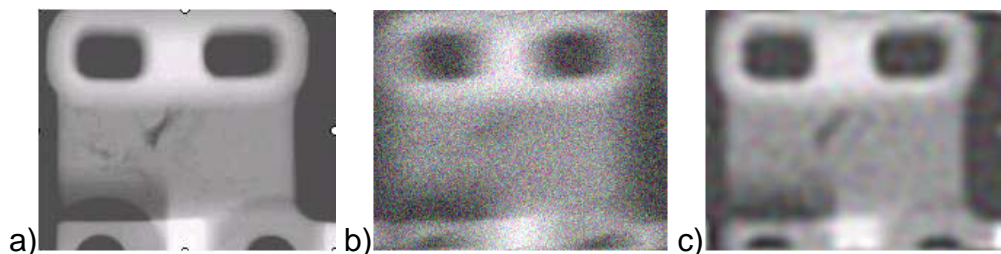


Figure.4.37: Neutron Radiography Image Restoration: a)Original, b)Blurred/Noisy, c)Restored image with BFO

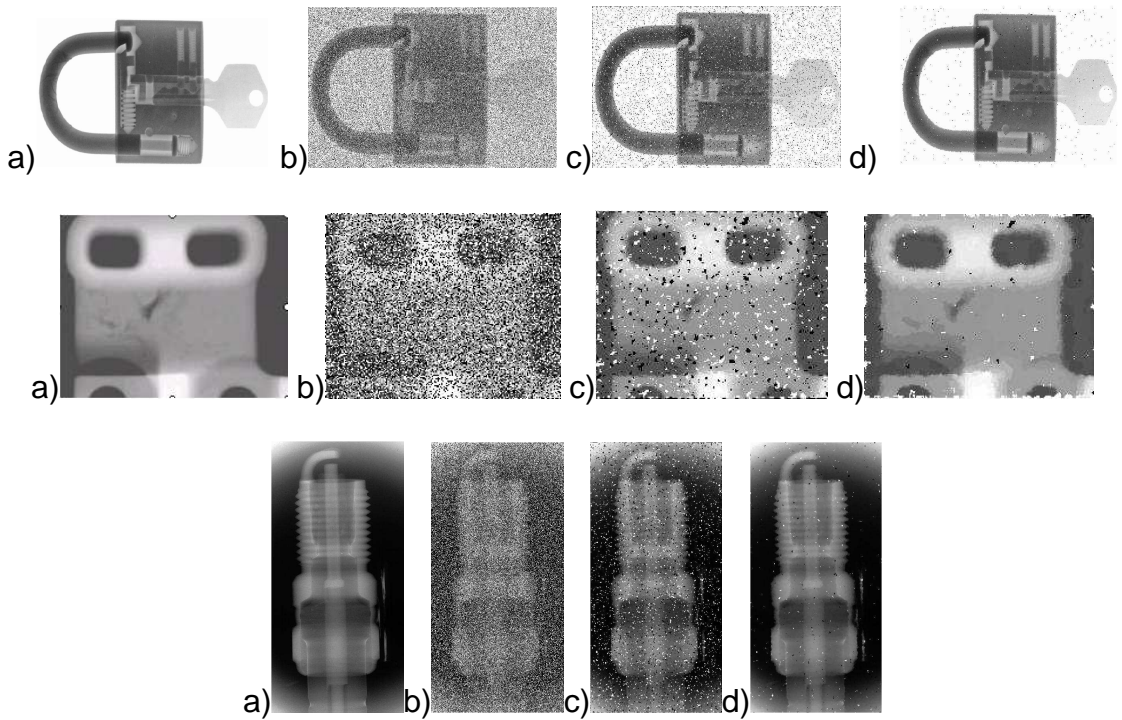


Fig.4.38: a) original image, b) with added noise, c) using median filter, d) using hybrid BFO-PSO

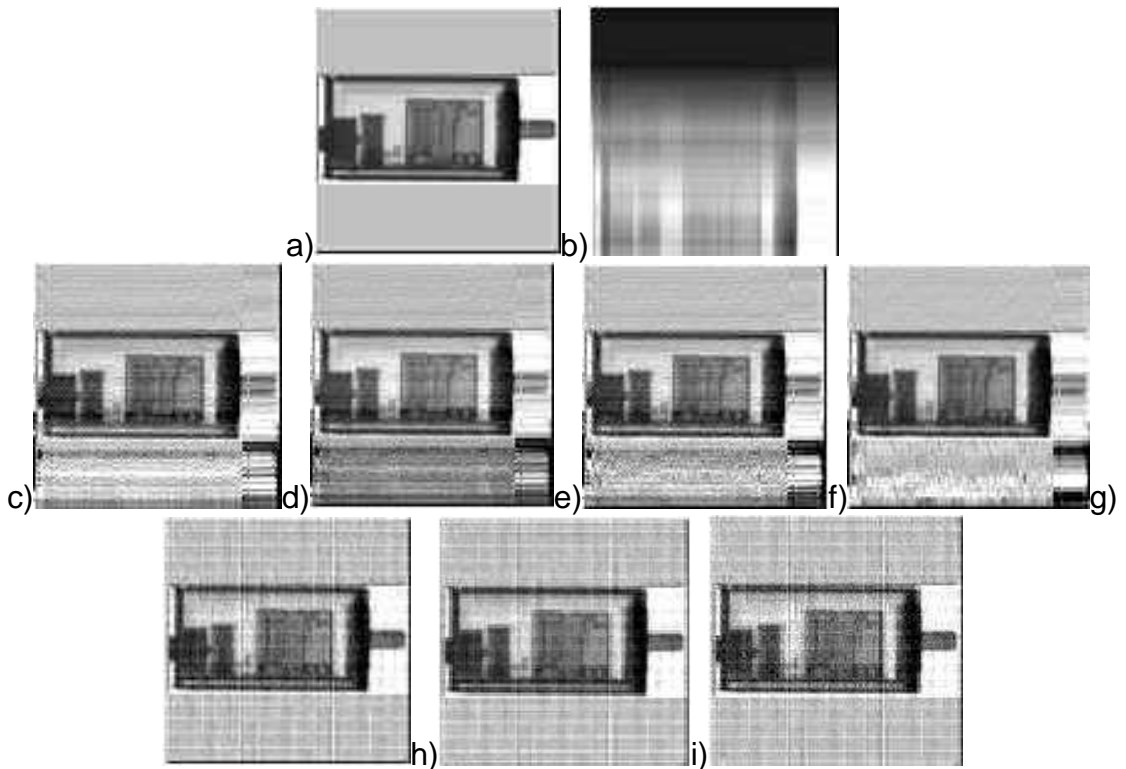


Figure.4.39: a)Original image of an electrical relay, b) Hardly motion blurred image, c)TSVD, d)Tikhonov regularization, e)Tikhonov (sobolev), f)TV regularization, g) Restored with PSO, h)Restored with BFO, i) restores with BFO-PSO Synergy

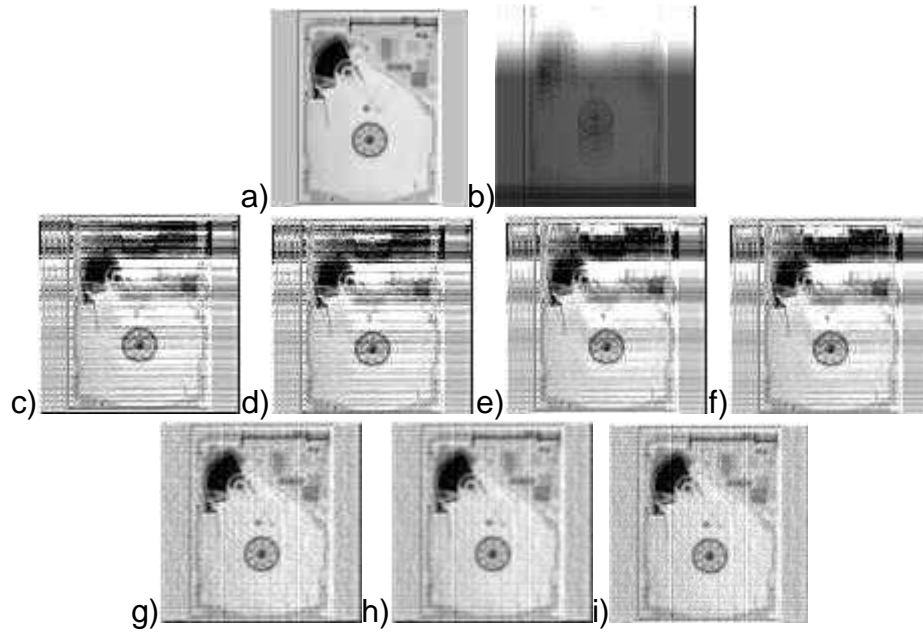

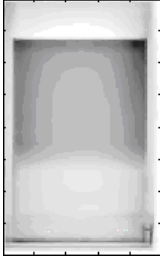






Figure.4.40: a) Original image of computer hard disk, b) Hardly motion blurred image, c) Restored with TSVD, d) Restored with Tikhonov regularization, e) Restored with Tikhonov (sobolev), f) Restored with TV regularization, g) Restored with PSO, h) Restored with BFO, i) restores with BFO-PSO Synergy

Table 4.18: Regularized Neutron Radiography Image Restoration with Hybrid BFO-PSO of mixing light water (H<sub>2</sub>O) and heavy water (D<sub>2</sub>O)

Original Image	Blurred Image	Restored Image
		
		

4.7.7. Some examples of image denoising and deblurring using PSO and BFO

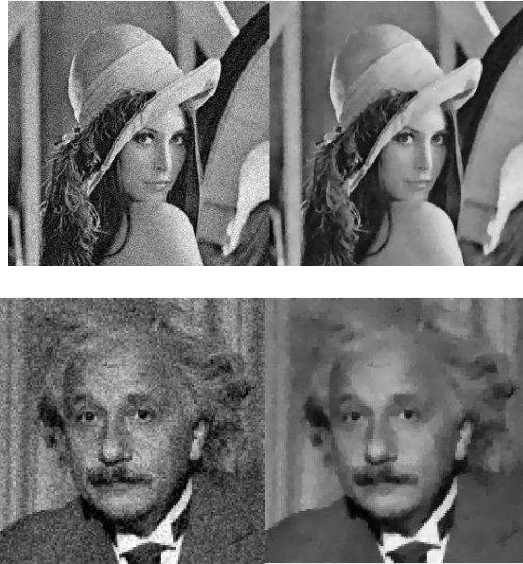


Figure.4.41: Gaussian Noise removal using (TV) Swarm Optimization

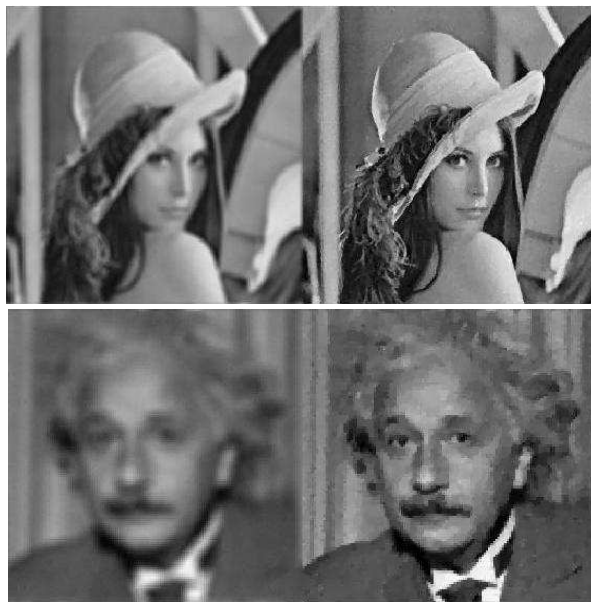


Figure.4.42: Image deblurring using (TV) Swarm Optimization



#### 4.8 Conclusion:

In our experiments, the proposed swarm methods always converges to acceptable results, from a quality point of view, with the computation time proportional to the matrix (image) size. Different types of blurring and noises are tested with the optimal regularization parameter  $\lambda$  chosen based on many trials and PSNR progress. Numerical results show that these methods are promising for many image restoration applications. We remark also that using TSVD as a direct method, the computed restorations are comparable to iterative methods but are computationally less expensive. However in Swarm Intelligence methods, we can obtain a closer approximation of the true image with very good RMSE and PSNR compared to the other existing methods; the number of iterations is a little larger and requires long computation time which merits further research, and regularization deserves a rigorous study to attain better results.

## CONCLUSIONS AND FUTURE WORK

In this thesis, we have introduced Swarm intelligence optimization algorithms in image restoration to solve the ill-posed inverse problem based on total variations (TV) approach that deals with the problem of minimizing a combination of a residue norm (one-norm) and regularization for the the Laplacian constraint has been used to smooth deblurred images in the presence of noise.

Different types of blurring and noises have been tested with optimal regularization parameter  $\lambda$  chosen based on many trials and PSNR progress through algorithms balancing parameters. Numerical results show that these methods are promising for many image restoration applications. To achieve further improvements in visual quality, intensive research is needed that could significantly improve performance in practical applications. We can not say that our proposed solutions are the best but they can be considered as additional solutions to former ones.

In the light of this thesis, we conclude that Total Variation algorithms combined with swarm intelligence algorithms is capable of restoring images from data with noise. According to our experiments, this is even good solution for gray level neutron radiography images taken in a hostile medium due to neutron flux non linearity and presence of gamma radiations. We can judge that such methods always converges to acceptable results, we obtained a closed approximation to the true image with good PSNR compared to the strong existing methods, from quality point of view. The computation time is a little larger and proportional to matrix (image) size which merits further investigation; also regularization deserves a rigorous study to attain better results.

The new approach that combines two swarm algorithms appears to be promising as we stated before, but more investigations need to be undertaken on all swarm methods in order to take advantage of each method in a hybrid implementation. This will be our subject of research to enhance results in many applications, in addition to reducing computation time with maintaining restoration quality by implementation on real time devices, and digital signal processors are certainly valid alternatives.

The ARMA (autoregressive moving average) model used for the non linearly degraded image deconvolution, which is identified using a fast trained neural network by a hybrid implementation of the two swarm algorithms: PSO and BFO. This optimized model will be implemented, in a future work, on reconfigurable hardware by means of field programmable gate array (FPGA). Our objective is to combine: the swarm intelligence optimization power, the parallel computing scheme of neural networks and real time functioning of the hardware and put all into practice in an embedded design.

## References

1. Per Christian Hansen, James G. Naqg, Dianne P OLearg, "Deblurring Images : Matrices, Spectra and Filtering ", SIAM, Society for Industrial and Applied Mathematics.Philadelphia.2006.
2. A. Khireddine, K. Benmahammed, W. Puech." Digital image restoration by Wiener filter in 2D case", Advances in Engineering Software 38 (2007) 513–516. [www.elsevier.com/locate/advengsoft](http://www.elsevier.com/locate/advengsoft).
3. J.L. Lamotte, R. Alt, "Comparison of simulated annealing algorithms nfor image restoration". Mathematics and Computers in Simulation 37 (1994) 1-15. 1994 Elsevier Science B.V.
4. Z. Riéti, "Deblurring Images Blurred by the Discrete Gaussian". 0893-9659(95)00042-9. 1995 Elsevier Science Ltd.
5. Robert A. Hummel, B. Kimia and Steven W. Zucker. "Deblurring Gaussian Blur". Computer Vision, Graphics, And Image Processing 38, 66-80 (1987). By Academic Press, Inc.
6. D. Firsov, S.H. Lui." A fast deblurring algorithm", Applied Mathematics and Computation 183 (2006) 285–291. [www.elsevier.com/locate/amc](http://www.elsevier.com/locate/amc).
7. Julie Kamm, James G. Nagy b, "Kronecker product and SVD approximations in image restoration", Linear Algebra and its Applications 284 (1998) 177-192. 1998 Elsevier Science Inc.
8. Yen-Wei Chen, Zensho Nakao, Kouichi Arakaki, Xue Fang, Shinichi Tamura, "Restoration of gray images based on a genetic algorithm with Laplacian constraint". Fuzzy Sets and Systems 103 (1999) 285-293, 1999 Elsevier Science...intro
9. C. A. Z. Barcelos, Y. Chen. "Heat Flows and Related Minimization Problem in Image Restoration", Computers and Mathematics with Applications 39 (2000) 81-97. [www.elsevier.nl/locat e/camwa](http://www.elsevier.nl/locat e/camwa).

10. Masashi Sugiyama , Hidemitsu Ogawa. "A unified method for optimizing linear image restoration filters", *Signal Processing* 82 (2002) 1773 – 1787. [www.elsevier.com/locate/sigpro](http://www.elsevier.com/locate/sigpro).
11. Tzu-Chao Lin, Pao-Ta Yu. "Partition fuzzy median filter based on fuzzy rules for image restoration". *Fuzzy Sets and Systems* 147 (2004) 75–97. [www.elsevier.com/locate/fss](http://www.elsevier.com/locate/fss).
12. P.E. Undrill, K.Delibassis,"Stack Filter Design for Image Restoration Using Genetic Algorithms". *Proceedings of the International Conference on Image Processing* , 1997.
13. Yuk-Hee Chan, Yik-Hing Fung. "A regularized constrained iterative restoration algorithm for restoring color-quantized images". *Signal Processing* 85 (2005) 1375–1387. [www.elsevier.com/locate/sigpro](http://www.elsevier.com/locate/sigpro)
14. Yik-Hing Fung, Yuk-Hee Chan, "A simulated annealing restoration algorithm for restoring halftoned color-quantized images", *Signal Processing: Image Communication* 21 (2006) 280–292. [www.elsevier.com/locate/image](http://www.elsevier.com/locate/image).
15. Shin-Min Chao, Du-Ming Tsai, «Astronomical image restoration using an improved anisotropic diffusion». *Pattern Recognition Letters* 27 (2006) 335–344. [www.elsevier.com/locate/patrec](http://www.elsevier.com/locate/patrec).
16. L. Jaafar Belaid, M. Jaoua, M. Masmoudi, L. Siala. « Application of the topological gradient to image restoration and edge detection", *Engineering Analysis with Boundary Elements* 32(2008)891–899, [www.elsevier.com/locate/enganabound](http://www.elsevier.com/locate/enganabound).
17. K. Rajesh, K.C. Roy, S. Sengupt, S. Sinh. "Satellite image restoration using statistical models", *Signal Processing* 87 (2007) 366–373. [www.elsevier.com/locate/sigpro](http://www.elsevier.com/locate/sigpro).
18. T. Barbu, et al. "A PDE variational approach to image denoising and restoration", *Nonlinear Analysis: Real World Applications* (2008), doi:10.1016/j.nonrwa.2008.01.017. article in press.
19. G. Landi. "A fast truncated Lagrange method for large-scale image restoration problems". *Applied Mathematics and Computation* 186 (2007) 1075–1082. [www.elsevier.com/locate/amc](http://www.elsevier.com/locate/amc).
20. X. Gu, L. Gao,"A new method for parameter estimation of edge-preserving regularization in image restoration", *Journal of Computational and Applied*

- Mathematics (2008), doi:10.1016/j.cam.2008.08.013. Article in press. [www.elsevier.com/locate/cam](http://www.elsevier.com/locate/cam).
21. Barzilai, J. and Borwein, J., 1988, "Two-point step size gradient methods". *IMA Journal of Numerical Analysis*, 8, 141–148.
  22. A. Bouzerdoum, "A combined quadratic optimization median filtering technique for image restoration", 0-7803-4778-1/98 \$10.00 ©1998 IEEE.
  23. Rafael Gonzalez, "*Digital Image Processing Using Matlab*", 3rd edition, 2004, Prentice Hall, Upper Saddle River.
  24. P. Campisi, K. Egiazarian, «blind image deconvolution, Theory and Applications», CRC Press. © 2007 by Taylor & Francis Group, LLC.
  25. I. Larrabide, «Processamento de imagens via Derivada Topológica e suas aplicações na modelagem e simulação computacional do Sistema Cardiovascular Humano». DSc Tesis. Laboratório Nacional de Computação Científica-LNCC/MCT. Petrópolis, RJ, Brazil. March 2007.
  26. Tikhonov, A.N. and Arsenin, V.Y., 1977, « Solution of Ill-posed Problems », (New York: John Wiley).
  27. D. Krawczyk, Stand, M. Rudnicki, « Regularization Parameter Selection in Discrete Ill-Posed Problems –The Use of The U-Curve », *Int. J. Appl. Math. Comput. Sci.*, 2007, Vol. 17, No. 2, 157–164. DOI:10.2478/v10006-007-0014-3.
  28. L. Rudin, S. Osher and E. Fatemi, « Nonlinear Total Variation based noise removal algorithms », *Physica D.*, 60:259–268, 1992.
  29. A. Chambolle, « An algorithm for Total Variation minimization and applications ». *Journal of Mathematical Imaging and Vision*, 20:89–97, 2004.
  30. Bermúdez, A., Moreno, C.: Duality methods for solving variational inequalities. *Comput. Math. Appl.* 7, 43-58 (1981).
  31. K. Edoh, J.P. Roop, «A Fast Wavelet Multilevel Approach to Total Variation Image Denoising », *International Journal of Signal Processing, Image Processing and Pattern Recognition*, Vol. 2, No.3, September 2009.
  32. Nnolim, U. Lee, P, « Homomorphic Filtering of colour images using a Spatial Filter Kernel in the HSI colour space », *Instrumentation and Measurement Technology Conference Proceedings*, 2008. IMTC 2008. IEEE.

33. Haupt, RL & Haupt, SE 2004, Practical Genetic Algorithms, 2 ndedn, Wiley-Interscience, Canada.
34. Abebe Geletu, "Solving Optimization Problems using the Matlab Optimization Toolbox - a Tutorial", December 13, 2007.
35. J. Kennedy and R. C. Eberhart. Particle swarm optimization. In Proceeding of IEEE International Conference on Neural Networks, pages 1942–1948, Perth,Australia, November 1995.
36. Mahamed G. H. Omran"Particle Swarm Optimization Methods for Pattern Recognition and Image Processing", PhD thesis, University of Pretoria,2004.
37. Xiaolan Wu,; Bo Cheng,; Jianbo Cao,; Binggang Cao, "Particle swarm optimization with normal cloud mutation", 7th World Congress on Intelligent Control and Automation , 2008 Pages: 2828-2832.
38. Jianping Wen; Xiaolan Wu; Kuo Jiang; Binggang Cao, "Particle swarm algorithm based on normal cloud", IEEE Congress on Evolutionary Computation (IEEE World Congress on Computational Intelligence) 2008 Pages: 1492-1496.
39. Kevin M. Passino, "Biomimicry of Bacterial Foraging, for Distributed Optimization and Control", 0272-1708/02/, IEEE Control Systems Magazine, June 2002.
40. W. J. Tang, Q. H. Wu, J. R. Saunders. "A Bacterial Swarming Algorithm For Global Optimization" , 2007 IEEE Congress on Evolutionary Computation (CEC 2007). 1-4244-1340-0/07/c\_2007 IEEE.
41. Abebe Geletu, "Solving Optimization Problems using the Matlab Optimization Toolbox, a Tutorial", December 13, 2007.
42. S.Saadi, M.Bettayeb, A.Guessoum, «Optimal Approach for Neutron Images Restoration Using Particle Swarm Optimization (PSO) Algorithm with Regularization», N°:16554-16554, Journal of Applied Sciences, 2010, ISSN 1812-5654 ©2010 Asian Network for Scientific Information.
43. S.Saadi, M.Bettayeb, A.Guessoum, «Novel Approach for Gray Images Restoration and Enhancement Using Bacterial Foraging Algorithm: Application to Neutron Imaging », IC-MED Journal, Vol. 4, No. 1, 2, Page 25-39 Copyright © 2011, TSI® Press Printed in the USA. All rights reserved.

44. S.Saadi, M.Bettayeb, A.Guessoum, «Deconvolution of Neutron Degraded Images: Comparative Study between TSVD, Tikhonov Regularization and Particle Swarm Optimization Algorithm », EL\_2009\_10\_26a, Engineering Letters Journal, accepted for publication, 2010.
45. S.Saadi, A.Guessoum, M.Bettayeb, Regularized Total Variation Image Enhancement Using E.Coli Bacteria Foraging Algorithm: Application to Neutron Radiography Projections, PRZEGLĄD ELEKTROTECHNICZNY (Electrical Review), ISSN 0033-2097,R. 03b/2012, <http://www.red.pe.org.pl/index.php?lang=1>
- 46.S.Saadi, A.Kouzou, A.Guessoum, M.Bettayeb, «Bacterial Foraging Algorithm for Neutron Radiography Image Quality Improvement », The 7th IEEE International Multi-Conference on Systems, Signals and Devices (SSD'2010),27-29 June 2010, Amman-Jordan. DOI: 10.1109/SSD.2010.5585541.
- 47.S.Saadi, A.Kouzou, A.Guessoum, M.Bettayeb, «A Comparative Study to Select an Image Deconvolution Method», The 7<sup>th</sup> IEEE International Multi-Conference on Systems, Signals and Devices (SSD'2010), 27-29 June 2010, Amman-Jordan. DOI: 10.1109/SSD.2010.5585542
- 48.S.SAADI, A.GUESSOUM, M.BETTAYEB, “A hybrid Implementation of PSO and BFO for Stained and blurred Images Restoration”, Paper ID37. Second International Conference on Image and Signal Processing and their Applications, 6<sup>th</sup> to 8<sup>th</sup> December 2010, university of Biskra, Algeria. <http://www.univ-biskra.dz/ispa2010>
- 49.S.SAADI, A.GUESSOUM, M.BETTAYEB, “A Novel Approach for Impulse Noise Removal Using Bacterial Foraging Optimization Algorithm with Regularization”, Paper ID38. Second International Conference on Image and Signal Processing and their Applications, 6th to 8th December 2010, university of Biskra, Algeria. <http://www.univ-biskra.dz/ispa2010> .
- 50.Slami SAADI, Abderrezak GUESSOUM, Maamar BETTAYEB, A Novel Approach for Regularized Signal Deconvolution Based on Hybrid Swarm Intelligence: Application to Neutron Radiography, 15th International Workshop on Nature Inspired Distributed Computing (NIDISC 2012), May 21-25, 2012 Shanghai, China.



## APPENDIX

### Scientific Participations and Publications (2008-2012)

#### Journal Papers

1. **S.Saadi**, A.Guessoum, M.Bettayeb, Regularized Total Variation Image Enhancement Using E.Coli Bacteria Foraging Algorithm: Application to Neutron Radiography Projections, PRZEGLĄD ELEKTROTECHNICZNY (Electrical Review), ISSN 0033-2097,R. 03b/2012, (Impact Factor (2010): 0.242). <http://www.red.pe.org.pl/index.php?lang=1>
2. **S.Saadi**, A.Guessoum, M.Bettayeb, FPGA Embedded Implementation for Neutron Radiography Images Restoration Based on Tikhonov and Total Variation Algorithms, PRZEGLĄD ELEKTROTECHNICZNY (Electrical Review), ISSN:0033-2097,R.07/2012, (Impact Factor (2010): 0.242). <http://www.red.pe.org.pl/index.php?lang=1> .
3. **S.Saadi**, M.Bettayeb, A.Guessoum, «Deconvolution of Neutron Degraded Images: Comparative Study between TSVD, Tikhonov Regularization and Particle Swarm Optimization Algorithm », Volume 18 Issue 3, EL\_18\_3\_03. (IAENG) Engineering Letters Journal, 2010. [http://www.engineeringletters.com/issues\\_v18/issue\\_3/index.html](http://www.engineeringletters.com/issues_v18/issue_3/index.html)
4. **S.Saadi**, M.Bettayeb, A.Guessoum, «Novel Approach for Gray Images Restoration and Enhancement Using Bacterial Foraging Algorithm: Application to Neutron Imaging », IC-MED Journal, Vol. 4, No. 1, 2, Page 25-39 Copyright © 2011, TSI® Press Printed in the USA. All rights reserved.
5. **S.Saadi**, M.Bettayeb, A.Guessoum, «Optimal Approach for Neutron Images Restoration Using Particle Swarm Optimization (PSO) Algorithm with Regularization», N°:16554-16554, DOI: 10.3923/jas.2010.517.525. Journal of Applied Sciences, 2010, ISSN 1812-5654 ©2010 Asian Network for Scientific Information. <http://scialert.net/abstract/?doi=jas.2010.517.525>

6. Aissa SOULI, Abdelhafid HELLAL, **Slami SAADI**, Programming EMTP-ATP-PSCAD Software Functions Using MATLAB for Power Systems Transients Analysis, PRZEGLĄD ELEKTROTECHNICZNY (Electrical Review), ISSN 0033-2097, R. 86 NR 3/2010. (<http://www.red.pe.org.pl/index.php?lang=1> )
7. **SLAMI SAADI**, HAMZA MEKKI, ABDERREZAK GUESSOUM, «Object Detection and Segmentation Algorithm Implemented on a Reconfigurable Embedded Platform Based FPGA », WSEAS TRANSACTIONS on SIGNAL PROCESSING, Issue 9, Volume 4, September 2008, ISSN: 1790-5022. WSEAS is indexed by ACM and IEEE. <http://www.worldses.org/journals/signal/signal-2008.htm>

### **International Conferences with Refereed Proceedings**

1. **S.Saadi**, A.Guessoum, M.Elaguab, M.Bettayeb “Hybrid Swarm Optimized ARMA Model For Radiological Image Deblurring with its FPGA Implementation”, The 2nd International Conference on Industrial Engineering and Manufacturing ICIEM'2012, Batna, Algeria, May 06-07, 2012.
2. **S.Saadi**, A.Guessoum, M.Elaguab, M.Bettayeb “Artificial Bees Colony Optimized Model for Image Restoration and its FPGA Implementation”, The 3<sup>rd</sup> IEEE International Conference on Multimedia Computing and Systems (ICMCS'12), May 10-12 2012, Tangier, Morocco.
3. **Slami SAADI**, Abderrezak GUESSOUM, Maamar BETTAYEB, A Novel Approach for Regularized Signal Deconvolution Based on Hybrid Swarm Intelligence: Application to Neutron Radiography, 15<sup>th</sup> International Workshop on Nature Inspired Distributed Computing (NIDISC 2012), May 21-25, 2012 Shanghai, China.
4. **Slami SAADI**, Mohamed Elaguab, Abderrezak GUESSOUM, Maamar BETTAYEB, Optimizing UPFC Parameters via Two Swarm, 9th IEEE International Multi-Conference on Systems, Signals and Devices (SSD'2012), March 20 - 23, 2012, Chemnitz, Germany.
5. **Slami SAADI**, Abderrezak GUESSOUM, Maamar BETTAYEB, Neutron Radiography Images Restoration on FPGA Embedded Implementation,

- 9th IEEE International Multi-Conference on Systems, Signals and Devices (SSD'2012), March 20 - 23, 2012, Chemnitz, Germany.
6. **S.Saadi**, A.Kouzou, A.Guessoum, M.Bettayeb, «Bacterial Foraging Algorithm for Neutron Radiography Image Quality Improvement », The 7th IEEE International Multi-Conference on Systems, Signals and Devices (SSD'2010),27-29 June 2010, Amman-Jordan. DOI: 10.1109/SSD.2010.5585541.
  7. **S.Saadi**, A.Kouzou, A.Guessoum, M.Bettayeb, «A Comparative Study to Select an Image Deconvolution Method», The 7<sup>th</sup> IEEE International Multi-Conference on Systems, Signals and Devices (SSD'2010), 27-29 June 2010, Amman-Jordan. DOI: 10.1109/SSD.2010.5585542
  8. **S.SAADI**, A.GUESSOUM, M.BETTAYEB, “A hybrid Implementation of PSO and BFO for Stained and blurred Images Restoration”, Paper ID37. Second International Conference on Image and Signal Processing and their Applications, 6<sup>th</sup> to 8<sup>th</sup> December 2010, university of Biskra, Algeria. <http://www.univ-biskra.dz/ispa2010>
  9. **S.SAADI**, A.GUESSOUM, M.BETTAYEB, “A Novel Approach for Impulse Noise Removal Using Bacterial Foraging Optimization Algorithm with Regularization”, Paper ID38. Second International Conference on Image and Signal Processing and their Applications, 6th to 8th December 2010, university of Biskra, Algeria. <http://www.univ-biskra.dz/ispa2010> .
  - 10.A.kouzou, **S.Saadi**, M.O.Mahmoudi, M.S.Boucherit, «Particle Swarm Optimization Applied for the Improvement of the PWM AC/AC Choppers Voltage», 2009 COMPATIBILITY AND POWER ELECTRONICS, CPE2009 6th INTERNATIONAL IEEE CONFERENCE-WORKSHOP. DOI: 10.1109/CPE.2009.5156027.
  - 11.Kouzou A, **Saadi S**, Mahmoudi M.O, Boucherit M.S, “Voltage Quality Enhancement of PWM AC Voltage Controller Using Particle Swarm Optimization”, IEEE POWERENG 2009, Lisbon, Portugal, March 18-20, 2009, DOI: 10.1109/POWERENG.2009.4915243.
  - 12.Kouzou A, **Saadi S**, Mahmoudi M.O, “THE USE OF THE PARTICLE SWARM OPTIMIZATION FOR THE IMPROVEMENT OF THE AC/AC CHOPPERS OUTPUT VOLTAGE”, 2009, 6<sup>th</sup> IEEE International Multi-

conference on systems, signals and devices, (SSD'2009).  
*DOI:10.1109/SSD.2009.4956744*

13. **Slami SAADI**, Abdelhamid DZANOUNI, Hamza MEKKI, Abderrezak GUESSOUM, "Color Detection Algorithm Implemented on Embedded Platform Based FPGA, Application to Irradiation Target Manipulation", 2<sup>nd</sup> International Conference on Electrical and Electronics Engineering 21-23 April 2008. University of Laghouat, Algeria.
14. Kouzou, A.; Khaldi, B.S.; **Saadi, S.**; Mahmoudi, M.O.; Boucherit, M.S, "Apparent power ratio of the Shunt Active Power Filter", 13th IEEE Power Electronics and Motion Control Conference, 2008. EPE-PEMC 2008. *DOI: 10.1109/EPEPEMC.2008.4635557.*

### **Participation as a Reviewer**

1. Review process of research articles for the ARI ELSEVIER Journal: Applied Radiation and Isotopes, (2010). <http://ees.elsevier.com/ari/>.
2. Review process of research papers for the SWEVO ELSEVIER Journal: Swarm and Evolutionary Computation, (2011). <http://ees.elsevier.com/swevo/>

### **Course Book**

**« Introduction à l'Optimisation Métaheuristique: Cours, Exercices & Applications en Génie Electrique »**

*Pour les étudiants en fin de cycle (Ingénieur, Master & Doctorat)*

Par: **Slami Saadi**, Enseignant-Chercheur

Faculté des Sciences et Technologie, Université Ziane Achour de Djelfa